2017

Heavy metal concentration and transport from existing copper slag emplacements along the Windang Peninsula, through the unconfined sandy aquifer to Lake Illawarra

Michael Trajcevski

Heavy metal concentration and transport from existing copper slag emplacements along the Windang Peninsula, through the unconfined sandy aquifer to Lake Illawarra

Abstract

Up until recently, copper slag was widely considered to be chemically inert, and was thought to pose no significant environmental risks when deposited. Since the late 20th century there have been many reports claiming that copper slag can pose a risk to groundwater systems once it has degraded in its depositional environment over time.

Wollongong City Council is interested in examining the possible environmental impacts of a copper slag emplacement located on the Windang peninsula, a narrow strip of estuarine sand on the south coast of NSW. In the past, high concentrations of zinc, iron, cadmium and copper have been observed in the emplacement groundwater. The concerns were the possibility of dissolved metals in the groundwater increasing over time due to increased metal leaching from weathering, and also the transport of these dissolved metals through the Windang unconfined sandy aquifer to nearby Lake Illawarra.

Dissolved metal concentrations in groundwater were analysed in this study from a number of new and existing bores within the slag emplacement, and results were compared with existing data gathered in past reports. Weathered and unweathered slag samples were also inspected visually using reflected light microscopy and scanning electron microscopy (SEM) to determine structural differences in the outer perimeter of the slag granules. The slag samples also underwent elemental analysis using EDS to determine the distribution and abundance of various elements throughout the slag granules, and help determine which metals leach out fastest.

The groundwater analysis yielded results similar to background levels for most samples, with the exception of zinc in groundwater from BH9 only, which on all four sampling rounds exceeding the ANZECC (2000) guidelines. When compared to past results from equivalent bores, the concentration of most metals in the groundwater decreased on average over time. The only metals which increased over time contained concentrations equal to or lower than background levels in all samples, suggesting the slag is not a major source of these metals.

XRF and EDS results consistently displayed significant depletion of zinc from the weathered zones of slag. As the main source of zinc in groundwater is the weathered outer rim of the slag granule, it suggests that any new zinc being leached into the groundwater must be originating from the weathering of the unweathered, inner zone of the slag granule. With the production of this weathering rind around the perimeter of partly weathered slag granules, it is hypothesised that the rate of weathering of the unweathered inner section of the slag granule is greatly decreased due to the reduced exposure to air and moisture as a result of the “shielding” effect of this weathering rind. The reduced supply of zinc from slag into groundwater through leaching, and the dispersion of existing dissolved zinc throughout the aquifer, provides a possible explanation for the reduced zinc concentrations in the Windang aquifer over time. With the likely continuation of this trend, as long as the emplacement site is not agitated or disturbed, no action is necessary regarding metal immobilisation within the groundwater.

Degree Type

Thesis

Degree Name

BEnviSc Hons

UNIVERSITY OF WOLLONGONG AUSTRALIA

Heavy metal concentration and transport from existing copper slag emplacements along the Windang Peninsula, through the unconfined sandy aquifer to Lake Illawarra

Michael Trajcevski

A thesis submitted in partial fulfilment of the Bachelor of Environmental Science (Honours)

School of Earth and Environmental Sciences

Faculty of Science, Medicine and Health

University of Wollongong

October 2017

Declaration

The information in this thesis is entirely the result of investigations conducted by the author unless otherwise acknowledged, and has not been submitted in part, or otherwise, for any other degree or qualification.

Michael Trajcevski

24 October 2017

Acknowledgements

First and foremost I would like to sincerely thank my supervisors at the University of Wollongong, Associate Professor Brian Jones, and Dr John Bradd for your extensive knowledge and invaluable guidance throughout this year. I would also like to thank my supervisor at the council, Dr Iradj Yassini, for your valuable insight and direction in planning and developing this project. Recognition and thanks to Brent Peterson, who has been of tremendous help both out in the field and on campus. Gratitude to Jose Abrantes for your work in XRF analysis and Polished Block preparation. Thanks to Solomon Buckman, for your knowledge in interpreting structures and species present in the polished blocks under reflected light microscopy. Thank you to Lili Yu for ensuring the YEO-KAL water quality analyser was calibrated and ready to go when needed. Thank you to Thomas Mcmahon and Mitchell Nancarrow for your guidance and assistance in SEM and EDS analysis. I also give thanks to Marina McGlinn for providing assistance and advice both prior to and during this year. Finally, thank you to my parents who have supported and helped me along the way.

Abstract

Up until recently, copper slag was widely considered to be chemically inert, and was thought to pose no significant environmental risks when deposited. Since the late 20th century there have been many reports claiming that copper slag can pose a risk to groundwater systems once it has degraded in its depositional environment over time.

Wollongong City Council is interested in examining the possible environmental impacts of a copper slag emplacement located on the Windang peninsula, a narrow strip of estuarine sand on the south coast of NSW. In the past, high concentrations of zinc, iron, cadmium and copper have been observed in the emplacement groundwater. The concerns were the possibility of dissolved metals in the groundwater increasing over time due to increased metal leaching from weathering, and also the transport of these dissolved metals through the Windang unconfined sandy aquifer to nearby Lake Illawarra.

Dissolved metal concentrations in groundwater were analysed in this study from a number of new and existing bores within the slag emplacement, and results were compared with existing data gathered in past reports. Weathered and unweathered slag samples were also inspected visually using reflected light microscopy and scanning electron microscopy (SEM) to determine structural differences in the outer perimeter of the slag granules. The slag samples also underwent elemental analysis using EDS to determine the distribution and abundance of various elements throughout the slag granules, and help determine which metals leach out fastest.

The groundwater analysis yielded results similar to background levels for most samples, with the exception of zinc in groundwater from BH9 only, which on all four sampling rounds exceeding the ANZECC (2000) guidelines. When compared to past results from equivalent bores, the concentration of most metals in the groundwater decreased on average over time. The only metals which increased over time contained concentrations equal to or lower than background levels in all samples, suggesting the slag is not a major source of these metals.

XRF and EDS results consistently displayed significant depletion of zinc from the weathered zones of slag. As the main source of zinc in groundwater is the weathered outer rim of the slag granule, it suggests that any new zinc being leached into the groundwater must be originating from the weathering of the unweathered, inner zone of the slag granule. With the production of this weathering rind around the perimeter of partly weathered slag granules, it is hypothesised that the rate of weathering of the unweathered inner section of the slag granule is greatly decreased due to the reduced exposure to air and moisture as a result of the “shielding” effect of this weathering rind. The reduced supply of zinc from slag into groundwater through leaching, and the dispersion of existing

dissolved zinc throughout the aquifer, provides a possible explanation for the reduced zinc concentrations in the Windang aquifer over time. With the likely continuation of this trend, as long as the emplacement site is not agitated or disturbed, no action is necessary regarding metal immobilisation within the groundwater.

Contents

List of figures

List of tables

List of abbreviations

AGC = Acid Generation Capacity

ALS = Australian Laboratory Services

ANC = Acid Neutralization Capacity

ANZECC = Australian and New Zealand Environment Conservation Council

BH = Borehole

D.O. – Dissolved Oxygen

DR = Driving Range

E.C. = Electrical Conductivity

LOD = Limit of Detection

LTV = Long Term Trigger Value

MASL/ASL = Metres Above Sea Level / Above Sea Level

NAPP = Net Acid Production Potential

NTU = Nephelometric Turbidity Unit

ORP = Oxidation-Reduction Potential

Sat = Saturation

STV = Short Term Trigger Value

TCLP = Toxicity Characteristic Leaching Procedure

TDS = Total Dissolved Solids

Chapter 1. Introduction

1.1. Project background

Copper slag was widely considered to be chemically inert in the past, and minimal environmental regulations were put in place regarding its disposal into the environment. As copper slag was thought to be of little to no risk of producing harmful leachate, the main method of disposal was to dump the slag on a site as is, with no isolation system separating the potential leachate from the surrounding groundwater system. As well as this, no proper post-disposal groundwater monitoring plans were developed, as no risk was thought to exist.

In the last 20 years there have been numerous reports (Gee et al., 1997; Manz and Castro, 1997; Sobanska et al., 2000; Ettler et al., 2003; Piatak et al., 2004; Reuter et al., 2004; Ettler et al., 2009 Vitkova et al., 2010; Piatak and Seal, 2010; Kierczak et al., 2013; Ettler and Johan, 2014; Piatak et al., 2015) claiming that copper slag can pose an environmental risk once it has been in its depositional environment for a number of years, due to the production of a leachate containing heavy metals released from the weathering of the slag over time.

A report by Lottermoser (2002) focuses on the chemical stability of several slag dumps from historical smelting sites in North Queensland. The weathering of slag due to a contemporaneous reaction with air and rainwater has triggered the release of metals and semi-metals from the slag granules into the surrounding groundwater. Zinc in particular is of great concern due to its high mobility, and thus presents a long-term risk to surrounding groundwater systems.

Wollongong City Council is interested in determining the impact that a copper slag emplacement has on surrounding groundwater quality, and determine how contaminants in the groundwater surrounding the emplacement transport through the Windang unconfined sandy aquifer into Lake Illawarra, a local recreational and fishing destination. The mechanisms of slag weathering are also of interest. The copper slag was produced by Southern Copper Inc. at nearby Port Kembla as a waste product of copper smelting. The oldest of the copper slag on the site dates back to 1947, and the most recent was deposited in 1993. After the last of the copper slag was deposited, the emplacement was sealed with a layer of clay and capped with soil in an attempt to limit groundwater infiltration from above (Pugh, 2002).

A number of reports have previously been completed on the Windang slag emplacement, focusing on contaminant leaching and transport in groundwater (Coffey Partners International Pty. Ltd. 1994, 1995, 1996; Pugh, 2002; Yassini, 1994; Forbes Rigby Pty Ltd, 1998) and also the mineralogy and weathering mechanism affecting the slag (Gay, 1995; Southern Copper Pty Ltd, 1992). This report will

seek to add to the information gathered collectively in these previous reports by examining how slag weathering and contaminants in groundwater has changed over time.

1.2. Site description

The copper slag emplacement of interest is located on the Windang Peninsula; a narrow strip of estuarine sand running north-south, with the Tasman Sea to the east and Lake Illawarra to the west (Figures 1 to 3). The width of the peninsula varies as you travel along north-south, however at the slag emplacement the sand barrier measures 900m across from the Pacific Ocean to Lake Illawarra (Figure 3). The site is relatively flat, with the largest variation in height above sea level being around 5m; one exception being the sand dunes on the eastern side of the peninsula which rise to 15m asl. The land used to dispose of the slag was previously described as a swamp with a high water table (Yassini, 1994).

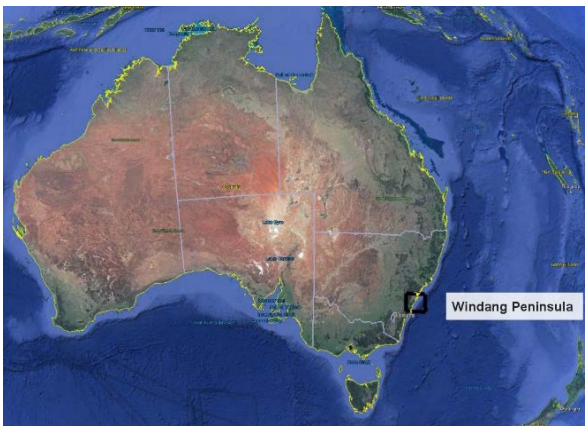

Figure 1: Windang Peninsula, South Coast NSW, Australia

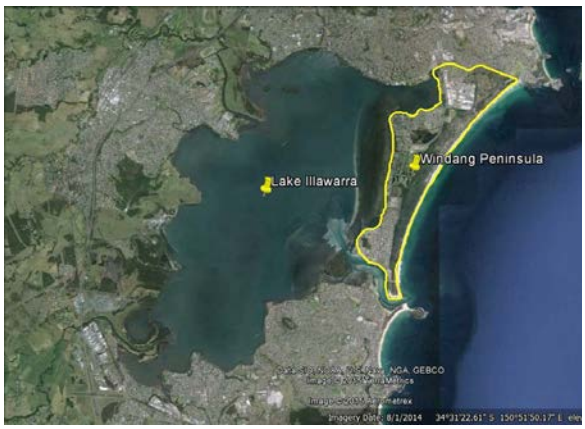

Figure 2: Windang Peninsula, South Coast NSW, Australia (From Longhurst, 2015)

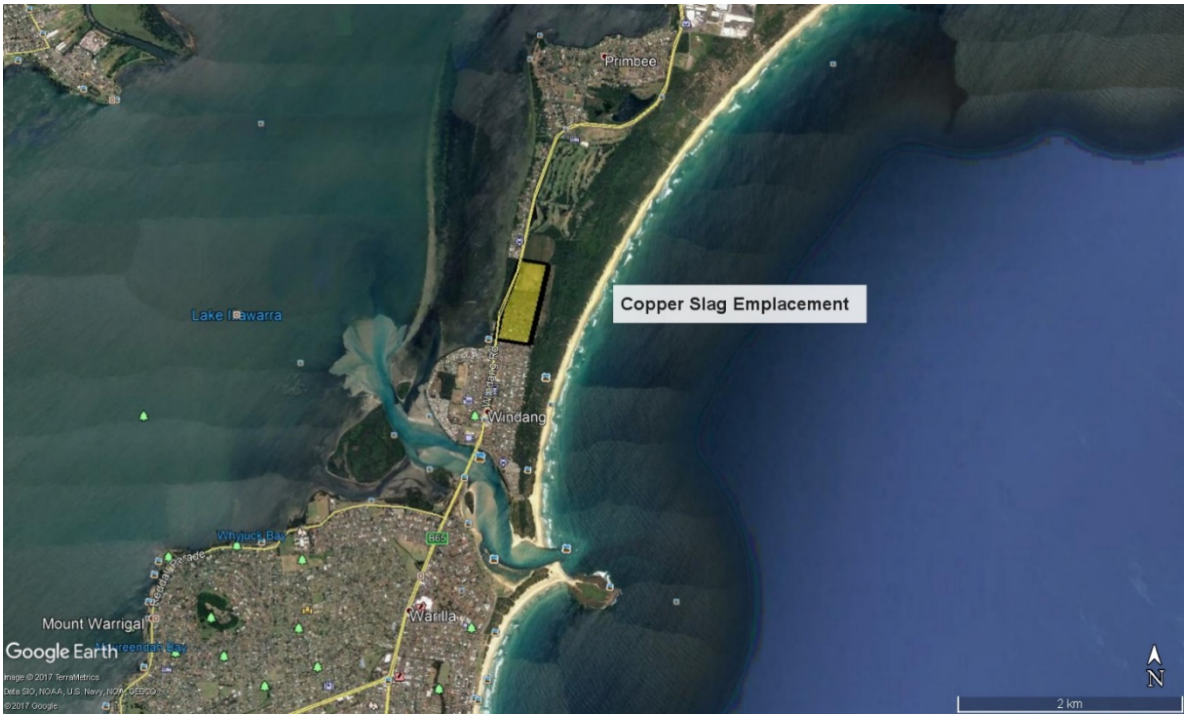

Figure 3: Copper Slag Emplacement (Adapted from Coffey, 1996)

The layer of soil and clay on the surface measures around 0.4m thickness. The copper slag emplacement lies directly below, and measures between 2m to 2.5m thick across the landfill site. Below the slag is unconsolidated, unconfined Quaternary estuarine sands, down to a depth of 30m (Coffey Partners International, 1996). There is no clay barrier between the bottom of the slag and the marine sand below, allowing mixing of the two groundwater zones. Below the dune sand lies bedrock composed of volcanic sandstones from the Permian Broughton Formation (Coffey Partners International, 1994).

The water table is on average at around 1m to 2m depth. This creates a vadose zone which ends within the slag layer, meaning the lower portion of slag is submerged in groundwater constantly except for during extreme drought. It is therefore expected that the bottom portion should show significantly less weathering than the top portion of slag which is exposed to oxygen and is wetted/dried repeatedly. As samples were able to be obtained from slag in both groundwater zones, this theory was able to be tested.

1.3. Aims and objectives

The aims of this study are to determine if there are any heavy metal pollution plumes present in the Windang unconfined sandy aquifer immediately surrounding a copper slag emplacement, and evaluate if the concentration and transport of these plumes through the unconfined sandy aquifer to nearby Lake Illawarra is a cause for concern. The mechanism of slag weathering will also be investigated.

In order to meet the project aims, topics that were investigated include:

1. Monitor water table fluctuations and use this information in conjunction with rainfall data to determine delay in aquifer recharge/depletion and relate magnitude of water table change to amount of rainfall received
2. Determining the concentration of dissolved heavy metals in groundwater via sampling through a number of bores of different depth and location relative to the slag emplacement
3. Compare the attributes of weathered vs unweathered slag by looking at characteristics such as grain size, mineralogy and elemental composition.
4. Examine the structure and weathering mechanism of the slag by reflected light microscopy, SEM and analyse elemental composition using EDS
5. Test the pH of the groundwater and soil, as well as the Acid Neutralization/Acid Generation Capacities (ANC/AGC) of the slag to help predict heavy metal mobility as a result of changes in pH
6. Determine major anions/cations present in the groundwater, and compare differences between bores of different locations and depths

Chapter 2. Literature review

2.1. Production and characteristics of copper slag

Copper slag is a waste material produced from the matte smelting and pyrometallurgical production of copper from ore. The ratio of slag production to copper production is around 2.2:1, which equates to approximately 24.6 million tonnes of slag generated per year from world copper production. Slags containing less than 0.8% copper are not post-processed, and are either discarded or sold as a substitute to natural basalt or obsidian manufacturing materials (Gorai et al, 2003).

Copper is recovered from ore by matte smelting at high temperatures, followed by conversion. Throughout the smelting process, iron, copper, sulphur and oxygen are present, as well as oxides of iron and copper, Al_2O_3, CaO, MgO, and SiO_2. These constituents originate from either the original concentrate or in the added flux (Gorai et al, 2003). The total sulphur content is generally under 1% (Southern Copper, 1992). The proportion of each of these components play a large part in controlling the chemistry and physical properties of the end products. Matte smelting produces 2 liquid phases; a copper-rich matte (sulphides) and slag (oxides) (Gorai et al, 2003).

During the smelting process, silica is added to isolate copper in the matte. The added silica combines with oxides to form strongly bonded silicate anions which group together, forming the slag phase (Gorai et al, 2003). Lime and alumina are added to stabilise the slag structure (Shi and Qian, 2000). Quickly cooled slag gives an amorphous texture, whereas slow cooling produces a hard, crystalline slag (Gorai et al, 2003).

Table 1 outlines the typical chemical composition of copper slag based on data from multiple studies (see Appendix. 4). As can be seen by examining the average percentage of each component, almost three quarters of copper slag consists of iron and silicon dioxide. Other oxides such as calcium oxide, magnesium oxide, and aluminium oxide make up around two thirds of the remaining material. The rest of the slag is composed of a spread between sulphur, copper, cobalt, manganese, nickel and zinc. Looking at the ranges of the values for each component between the studies, and comparing that range to the relative average amounts, there seems to be high variability in the composition of slag depending on the source material and smelting methods used.

Table 1: Chemical composition of copper slag based on data from the following studies:

(1) Iranian National Copper Industries Co, (Marghussian and Maghsoodipoor, 1999).
(2) Etibank Ergani Copper Plant, Elazig-Turkey (Kiyak et al., 1999).
(3) Caletone Smelter Chile (Imris et al., 2000).
(4) Indian Copper Plants (Agrawal et al., 2000).
(5) Kure Copper Slag (Yucel et al., 1992).
(6) Copper Queen, Prince, USA (Mobasher et al., 1996).

	Minimum	**Maximum**	**Range**	**Average**
Fe (%)	34.62	47.80	13.18	43.83
SiO_2 (%)	24.70	40.97	16.27	30.68
CaO (%)	0.70	17.42	16.72	6.83
MgO (%)	1.00	3.51	2.51	2.04
Al_2O_3 (%)	2.40	15.6	13.20	8.66
S (%)	0.11	1.50	1.39	0.76
Cu (%)	0.60	2.10	1.50	1.01
Co (%)	0.10	0.40	0.30	0.21
Mn (%)	0.03	0.49	0.46	0.24
Ni (%)	0.002	0.06	0.06	0.03
Zn (%)	0.05	0.72	0.67	0.29

Table 2 compares the average elemental composition of copper slag from Table 1 with values obtained for the Windang slag emplacement by Gay (1995), and also values obtained from slag produced by flash smelting at Boliden Harjavalta, Finland (Kaksonen et al., 2017). Values from these studies are within relatively close proximity to each other, with the only exception being iron content. However, in the XRF analysis of the Windang slag by Gay (1995), it was noted that problems during the XRF analysis may have reduced the accuracy of results, which is perhaps an explanation of why the iron content was so low in the Windang slag when compared to a reading of approx. 40% in the other 2 papers. Also in the paper by Gay (1995), a notable difference between the elemental compositions of old slag and new slag produced by Southern Copper circa 1995 is identified. The newer, less oxidised slag contains an equal or smaller proportion of zinc, copper, lead and iron when compared to the old/oxidised slag. Results in the report by Gay (1995) show a slight increase in sulphur in the new slag; an important finding which will be discussed in section 2.3.1, mechanisms of slag weathering.

Table 2: Elemental compositions of copper slags originating from various sources as percentage by weight

1 - Oxidised and unoxidised copper slag from the Windang emplacement (Gay, 1995)

2 - Copper slag from the copper flash smelting process at Boliden Harjavalta, Finland (Kaksonen et al., 2017)

3 – Typical average chemical compositions of copper slag from 10 different sources worldwide (Gorai et al., 2003)

	1		2	3
Metal	**Old slag (%)**	**New slag (%)**	**(%)**	**(%)**
Zn	1.91	1.11	2.79	0.31
Cu	0.44	0.45	0.38	1.00
Pb	0.52	0.37	0.6	-
Fe	21.1	21.1	40.9	43.83
S	0.53	0.74	0.14	0.76

The particle size distribution of marine sand and oxidised/unoxidised slag from the Windang Slag Emplacement is shown below in Figure 4. Marine sand is much finer than both the oxidised and unoxidised slag. Due to the process of oxidation and ferric-hydroxide coating of slag particles, the oxidised slag contains a greater proportion of slightly larger particles compared to the unoxidised slag (Yassini, 1994).

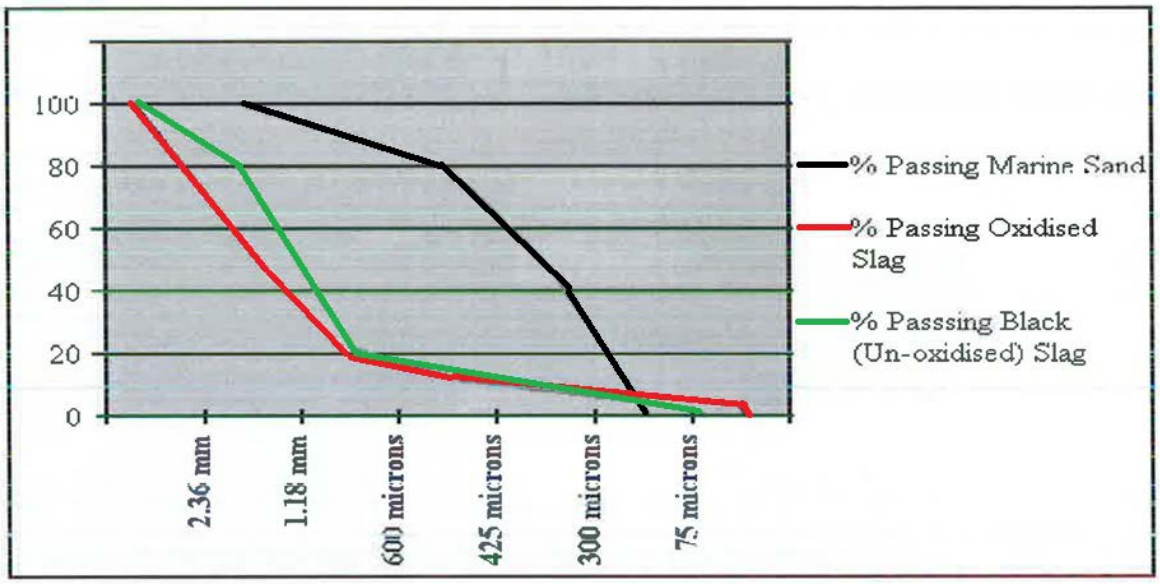

Figure 4: Grain size distribution of marine sand, unoxidised copper slag and oxidised copper slag in the Windang Slag Emplacement (Yassini, 1994)

2.2. Leachate from granulated copper slag

Chemical leaching of heavy metals occurs due to oxidation of the minerals in acidic environments, resulting in the release of ionic metals into solution. The rate of leaching can be accelerated by microorganisms, via a process called bioleaching (Larsson et al., 1993). Particular types of microorganisms, such as species belonging to the *Thiobacillus* genus, have been found to significantly increase the degree of heavy metal leaching over a wide range of pH (Kelly & Harrison, 1989). A report by Domel and Holden (1994) found that sulphur-oxidising (bioleaching) bacteria were present in the slag at the Windang landfill site. Leachate produced from the copper slag at Windang is generally highest in zinc, with lower concentrations of copper, lead and iron. When considering that zinc is the metal of highest concentration in the leachate, but one of the less abundant metals in the slag, we can infer that zinc is much more susceptible to leaching/bioleaching than the other metals. In addition to this, Gay (1995) reported, as a result of a number of leaching experiments, that the degree that each metal was leached depended on the type of bacteria present, as well as the pH. The leaching potential of slag in environments with a pH close to neutral or slightly alkaline (pH 7 to 10.5) was found to be lower over time than slag exposed to a more acidic environment. This is the case regardless of the slag structure or composition (Potysz et al, 2016).

In a study on a lead slag emplacement by Talpos et al. (2013), a large difference was noted in the leaching potential between fresh granulated lead slag and aged granulated lead slag. The degree of zinc leaching potential increased 25 times from fresh granulated slag to aged granulated slag; a notable difference that can most likely be attributed to both weathering, and a lower pH environment from the release of sulphates as a result of the weathering, leading to the production of sulfuric acid. Although this experiment was performed on lead slag, the same trend would likely be expected in copper slag, due to the fact that both slags contain zinc and sulphate, which are the key components in this process.

Talpos et al. (2013) described how to estimate the acid draining potential of an emplacement. Acid generation capacity is calculated by looking at quantitative measurements of the total amount of sulphur, whereas acid neutralisation capacity is determined through experimentation which involves hydrochloric acid being added to a finely ground sample, and then measuring the amount of acid consumed in the reaction with the base (sample).

An experiment on slag in the Windang and Korrongulla swamp area by Longworth and McKenzie (1983) involved trickling leachate water down a column filled with slag and monitoring the concentration of metals in the water. This was to establish data on the rate of heavy metal leaching, as well as the change in rate over time. The results of this experiment showed a linear increase in

dissolved zinc concentration over time, with no change in the rate of increase. The experiment was repeated under reflux conditions, which produced slightly different results. Zinc concentration in the leachate still increased at all times, however the rate of leaching also increased after around 100 hours, and remained at this higher rate for the duration of the experiment. The increase in rate of leaching coincides with the increased oxidation of slag sulphides and subsequent increase in sulphates in the water, lowering the pH due to the production of sulfuric acid. This could be an explanation for the sharp increase in leaching rate at 100 hours. A note made in the report highlights the significance of uncontrolled factors such as pH and Eh during the experiment, and how the amount of zinc dissolved should be much higher given a representative groundwater sample.

2.3. Mechanisms of copper slag weathering

Based on extensive TCLP (toxicity characteristic leaching procedure) testing of slag from the Windang emplacement between 1984 and 1992, the general consensus was that the copper slag is chemically inert, and has thus been thought to pose no environmental threat to soil and groundwater in a landfill environment (Yassini, 1994). However, the TCLP testing failed to take into account how weathering of the exposed copper slag over time affects leaching characteristics. The work by Gay (1995) has demonstrated that heavy metal concentrations in the groundwater at the Windang copper slag landfill site have increased over time since the slag was deposited. The mechanism behind the weathering of the slag is still not fully understood, however electron micrographs have demonstrated that metal sulphides have been removed from the slag granules. The removal of metal sulphides can be attributed to sulphur-oxidising bacteria, causing biologically catalysed solubilisation. This means in theory, the bacteria can cause an increased degree of heavy metals leaching from the slag. However, during Gay's experiment, which involved growing the sulphur-oxidising bacteria, it was found that the bacterial leach solution was only able to leach zinc, copper and iron when excess sulphur was added. When no additional sulphur was added, then leaching of the slag did not occur. This creates doubt as to whether in-situ sulphur concentrations in the copper slag at Windang are high enough for the sulphur-oxidising bacteria to leach out the three metals. However, an important result outlined in Gay's 1995 paper was a higher concentration of sulphur found in the newer slag (Table 1), possibly correlating to an increased likelihood of bioleaching in-situ.

An experiment by Potysz et al. (2016) examined the effects of the *Pseudomonas aeruginosa* bacteria, in a comparison of leaching behaviour resulting from biotic weathering vs abiotic weathering. Results showed between a 20% to 99% increase in Si, Fe, Cu, Zn and Pb concentrations in the biotic solution when compared to the abiotic solution. These results were supported by examination of the abiotic and biotic slags under an electron microscope, with the biotic slag sample visibly displaying a greater extent of weathering around the outer margins. This result was consistent for both granulated slag

and crystalline massive slag, thus inferring that a similar trend could possibly be established for all types of slag chemistry and structure.

2.3.1. Sulphur in copper slag

Sulphur in copper slag is only found in the form of sulphide. Sulphide in slag is responsible for the production of sulphuric acid as a product of weathering, as well as being a requirement for biological weathering/oxidation to take place. More than 95% of the sulphide particles found in the slag are iron sulphide, with small amounts of copper-iron sulphide, copper sulphide and lead sulphide. Reflected light microscopy images (Figures 5 to 8) of exfoliated weathered slag from the Windang emplacement show submicron sulphide particles (ssp), voids (v) and very fine fissures (E) (Yassini, 1994).

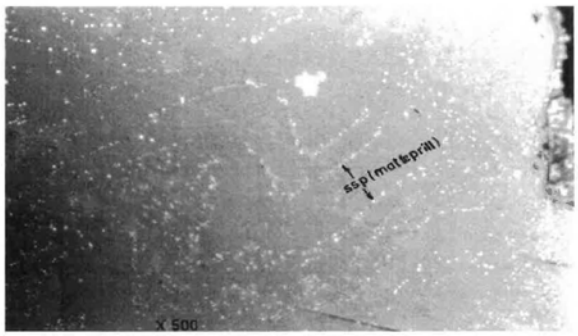

Figure 5: Distribution of submicron sulphide particles (ssp) in copper slag iron-silica matrix (matte prill) (from Yassini, 1994)

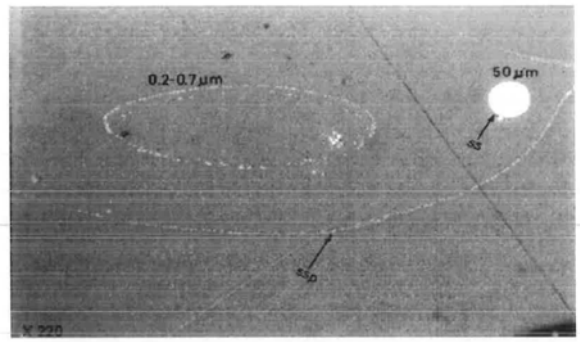

Figure 6: Large (50 µm) sulphide particles (ss) and sub-concentric submicron sulphide particles (ssp) (from Yassini, 1994)

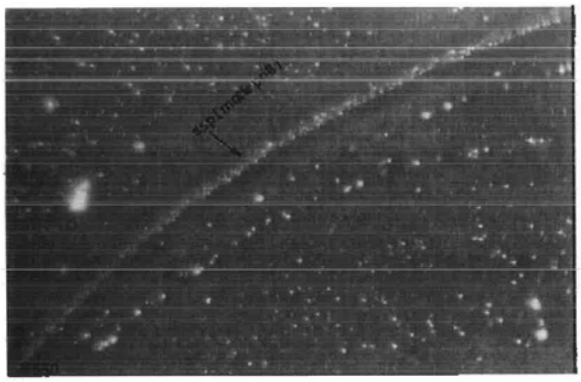

Figure 7: Quasi-continuous sulphide layers (ssp) and irregularly disseminated sulphide particles (from Yassini 1994).

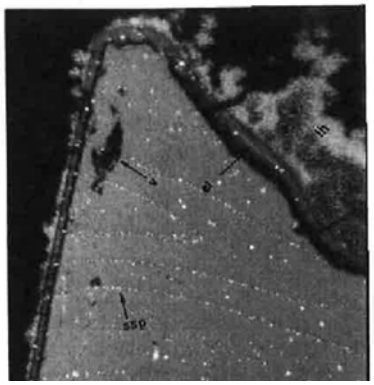

Figure 8: Sub-concentric and irregularly disseminated sulphide particles (from Yassini, 1994).

Fluctuations in groundwater level create an oxygen-rich zone within the slag emplacement subject to constant wetting and drying (vadose zone). Presence of oxygen as well as carbon allows two major biochemical reactions to take place in the slag:

- Vadose zone oxidation reaction (Starkey, 1945):
    - Caused by aerobic sulphur oxidising bacteria such as *Thiobacillus ferrooxidans* and *Thiobacillus thiooxidans*
    - Due to catalytic reactions of metalloenzymes produced by the bacteria, potentially increasing the rate of sulphur oxidation by up to 1000X
    - Sulphuric acid is a by-product of the reaction.
- Oxidation of iron sulphates to produce ferric sulphate (Reedy & Machin, 1923)
    - Faster rate of oxidation compared to vadose zone oxidative reaction
    - Also produces sulphuric acid

Sulphide oxidation is evident in the slag at Windang by the presence of a reddish brown precipitate of ferric hydroxide around the outer perimeter of the oxidised slag (Figure 9).

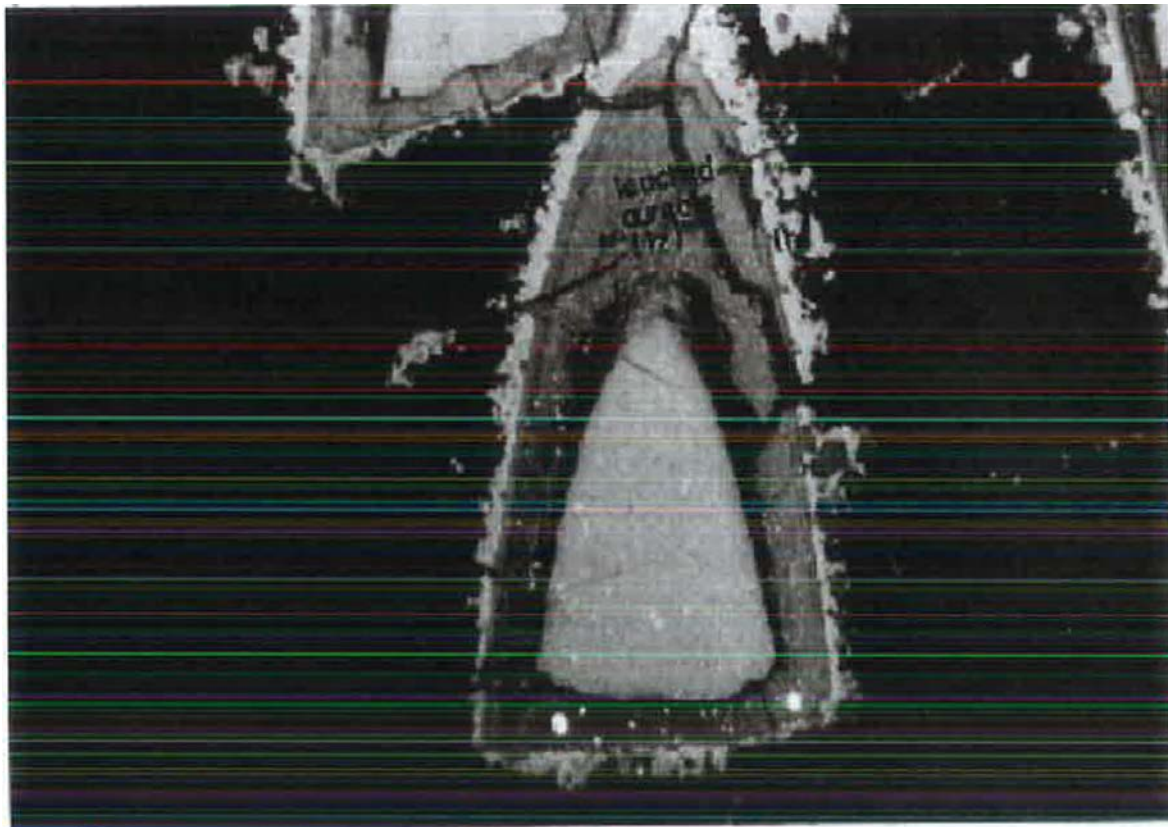

Figure 9: Iron hydroxide precipitate around the perimeter of the leached zone of an exfoliated weathered slag, view under reflected light (From Yassini, 1994)

The effect that this sulphuric acid has on leaching behaviour depends on the acid neutralising capabilities of the particular slag in question, as well as the presence and abundance of shell fragments in surrounding sand. Both the slag and shell fragments act as a buffer, preventing significant decreases in pH from the production of the sulphuric acid. However, the buffering effect of shelly fragments is somewhat limited to the groundwater surrounding the fragments. As the shelly fragments only occur in the estuarine sand layers, and not within the slag, the neutralizing effect of the fragments on leaching behaviour is limited (Pugh, 2002).

2.4. Heavy metal contaminant transport in groundwater

Previous reports (Coffey Partners Pty Ltd 1995; 1996) have used soil characteristics analysed in a laboratory to predict contaminant transport in the field at Windang. Results demonstrated that there is little advective transport of contaminants through groundwater movement, the main reason being the small hydraulic gradient present at the site. It was concluded from these studies that leached chemicals within the groundwater of the landfill site would take between 5 and 24 years to reach Lake Illawarra. However, these studies did not take into account less significant transport mechanisms such as the hydrodynamic dispersion coefficient. In the report by Pugh (2002), the significance of these less dominant transport mechanisms were explored.

A series of bores were installed at the Windang slag landfill site within a close proximity to the west and south-west of an existing bore, as the general direction of flow was determined previously through groundwater flow experiments in papers by Coffey Partners (1994, 1996). The purpose of this was to run an experiment involving the injection of a sodium chloride solution of known quantity and concentration into the existing bore and to then monitor the movement of the sodium chloride solution through the groundwater. This was done by regular sampling and testing of groundwater obtained from the new bores to see how long it would take for NaCl concentrations to rise, and by how much, as well as the time taken to achieve a stable concentration. The new bores were at varying depths in order to test the dispersion of sodium chloride vertically as well as horizontally within the groundwater. Using this method to test the rate and quantity of NaCl dispersion can help us infer how far and how fast slag leachate travels, and thus help to develop a conclusion as to whether some leachate may reach Lake Illawarra, and if so how long it would take. The findings concluded that transport of slag leachate containing heavy metals would only take 10 years to reach Lake Illawarra, and be at the same concentration as the source. However, it is important to consider that sodium chloride does not adsorb to clay-rich soil like heavy metals would, so it is unlikely that the mobility of heavy metals through the aquifer would be as high as sodium chloride.

2.4.1. Windang groundwater chemistry

The background groundwater chemistry at Windang was examined in the report by Yassini (1994) by analysing groundwater samples from wells east of the slag emplacement, seeing as groundwater flow has been determined to be in a west to southwest direction. The results concluded that background trace metal concentrations were generally very low. Conductivity measurements were also generally very low (100-400 µS/cm). The aquifer is in a reduced state, indicated by negative ORP values.

Conductivity of the groundwater within the Windang emplacement was generally higher than background levels, ranging from 155 to 855 µS/cm. ORP readings remained negative in most bores except those showing high concentrations of zinc (Yassini, 1994). Another report by Coffey Partners International Pty Ltd in 1994 found that zinc concentrations in groundwater peaked shortly after high rainfall events. This finding will form part of the basis of the groundwater analysis conducted in this study, with sampling rounds separated into two categories; sampling after significant rainfall and sampling during a dry spell. An explanation for this spike in zinc concentration levels, hypothesised by Pugh and Yassini (2002), was an increased rate of sulphide decomposition during dry weather resulting in a greater release of zinc to the surrounding hydroxide deposits. When water infiltrates the hydroxide deposits during rain, zinc is released into the groundwater, resulting in an increase in zinc concentration. After the rainfall ceases, the zinc disperses throughout the aquifer, and zinc concentrations fall.

The bores used by Yassini (1994) for testing down-gradient groundwater chemistry are relatively close to Lake Illawarra, with the freshwater lens extending to a depth of around 5 to 6m from the surface (Figure 10). The bores in this location were approximately 3 to 4m deep and assumed to be largely unaffected by the lake water. Conductivity readings were slightly higher (between 620 and 1000 µS/cm) in the down-gradient groundwater compared to the emplacement groundwater and up-gradient (background) groundwater levels.

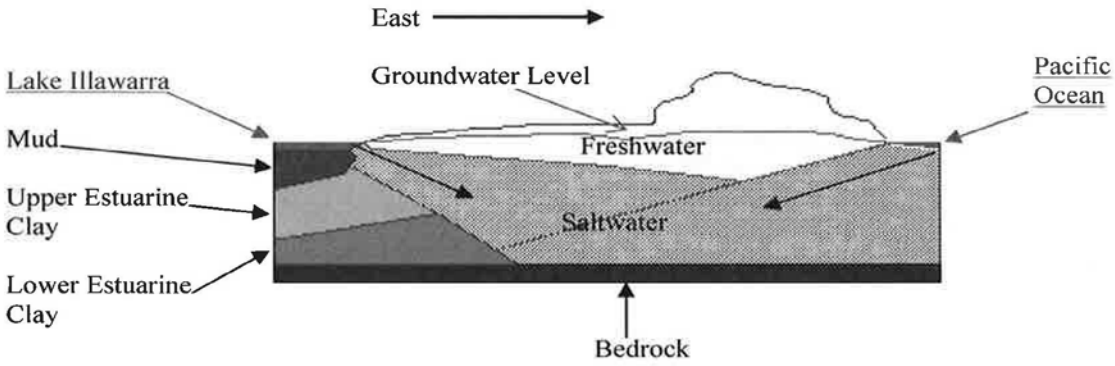

Figure 10: A diagram showing the approximate dimensions of the freshwater lens and partitioning of the groundwater at Windang (Pugh, 2002)

Heavy metal concentrations of manganese and copper in the down-gradient groundwater were slightly higher than background levels, possibly due to the transport of heavy metals from the slag emplacement groundwater. Other heavy metals showed no significant increase from background concentrations, with some metals showing a slight decrease.

2.4.2. Effect of groundwater and soil characteristics on heavy metal groundwater transport

The following studies conducted in various locations worldwide describe any apparent correlation between groundwater or soil characteristics and transport of heavy metals through aquifers. The study by Brown et al. (1999) looked at how transport behaviour differed between 3 zones of different pH, varying from acidic to neutral. The results show that in the transition zone where carbonate-mineral dissolution produces a rise in pH to around 5, metals such as zinc and nickel adsorb to an iron hydroxide precipitate. At pH of above 7.7, zinc hydrolyses and becomes more readily adsorbed to soil surfaces. However, in two other studies by McBride and Blasiak (1979) and Kuo and Baker (1980), an increase in zinc concentration in solution, and thus a decrease in zinc adsorbtion to soil, was noted when the pH was raised above 7.5. The explanation given by Kuo and Baker was the solubilisation of organic complexing ligands, which compete with zinc for adsorbtion sites on the soil surface.

McLean and Bledsoe (1992) discuss in their article the effect of retention capacity of soils in relation to contaminant transport through groundwater. The article claims that contaminant transport through groundwater should be minimal providing the retention capacity of the soil in question is not exceeded. The retention capacity of cations such as zinc has been correlated with soil characteristics such as pH, redox potential, surface area, cation exchange capacity, organic matter content, clay content, iron and manganese content and carbonate content. Methods of retention include adsorption and precipitation. Zinc is readily adsorbed at a higher pH by clay minerals, carbonates and

hydrous oxides, so acidic soils that are deficient in these components would be expected to have a greater extent of zinc transportation throughout the groundwater. Soils with Fe and Mn oxides were also found to have had the largest amount of zinc (Tessier et al., 1980). Zinc adsorbtion was lower in soils with an increased abundance of total organic carbon (TOC) and total soluble salts (TSS) (Boyle and Fuller, 1987).

Kurdi and Doner (1983) found that the adsorbtion of Zn to soil was inhibited completely by the presence of Cu at concentrations above 15 μg/L, however the opposite was true in another study by McBride and Blasiak (1979). The mechanism that prevented the adsorbtion of Zn in the first study was thought to most likely be competition between Cu and Zn for the limited number of adsorbtion sites available on the soil surface. However, the second study on a different site which resulted in increased Zn adsorbtion over Cu suggests that the adsorbtion of each metal may be site specific. Cavallaro (1982) found that phosphate at high concentrations also out-competed zinc for adsorbtion sites. However, other studies (Kuo and McNeal, 1984; Stanton and Burger, 1970; Bolland et al., 1977) found that lower concentrations of phosphate adsorbed on the oxide surface enhanced the adsorbion of zinc and other metal cations due to the increased negative charge on the oxide surface.

Chapter 3. Methods

3.1. Reactivation of existing piezometers

Existing bores from previous studies were located, reactivated and utilised for groundwater sample collection in this study (Figure 11 & Table 3). As the majority of these bores were originally installed for studies completed over 20 years ago and not utilised since, many of the caps were covered with a layer of topsoil or forest foliage, and not visible. The bores of interest that were not visible were tracked using Real Time Kinematics (RTK) satellite navigation, given the accurate coordinates found in the original studies. Bores were reactivated by "purging" the well of any sand, debris and stagnant water that may have accumulated over time due to inadequate capping and sealing. Purging was completed by withdrawing and discarding 6 to 8 well volumes worth of groundwater before any samples were collected. The well was also monitored during the withdrawal of water to establish a recharge rate and make sure water flow into the well appeared to be adequate in order to obtain a sample that was representative of the surrounding groundwater. In bores with water that was overly rich in Total Dissolved Solids (TDS) or sand, extra water was pumped from the well, until these parameters reduced. If these constituents remained in excess after the extra pumping, than the well was deemed to have a compromised textile, and avoided unless it was in a prime location. Luckily, all but one of the wells of interest were able to be successfully reactivated.

Bores that were reactivated, along with the study they were originally installed for are:

- BH12 - Coffey Partners International Pty Ltd, 1996
- BH2/BH9 - Coffey Partners International Pty Ltd, 1995

Figure 11: Map showing the location of the all bores sampled in this study

Table 3: Characteristics of each bore shown in Figure 11

Borehole	BH2	BH9	BH12	DR_NEW_EAST	DR_NEW_WEST
Depth (m)	4.03	3.28	8	8.2	9.08
Zone (MGA94)	56	56	56	56	56
Easting	304690.3	304873.545	304874.009	304785.785	304679.842
Northing	6177684	6177985.573	6177986.581	6178002.049	6178115.594
Elevation (MASL)	1.816	2.879	2.835	2.88	2.121

There were plans to utilise a bore (WCC-1) installed by Southern Copper Pty Ltd (1992) located around 200m north-west of BH2, however due to lack of a proper cap, a number of small rocks had been jammed down the bore, deeming any reactivation efforts impossible. This was unfortunate, as WCC-1 was of great interest to us, being one of the remaining bores located closest to the lake, and thus would have provided useful insight into risk of contamination of Lake Illawarra. However, this disadvantage was somewhat offset by the installation of the new DR_NEW_WEST bore, which measures around the same straight line distance to the lake (approx. 130m, measured using Google Earth).

3.2. Installation of new piezometers

Two new monitoring wells were installed (Figure 12) in order to get a better representation of the westward migration of heavy metals from the slag leachate. As contaminant transport at depth was of interest, the bores drilled were slotted in order to target the aquifer at between 8 and 9m depth. Wireline rotary sonic was used to drill the holes, with bentonite drilling muds used to stabilise the hole during drilling, and ensure sand was being adequately displaced from the hole (Longhurst, 2015).

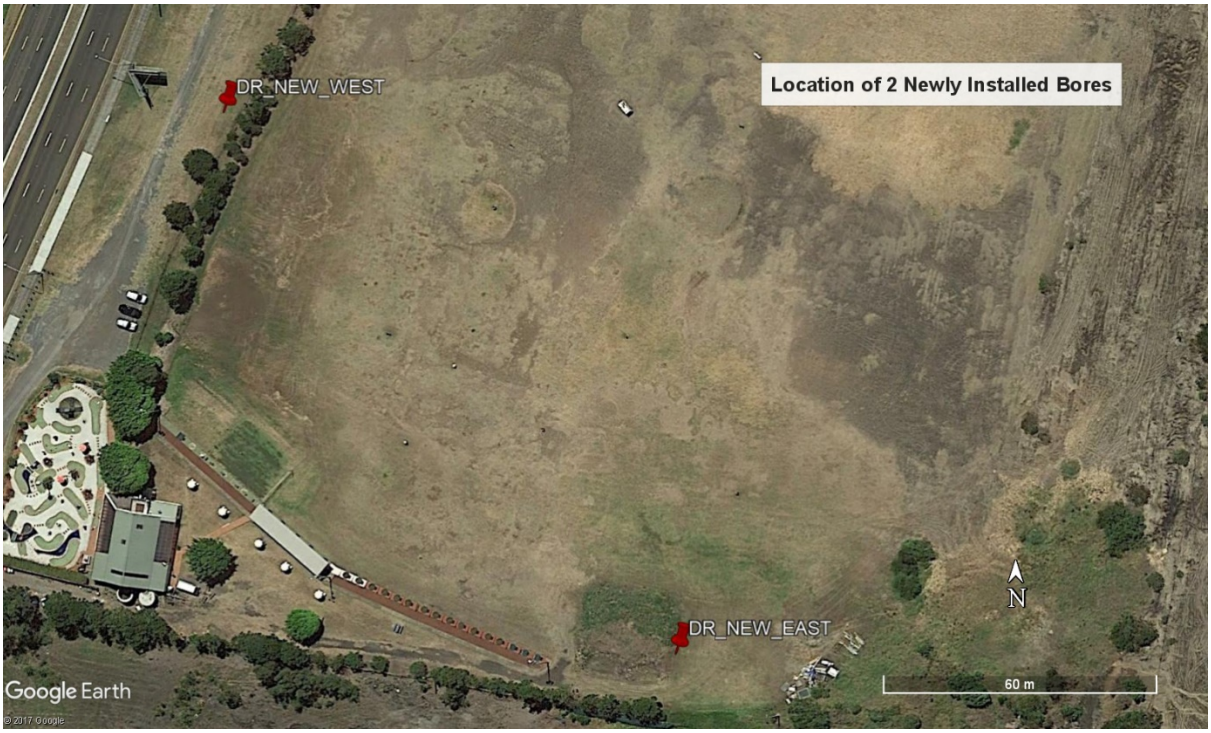

Figure 12: Map showing the location of the 2 new bores drilled specifically for this project, DR_NEW_EAST and DR_NEW_WEST

Permission was granted by both the council and the owner of Illawarra Golf Complex, John Hufton, to proceed with the installation of the new piezometers. Dial Before You Dig was used to obtain maps of the underground infrastructure in the area, and ensure the installation did not risk damaging any of these assets. A diagram of a piezometer similar to the ones installed at Windang is shown in Figure 13. The piezometer was constructed with 50mm PVC class 12 piping. Lengths of PVC were joined together using PVC solvent cement and a coupler attachment to make up the required length. Slots were cut at the bottom 0.5m to 1.5m of the PVC pipe, and a filter textile sock was fitted to prevent the ingress of sand into the piezometer. Once the drilling was complete, the piezometer was inserted into the drill hole. Small stones were poured around the piezometer to fill up around 2m from the bottom. This was to prevent collapsing sand from higher up the drill hole from collecting around the textile sock, theoretically enhancing the flow rate of the well. The space above the small stones around the piezometer was filled with material that was extracted during drilling. A lockable cap was then

positioned on top of the piezometer, flush with the ground. Quick set concrete was then mixed and poured around the cap to secure it in place. A smaller PVC cap was placed on top of the piezometer to seal the well from rainwater ingress in the event of flooding.

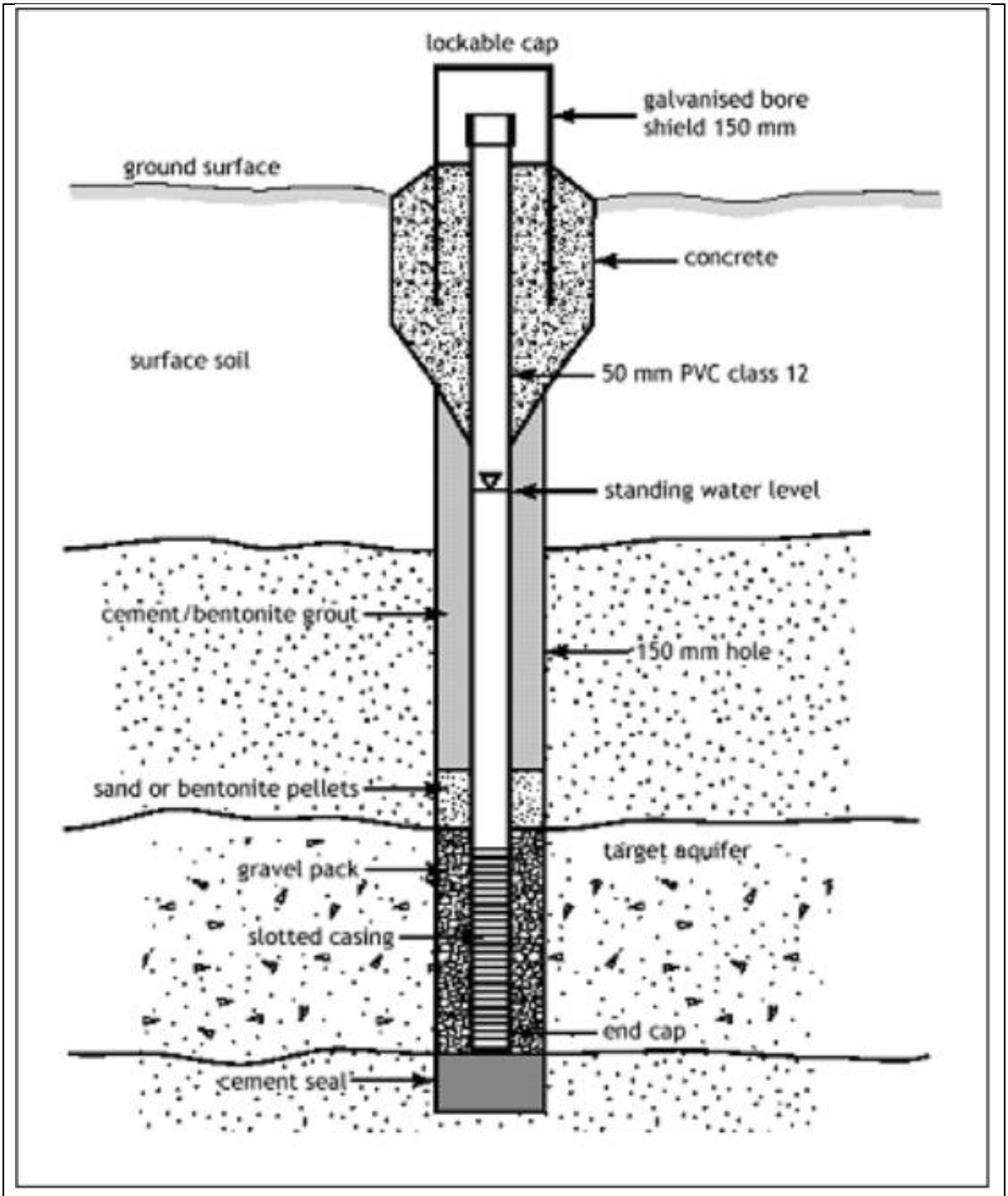

Figure 13: Diagram showing the features and layout of a Piezometer, with a similar method of construction used for the newly installed Windang bores (Longhurst, 2015)

The wells were then purged of any residual bentonite in the surrounding groundwater, as well as any sand or debris that may have fallen into the well during installation. Purging was completed using the same method as the reactivated wells, however pumping was extended to a 15 minute duration, due to the larger volume of contamination from the bentonite muds dissipated throughout the groundwater. Note that any residual bentonite that may have remained in the groundwater samples would not have an effect on the data values obtained, rather it just made field filtering difficult due to the rapid clogging of the filter pores.

3.2.1. Core collection and logging

Core samples were collected using sonic pre-coring. Three cores were collected from the DR_NEW_EAST drill hole only. The first two cores were obtained from 0.1m to 3.1m depth, and the third core from 7.7m to 9.2m depth. Cores from 3.1m to 7.7m depth were not obtained because the material was largely the same throughout this range (marine sand), however the bottom core was obtained due to a suspected presence of shelly fragments, which turned out to be confirmed upon core collection. This was of significance because the presence of calcium carbonate fragments affects the buffering characteristics of the soil.

3.3. Soil sampling and analysis

Two pits were dug within the slag emplacement (Figures 14 to 16, Table 4) in order to observe the relationship between depth and degree of slag weathering. The pit also allowed us to obtain solid samples from each different weathering layer for further analysis.

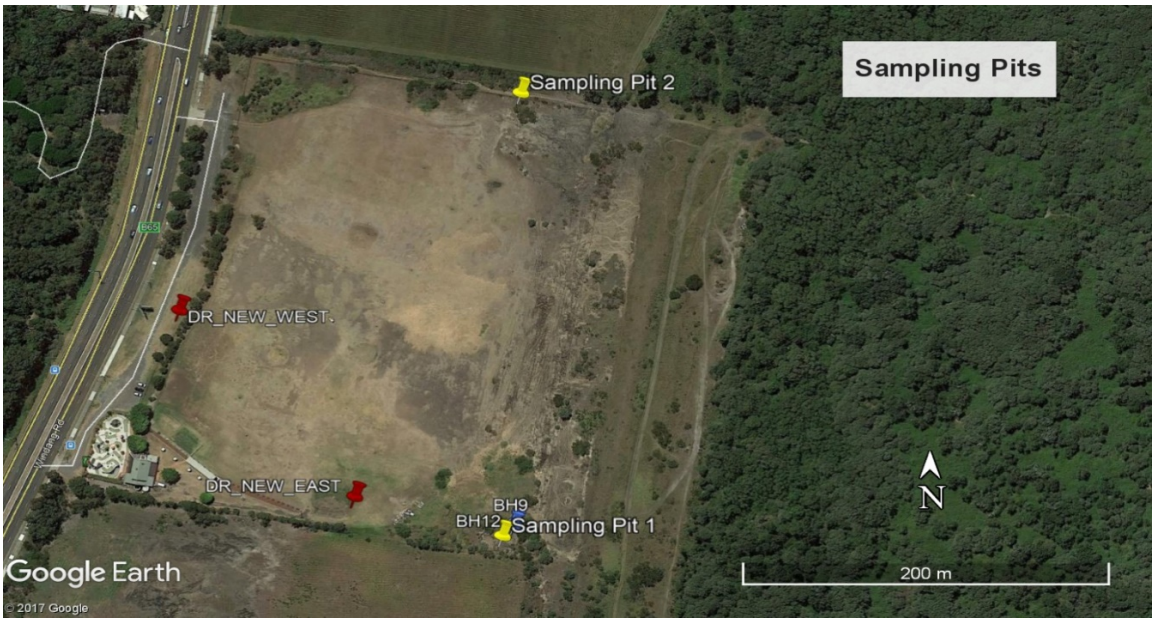

Figure 14: Location of sampling pit (b) (Figure 15) and sampling pit (c) (Figure 16) which were dug in order to collect slag samples from layers with variable levels of weathering. Descriptions of each pit are displayed in Table 4

Table 4: Location, depth, and elevation of sampling pits (b) and (c)

	Pit (b) (Figure 15)	Pit (c) (Figure 16)
Approx. depth (m)	1.55m	1.8m
Zone (MGA94)	56	56
Easting	304866.383	304871.402
Northing	6177978.231	6178260.174
Elevation (masl)	2.776	2.493

Figure 15: Pit (b)

Figure 16: Pit (c)

3.3.1. Acid Neutralization Capacity/Acid Generation Capacity

Analysis of the Acid Neutralization Capacity of the weathered and unweathered slag was completed by ALS environmental Wollongong, by submitting about 30g of solid sample in a sample bag. Net acidity was reported in moles H^+/tonne, which was converted to kg of sulfuric acid per tonne.

3.3.2. Grain size analysis

Grain size was performed on slag obtained from various depths. Each sample was weighed prior to analysis. The sample was then poured into a stack of sieves starting from the largest particle size sieve

at the top and smaller particle size sieve at the bottom. The stack of sieves was then sealed and clamped down to a sieve shaker, which agitated the stack of sieves in order to speed up the process of particle size sorting. After 5 minutes, the sieve shaker was turned off, and the stack of sieves removed. The particles caught in each sieve were weighed. What was left at the bottom catch pan was considered as fines, and further sorted using the Malvern Mastersizer 2000.

3.3.3. XRF

Soil samples from within the slag fill area were obtained from sampling pit (b) to be analysed for trace elements by XRF. Samples were first ground up to a fine powder using the TEMA. The fine powder was then mixed with a PVA binding agent, and the mixture was placed into an aluminium holder. The sample was then compressed using a hydraulic press in order to form a pellet, and placed in an oven at 70°C for at least 2 hours to cure prior to XRF analysis.

XRF data collected by Brian Jones in early 2017 (Figure 17) was also utilised in this report in order to determine average background metal concentrations and average emplacement metal concentrations based on data collected from various locations within each zone (Appendix 5).

Figure 17: Locations of sampled analysed by XRF (Jones, 2017)

3.3.4. Optical properties

A small range of the samples obtained from the pit were made into polished blocks in order to be able to observe the optical properties of the slag, and compare the slag structure between weathered and unweathered samples. The following code names were assigned to the polished blocks, accompanied by descriptions on the origin and status of the slag samples:

- MA – Unweathered, newer slag, 0.45m depth
- MB – Weathered Slag, 0.9m depth
- MC – Unweathered, older slag, 1.55m depth
- MD – Heavily Weathered Slag from the eastern side of Windang Road

All samples were examined by reflected light microscopy at magnifications of 40X, 100X, 200X and 500X. Solomon Buckman, a senior lecturer from the School of Earth and Environmental Science at the University of Wollongong, assisted with observations of the polished blocks. The polished blocks were observed predominantly using plane polarised light (PPL). Cross polarised light (XPL) was used when verification of optical properties was needed to determine foreign species.

Due to time constraints, only the least weathered sample (MA) and the most weathered sample (MD) underwent elemental analysis and visual examination under the scanning electron microscope (SEM).This was in order to simulate the largest potential differences between the most weathered and least weathered samples that exist in the Windang copper slag emplacement. In preparation for use in the Scanning Electron Microscope, the entire surface of the polished blocks were imaged in high resolution so that areas of interest could be marked out on a printed version of the image. The elemental analysis was performed by Energy Dispersive Spectroscopy (EDS) on a JEOL JSM-6490LV scanning electron microscope with an Oxford Instruments X-max^{N} 80mm SDD EDS system. Acquisition was performed using the Oxford Aztec software suite at 15kV and 30kV, where higher voltages were used for the definitive identification of lead.

3.4. Groundwater sampling, analysis and monitoring

3.4.1. Monitoring of groundwater levels

In order to collect continuous data for groundwater level fluctuations at Windang, Two HOBO U20 Water Level Data Loggers were anchored to the piezometer caps, and then placed down around 0.5 to 1 metre below the water level. This was to allow for any variation (lowering) of the water table over time, and ensure the data logger was underwater at all times; a vital condition for accurate readings. One data logger was located in BH9 for the entirety of the data collection period (8/4/17 to 10/9/17), and the other was located in BH2 for the first period (8/4/17 to 7/7/17) and DR_NEW_WEST for the second period (14/7/17 to 10/9/17). Data obtained was plotted as pressure (kPa) over time, and

ground water level measurements during sample events were used as baseline data points from which the pressure variation could be converted to a height variation in metres, since the pressure and water level change are correlated in a 1:1 relationship.

3.4.2. Groundwater sampling and analysis

A total of 4 sampling rounds were completed from 31st March 2017 to 7th July 2017, alternating wet and dry conditions. The wet sampling round occurred within 48 hours after a significant rainfall event (greater than 15mm). This was followed by a dry sampling round which occurred at least 7 days after last rainfall. Unfortunately, the two new bores, DR_NEW_EAST and DR_NEW_WEST were only sampled during the last two rounds (one wet and one dry), as they were not installed whilst the first two sampling rounds were being undertaken.

Groundwater samples were withdrawn from the piezometers using a petrol powered impeller pump. At each sampling event, at least one well volume, usually in the order of 50 litres was discarded in order to eliminate any stagnant water that may have been sitting in the well, and get a sample that was representative of the target aquifer. A 9L bucket was then filled with extracted groundwater, and the probe from the YEO-KAL 615 water quality analyser was submerged in the water. The analyser provided readings such as pH, electrical conductivity, ORP, dissolved oxygen, salinity, turbidity and total dissolved solids, which were recorded once readings stabilised.

All samples for trace metal analysis were field filtered using a pre-filter (25µm) followed by a 0.45µm syringe filter. The container for collecting trace metal samples was preserved with nitric acid to reduce bacterial activity. All samples for major ion analysis were not field filtered, and were collected in a non-preserved, sterile bottle. All samples were stored in an esky with ice immediately after collection while out in the field to reduce bacterial activity. Samples were then dropped off at the Wollongong Australian Laboratory Services (ALS) office. Throughout the analysis, one Laboratory Duplicate (DUP), Method Blank (MB), Matrix Spike (MS), and Laboratory Control Spike (LCS) were run as a part of the quality control procedures in place. The resulting quality control reports all returned acceptable results.

Chapter 4. Results

4.1. Core/pit analysis

The tables below describe the stratigraphy observed at borehole DR_NEW_EAST (a) (Table 5), sampling pit (b) (Table 6), and sampling pit (c) (Table 7). Depth refers the distance below the surface in metres. The degree of slag weathering was based solely on visual observation, with 1 being least weathered and 5 being the most weathered.

Table 5: Description of the drill core obtained during the installation of the DR_NEW_EAST bore (a)

Depth (m)	Description	Grain Size	Degree of Weathering
0.1-0.39	Clay rich soil, some organic matter	Mud to VF	N/A
0.39-0.58	Clay rich soil, some fine grained slag intermixed with organic matter	VF to Fine	1-2
0.58-0.65	Light grey slag	Fine	1-2
0.65-0.67	Light grey slag	Very Fine	1-2
0.67-0.69	Heavily Oxidised Brown slag	Med	4
0.69-0.77	Grey Slag	Med	1-2
0.77-1.26	Dark Grey Slag	Med	2
1.26-1.6	Grey slag	Coarse to VC	1-2
1.6-1.78	Dark grey slag intermixed with clay	Fine	1-2
1.78-1.89	Light Grey Slag	Med to Coarse	2
1.89-2.17	Grey slag intermixed with clay	Mud to Med	2
2.17-2.21	Slag	Coarse	2
2.21-2.26	Heavily oxidised brown slag	Fine	4
2.26-2.31	Greenish clay (Weathered Cu?) intermixed with slag	Mud to Med	2
2.31-9	Sand	VF to Fine	N/A
9-9.2	Sand with shells	VF to Fine	N/A

Table 6: Description of the stratigraphy observed from the excavation of Pit (b)

Depth (m)	Description	Grain Size	Degree of Weathering
0-0.36	Clay rich soil, some organic matter	Mud to VF	N/A
0.36-0.56	Clay rich soil, some fine grained slag intermixed with organic matter	VF to Fine	2
0.56-0.7	Sand	VF to Fine	1-2
0.7-0.8	Intermixed weathered and unweathered slag	Fine	1-4
0.8-0.9	Heavily Oxidised Brown slag	Med	3-4
0.9-1	Intermixed weathered and unweathered slag	Fine	1-4
1-1.25	Heavily Oxidised Brown slag	Med	3-4
1.25-1.5	Intermixed weathered and unweathered slag	Fine to Med	1-4
1.5-1.55	Unweathered Slag	Fine to Med	1-2

Table 7: Description of the stratigraphy observed from the excavation of Pit (c)

Depth (m)	Description	Grain Size	Degree of Weathering
0-0.1	Top Sand	VF to Fine	N/A
0.1-0.25	Coal Wash	VF	N/A
0.25-0.35	Sand	VF to Fine	N/A
0.35-0.55	Oxidised, dark brown slag	Med	2-3
0.55-0.8	Unoxidised, dark grey slag intermixed with clay	Med	1-2
0.8-0.95	Heavily oxidised, brown slag	Fine to Med	3-4
0.95-1.8	Unoxidised, dark grey slag	Med	1-2

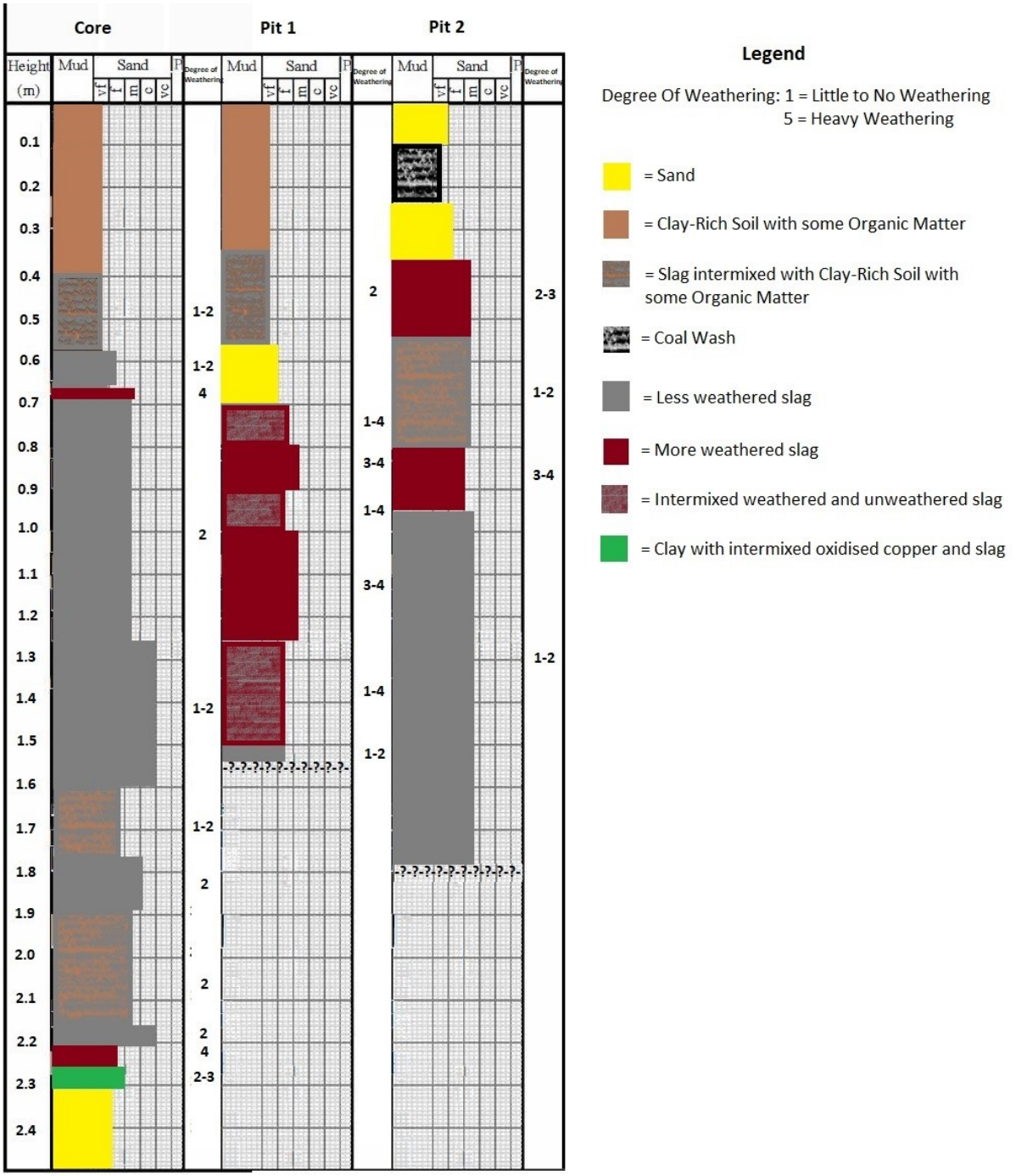

Figure 18: Comparison of the stratigraphy between the 3 subsurface analyses conducted

4.2. Groundwater analysis and monitoring

4.2.1. Dissolved metals

All the results for heavy metal concentrations are in mg/L. The results were compared to guidelines found in the ANZECC & ARMCANZ document "Australian and New Zealand Guidelines for Fresh and Marine Water Quality" (2000). As there were no specific guidelines applicable to groundwater, the guidelines used were long-term trigger values (LTV) and short-term trigger values (STV) for heavy metals and metalloids in irrigation water. The reasoning for using these guidelines are as follows:

- A number of properties within the housing estate on and just to the south of the slag emplacement utilise the groundwater for the irrigation of plants and veggie patches.
- If the concentration of trace metals in the groundwater within the emplacement is low enough to be deemed safe for irrigation of "crops", than it is reasonable to say that trace metals in groundwater originating from the emplacement pose little to no threat to nearby Lake Illawarra, regardless of the extent of metal transport through the aquifer.

Long-term trigger values outline the maximum concentrations acceptable in water used for irrigation up to 100 years, while short-term trigger values define use up to 20 years. Readings that breach the LTV are highlighted in orange, and readings exceeding the STV are highlighted in red. Note that in some cases the metal concentrations in the groundwater (iron in particular) exceeded the ANZECC LTV, but were still lower than background metal concentrations. These breaches were ignored, as the excessive amount of the metal in the groundwater is not as a result of leachate from the slag.

Table 8 refers to the average background concentrations of heavy metals in the Windang aquifer, as determined through sampling by Yassini (1994) of bores located up-gradient from the slag emplacement.

Table 8: Background metal concentrations in the groundwater at Windang (Yassini, 1994)

Arsenic (mg/L)	0.01
Cadmium (mg/L)	0.005
Copper (mg/L)	0.0085
Manganese (mg/L)	0.054
Nickel (mg/L)	0.005
Lead (mg/L)	0.01
Selenium (mg/L)	0.01
Zinc (mg/L)	0.1
Iron (mg/L)	1.2525

4.2.1.1. Sampling Event 1 – 31/03/2017 (after rainfall):

As the first round of sampling was only for preliminary testing purposes, only bores BH2 and BH9 were sampled, and water quality parameters such as pH and conductivity were not measured, as access to the YEO-KAL water quality tester was not yet arranged. The sampling event occurred immediately after 27mm of rainfall received 24 hours prior to collection. The previous 2 weeks were also notably wet, with a total of 250mm received over the 14 days, of which 151mm was received within a 24 hour period on 17th March 2017 (Source: BOM). All trace metal concentrations were generally around or below background levels. An exception was Zinc BH9, which exceeded the LTV defined by ANZECC (2000), and came within 0.5mg/L of the STV.

Table 9: Trace Metals Sampling Round After Rainfall, 31/03/2017

Cells shaded in orange contain readings that exceed the long-term trigger value (LTV) for irrigation water, as outlined in the ANZECC (2000) guidelines

Cells shaded in green contain readings that are equal to or below background concentrations, as defined by Yassini (1994)

Bore I.D.	**BH2**	**BH9**	**ANZECC (2000) LTV**	**ANZECC (2000) STV**
Arsenic (mg/L)	0.014	0.002	0.1	2
Cadmium (mg/L)	0.0001	0.0001	0.01	0.05
Copper (mg/L)	0.002	0.002	0.2	5
Manganese (mg/L)	0.038	0.067	0.2	10
Nickel (mg/L)	0.01	0.133	0.2	2
Lead (mg/L)	0.001	0.001	2	5
Selenium (mg/L)	0.01	0.01	0.02	0.05
Zinc (mg/L)	0.042	4.69	2	5
Iron (mg/L)	0.18	0.91	0.2	10

4.2.1.2. Sampling Event 2 – 17/05/2017 (after dry spell):

The second round of sampling took place during a dry spell lasting around 2 weeks, however during the month preceding the measurement, only 3mm of rain was received during a single 24 hour period on the 4th May 2017. A deeper bore (BH12) was included in the sampling rounds from here onwards, as the close proximity to BH9 allowed a direct comparison on the vertical mobility of the trace metal concentrations. The groundwater from the deeper bore contained lower concentrations of Zinc. In BH9, the zinc concentration exceeded the ANZECC (2000) STV. ORP readings were also highest in BH9, and slightly negative in BH2 and BH12. All samples had a pH close to neutral. Electrical conductivity and salinity were highest in BH2, followed by BH9.

Table 10: Trace Metals Sampling Round After a Dry Spell, 17/05/2017

Cells shaded in red contain readings that exceed the short-term trigger value (STV) in irrigation water, as outlined in the ANZECC (2000) guidelines

Cells shaded in green contain readings that are equal to or below background concentrations, as defined by Yassini (1994)

Bore I.D.	BH2	BH9	BH12	ANZECC (2000) LTV	ANZECC (2000) STV
Arsenic (mg/L)	0.002	0.002	0.001	0.1	2
Cadmium (mg/L)	0.0001	0.0001	0.0001	0.01	0.05
Copper (mg/L)	0.001	0.003	0.001	0.2	5
Manganese (mg/L)	0.05	0.097	0.02	0.2	10
Nickel (mg/L)	0.004	0.17	0.003	0.2	2
Lead (mg/L)	0.001	0.001	0.01	2	5
Selenium (mg/L)	0.01	0.01	0.01	0.02	0.05
Zinc (mg/L)	0.038	5.46	0.1	2	5
Iron (mg/L)	0.5	1.12	0.13	0.2	10
Turbidity (NTU)	24.4	3.75	299		
D.O. (% Sat)	58	147	54		
D.O. (mg/L)	5.01	12.25	4.76		
pH	6.8	7.23	6.9		
ORP (mV)	-32	176	-30		
Salinity (ppt)	0.32	0.24	0.14		
TDS (g/L)	0.4	0.3	0.2		
E.C. (µS/cm)	650	492	284		
E.C. (mS/cm)	0.65	0.49	0.28		

4.2.1.3. Sampling Event 3 – 09/06/2017 (after rainfall):

Sampling event 3 took place after 35mm of rainfall which was received in the preceding 48 hours prior to sampling on the 9th June 2017. Newly installed bores, DR_NEW_EAST and DR_NEW_WEST were included in sampling rounds from this event onwards. The purpose of sampling these bores was to

establish trends on westward migration of trace metals from the slag emplacement, and to also run analyses on major cations and anions present in the groundwater to determine similarity of sources. The pH readings from the two new bores are slightly elevated due to residual soda ash used in the bentonite drilling muds.

Heavy metal concentrations in groundwater from both new bores were generally as low or lower than concentrations found in groundwater from BH12 from both this sampling round and the last sampling round. Generally, the concentration of most metals were on par or lower than background levels except for zinc in BH9, which exceeded the STV by a small margin. ORP values were highest in BH9, DR_NEW_EAST and DR_NEW_WEST. Electrical conductivity and salinity were similar across all samples.

Table 11: Trace Metals Sampling Round After Rainfall, 09/06/2017

Cells shaded in red contain readings that exceed the short-term trigger value (STV) in irrigation water, as outlined in the ANZECC (2000) guidelines

Cells shaded in green contain readings that are equal to or below background concentrations, as defined by Yassini (1994)

Bore I.D.	BH2	BH9	BH12	DR_NEW_EAST	DR_NEW_WEST	ANZECC (2000) LTV	ANZECC (2000) STV
Arsenic (mg/L)	0.019	0.002	0.001	0.002	0.003	0.1	2
Cadmium (mg/L)	0.0001	0.0001	0.0001	0.0001	0.0001	0.01	0.05
Copper (mg/L)	0.009	0.002	0.001	0.002	0.005	0.2	5
Manganese (mg/L)	0.037	0.078	0.023	0.018	0.023	0.2	10
Nickel (mg/L)	0.009	0.162	0.002	0.003	0.001	0.2	2
Lead (mg/L)	0.001	0.001	0.006	0.001	0.001	2	5
Selenium (mg/L)	0.01	0.01	0.01	0.01	0.01	0.02	0.05
Zinc (mg/L)	0.044	5.28	0.1	0.051	0.064	2	5
Iron (mg/L)	0.21	1.24	0.05	0.05	0.09	0.2	10
Turbidity (NTU)	6.7	14.5	108	77.9	111		
D.O. (% Sat)	85.2	42.7	45.6	14.4	90.9		
D.O. (mg/L)	7.7	3.83	4.13	1.24	8.1		
pH	6.95	6.9	6.89	8.28	8.11		
ORP (mV)	6	158	-18	210	275		
Salinity (ppt)	0.26	0.23	0.14	0.2	0.22		
TDS (g/L)	0.3	0.3	0.2	0.3	0.3		
E.C. (µS/cm)	548	481	304	422	464		
E.C. (mS/cm)	0.53	0.46	0.27	0.41	0.45		

4.2.1.4. Sampling Event 4 – 07/07/2017 (after dry spell)

Sampling event took place on the 7th July 2017, after a dry spell lasting around a month (disregarding a few days of very light shower activity, adding up to no more than 1mm overall). The pH of the groundwater obtained from the two new bores was closer to neutral this sampling round, indicating the dispersion of the drilling fluids throughout the surrounding groundwater.

Most metal concentrations were near or below background levels, with the exception of zinc in BH9, which exceeded the ANZECC (2000) LTV. ORP was again highest in BH9, DR_NEW_EAST and DR_NEW_WEST. Salinity and electrical conductivity in BH2 was nearly double as high as the other bores.

Table 12: Trace Metals Sampling Round After a Dry Spell, 07/07/2017

Cells shaded in orange contain readings that exceed the long-term trigger value (LTV) for irrigation water, as outlined in the ANZECC (2000) guidelines

Cells shaded in green contain readings that are equal to or below background concentrations, as defined by Yassini (1994)

Bore I.D.	**BH2**	**BH9**	**BH12**	**DR_NEW_ EAST**	**DR_NEW_ WEST**	**ANZECC (2000) LTV**	**ANZECC (2000) STV**
Arsenic (mg/L)	0.002	0.002	0.001	0.001	0.003	0.1	2
Cadmium (mg/L)	0.0001	0.0001	0.0001	0.0001	0.0001	0.01	0.05
Copper (mg/L)	0.001	0.007	0.001	0.001	0.004	0.2	5
Manganese (mg/L)	0.071	0.066	0.021	0.041	0.057	0.2	10
Nickel (mg/L)	0.006	0.13	0.001	0.001	0.001	0.2	2
Lead (mg/L)	0.001	0.001	0.001	0.001	0.001	2	5
Selenium (mg/L)	0.01	0.01	0.01	0.01	0.01	0.02	0.05
Zinc (mg/L)	0.019	4.88	0.013	0.014	0.01	2	5
Iron (mg/L)	0.62	0.72	0.05	0.1	0.24	0.2	10
Turbidity (NTU)	8.4	5	2.5	1.1	4		
D.O. (% Sat)	6.97	45.8	42.8	23.6	34.9		
D.O. (mg/L)	6.27	4.09	3.85	2.11	3.12		
pH	6.3	6.59	6.5	7.61	7.48		
ORP (mV)	3	207	-54	171	211		
Salinity (ppt)	0.42	0.23	0.16	0.23	0.23		
TDS (g/L)	0.5	0.3	0.2	0.3	0.3		
E.C. (µS/cm)	870	485	343	472	511		
E.C. (mS/cm)	0.84	0.46	0.31	0.42	0.46		

4.2.2. Difference in heavy metal concentrations between "dry" sampling events and "wet" sampling events

Table 13 shows the difference in metal concentrations between "dry" sampling events and "wet" sampling events. There is a wide spread of results obtained, which make it hard to determine any significant trends relating rainfall and groundwater concentration. In relation to zinc, four out of the five bores contained higher zinc concentrations after rainfall.

Table 13: Differences in metal concentrations between "dry" sampling rounds and "wet" sampling rounds

Yellow = No Change Red = Increased concentration after wet Green = Increased concentration during dry					
Differences between Wet vs Dry	**BH2**	**BH9**	**BH12**	**DR_NEW_EAST**	**DR_NEW_WEST**
Arsenic (mg/L)	0.0145	0	0	0.001	0
Cadmium (mg/L)	0	0	0	0	0
Copper (mg/L)	0.0045	-0.003	0	0.001	0.001
Manganese (mg/L)	-0.023	-0.009	0.0025	-0.023	-0.034
Nickel (mg/L)	0.0045	-0.0025	0	0.002	0
Lead (mg/L)	0	0	0.0005	0	0
Selenium (mg/L)	0	0	0	0	0
Zinc (mg/L)	0.0145	-0.185	0.0435	0.037	0.054
Iron (mg/L)	-0.365	0.155	-0.04	-0.05	-0.15

4.2.3. Metal concentration vs bore depth

The scatterplots shown in Figure 19 below display the relationship between metal concentration and depth of the bore from which the groundwater was obtained. A weak correlation (R^2 = 0.0539) of decreasing zinc concentration with increasing bore depth exists. One consideration to add regarding this analysis is that results may not be totally representative of the relationship between metal concentration and bore depth, as a lot of the data from the deeper bores was from studies conducted over 20 years ago when concentrations were significantly higher in all bores. This means realistically the correlation between zinc concentration and bore depth could be a lot stronger than what is displayed in Figure 19 if sampling occurred all at one time, however in that case conclusions would be insignificant due to the small number of bores sampled, as well as the poor range of depths (either 3-4m or 8-9m depth, no bores at 5-6m).

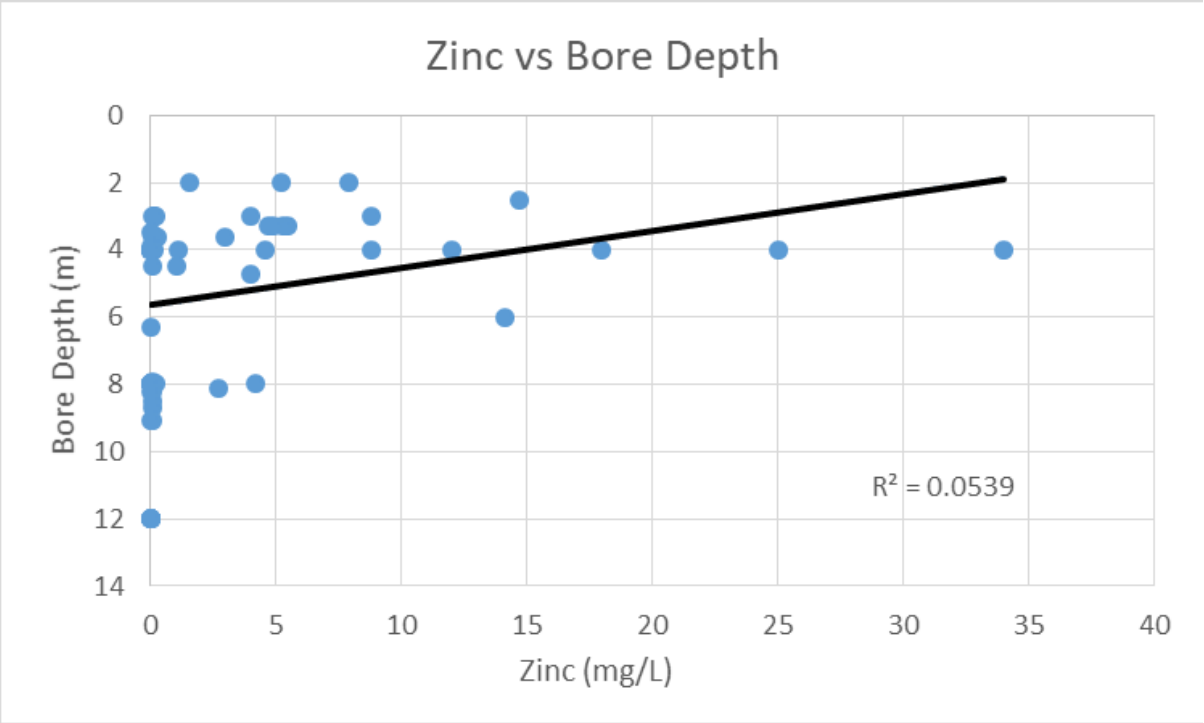

Figure 19: Zinc concentration vs depth of bore from which the groundwater was obtained, based on data from studies conducted between 1992 and 2017 (Appendix 2)

4.2.4. Changes in heavy metal concentrations over time

The following results show changes in groundwater concentrations over time using data collected in previous studies as well as this study (Appendix 1 and 2). The trendline type was chosen based on the highest R^2 value, indicating the most suitable fit. It is important that too much weighting is not placed on these trends, as the relatively small sample size (around 6 to 8 sampling rounds between 1994 and 2017) as well as the lack of even temporal distribution between sampling events means that trends developed from this data are generally weak, and can be misleading if the results from some sampling rounds happened to be compromised.

4.2.4.1. Zinc

The zinc concentration in BH9 has reduced over time from values significantly higher than the ANZECC (2000) STV down to readings slightly above or on par with the guideline (Figures 20 & 21). Based on the trend established in Figure 20, the rate of decrease of zinc in groundwater should continue into the future, and perhaps stabilise at a concentration slightly below the ANZECC LTV. The same trend is apparent in BH12 (Figure 21), with values dropping from up to 2 times above the ANZECC LTV in 1994 (Yassini) down to background levels in 2017. Zinc concentrations in BH2 (Figure 22) increased slightly over time from 1994 to 2017, however the significance of this trend is questionable, as all recorded concentrations were so close to background levels that small changes like this may be caused by other factors, and not specifically from increased weathering of the slag.

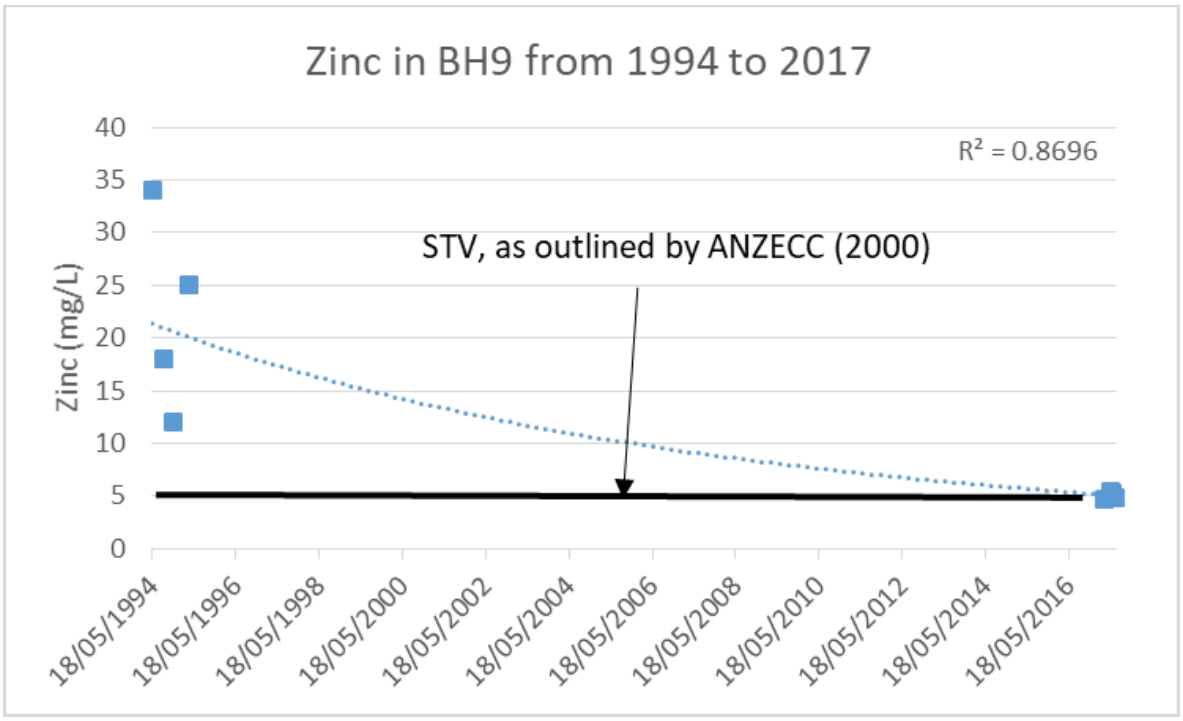

Figure 20: Changes in zinc concentration in BH9 from 1994 to 2017

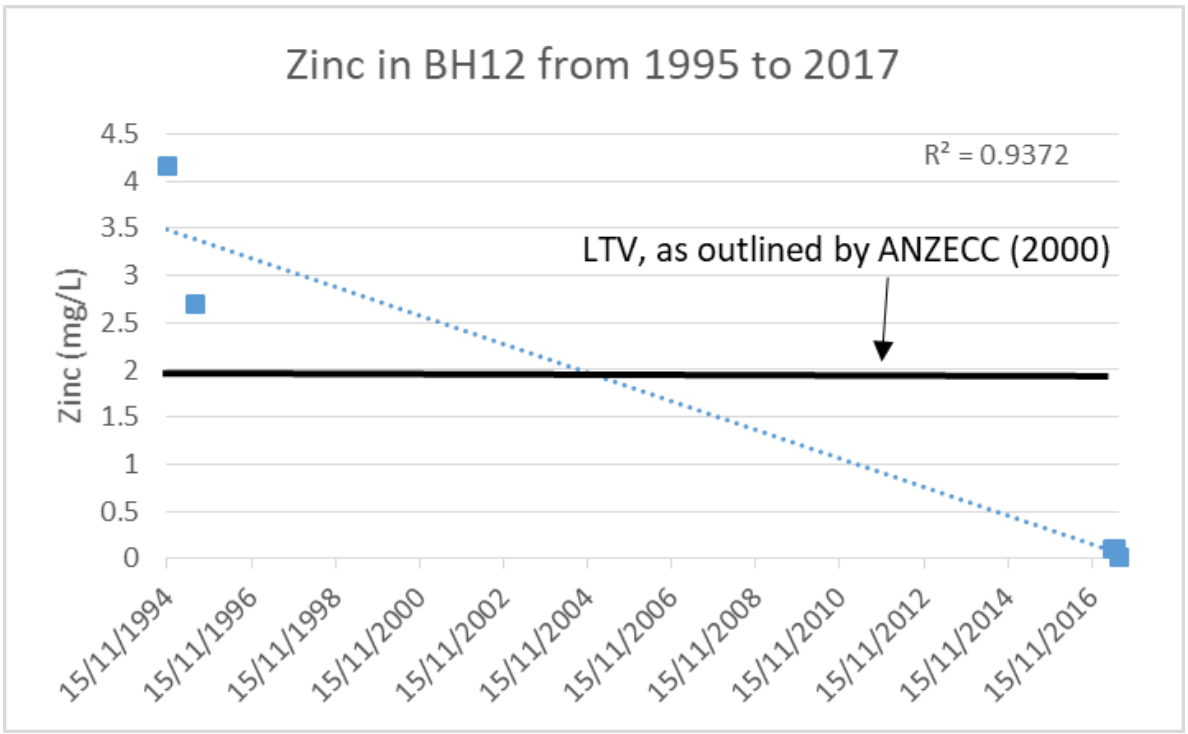

Figure 21: Changes in zinc concentration in BH12 from 1995 to 2017

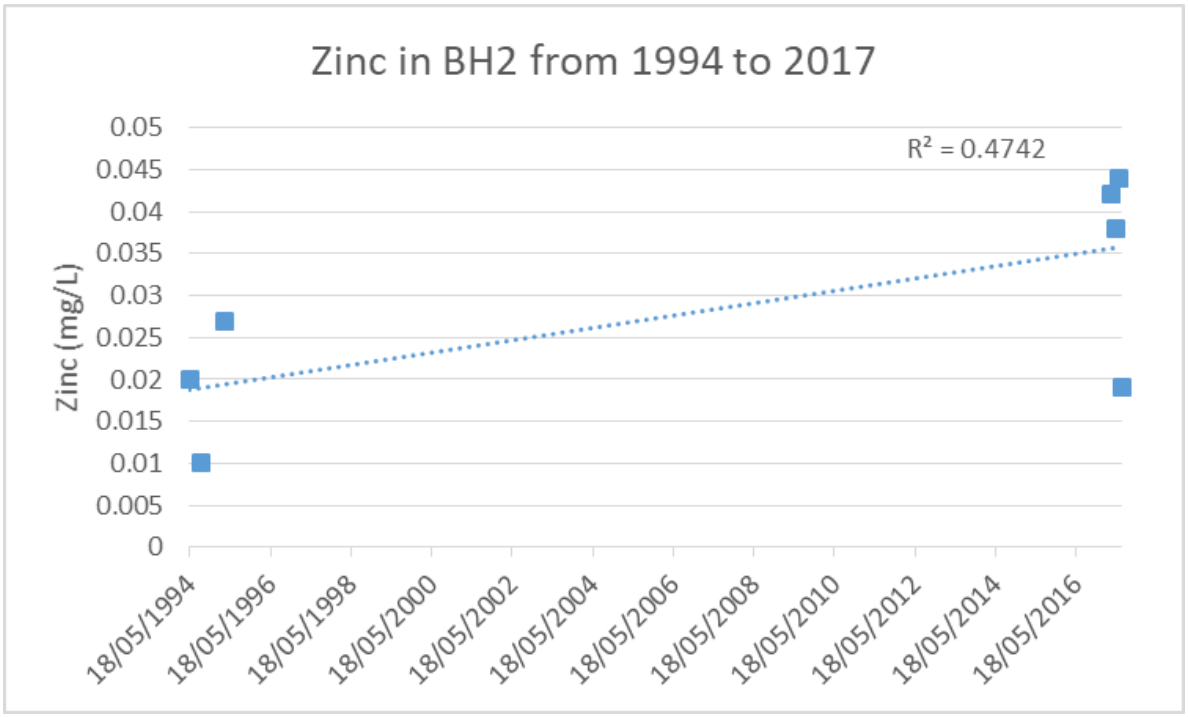

Figure 22: Changes in zinc concentration in BH2 from 1994 to 2017

4.2.4.2. Iron

The iron concentration has, in contrast to the zinc concentration, increased over time in BH9 and BH2 (Figures 23 and 24). However it must be noted that although values obtained in 2017 are above the ANZECC (2000) LTV, they are still equal to or lower than background values obtained for the Windang area by Yassini (1994). Iron content dropped to around 1% of the initial reading in BH12 from 1994 to 2017 (Figure 25), down to concentrations far below background levels for the Windang region (Yassini, 1994).

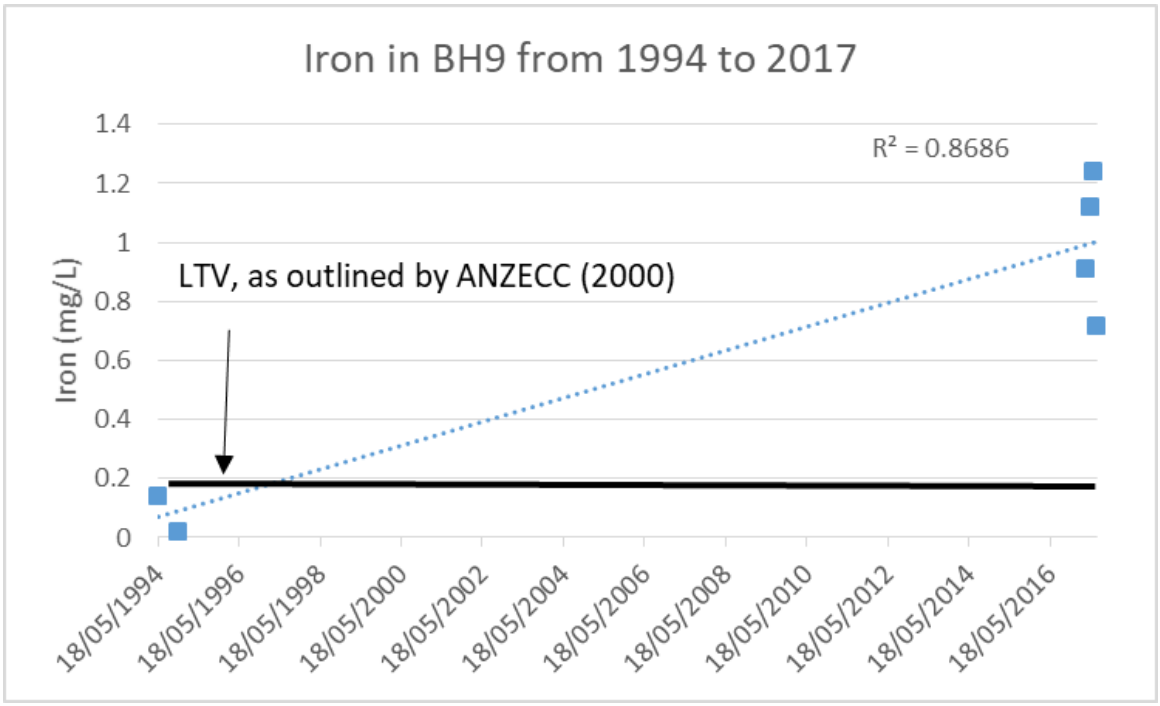

Figure 23: Changes in iron concentration in BH9 from 1994 to 2017

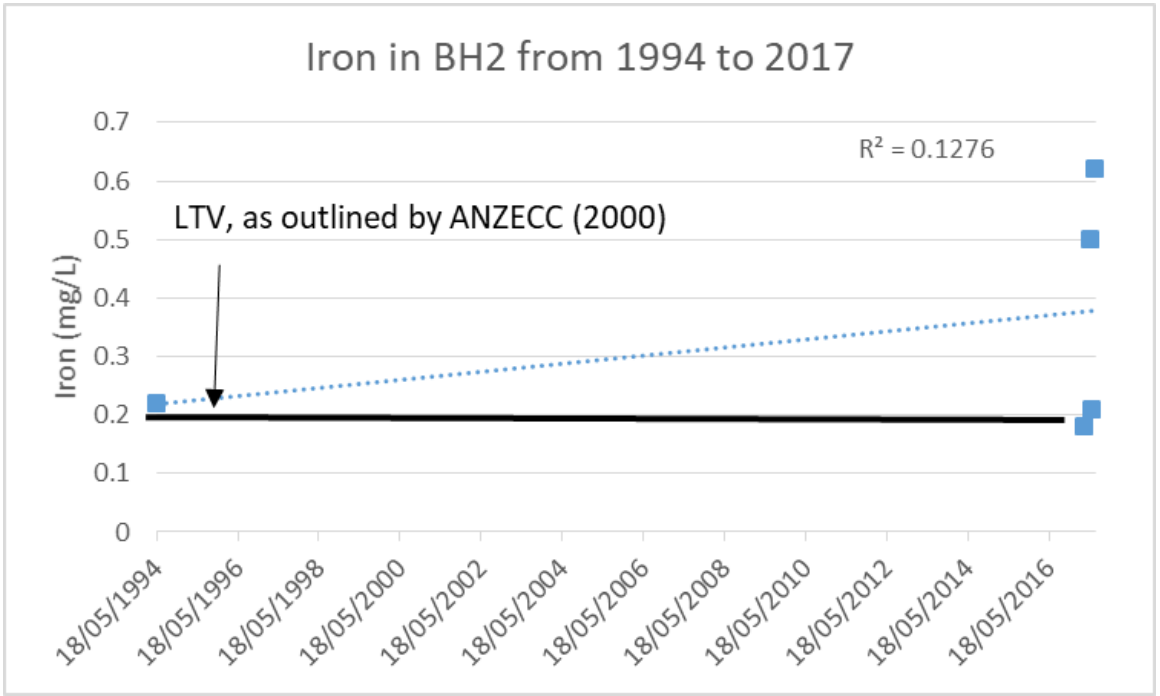

Figure 24: Changes in iron concentration in BH2 from 1994 to 2017

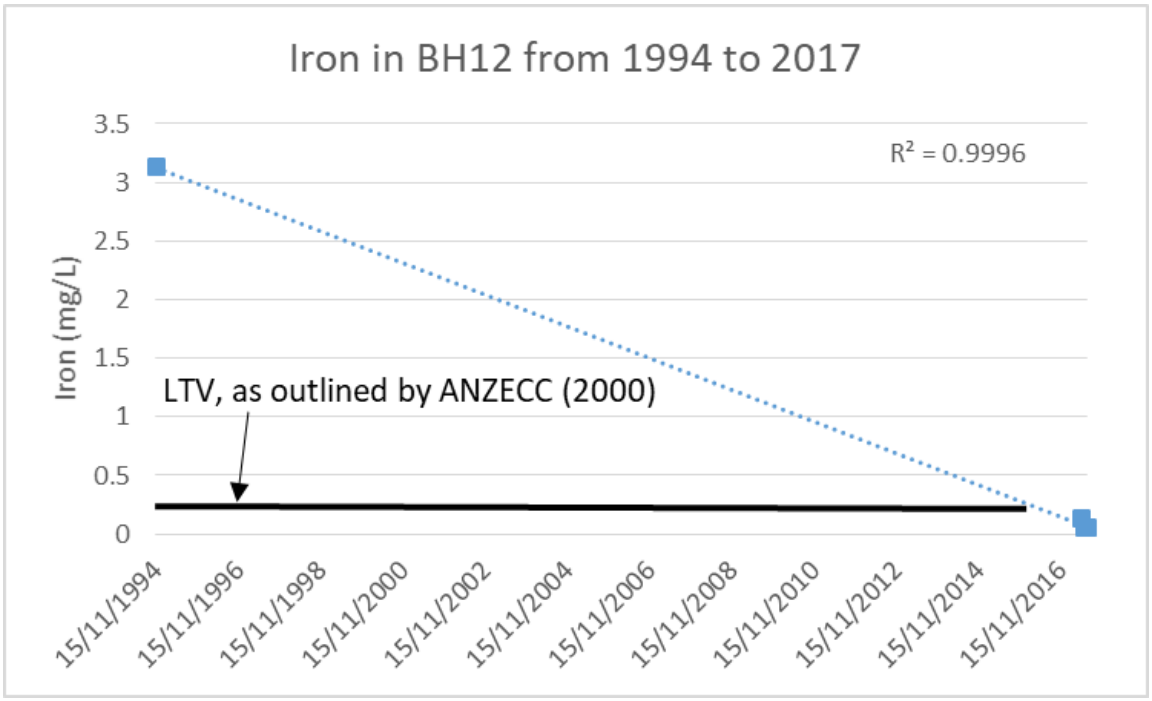

Figure 25: Changes in iron concentration in BH12 from 1994 to 2017

As groundwater from BH9 contained trace metal concentrations significantly above background levels in the past, it provided a good opportunity to develop trends of some of the less abundant trace metals over time. Although the concentration of the following less significant trace metals are below ANZECC (2000) guidelines at the moment, developing a trend based on data from the past 23 years can help predict if concentrations may reach a level in the future where action would be required. The metals shown in Figures 26 to 31 follow a trend similar to zinc, i.e. showing a decrease in concentration over time.

4.2.4.3. Copper

Concentrations of copper reported in papers from the mid 1990's in BH9 varied, from levels slightly below the ANZECC LTV, to one sample with a concentration almost twice the guideline (Figure 26), however concentrations have decreased overall over time. In BH2 and BH12 (Figures 27 and 28), concentrations were consistently under 0.1mg/L, and have trended down further over time.

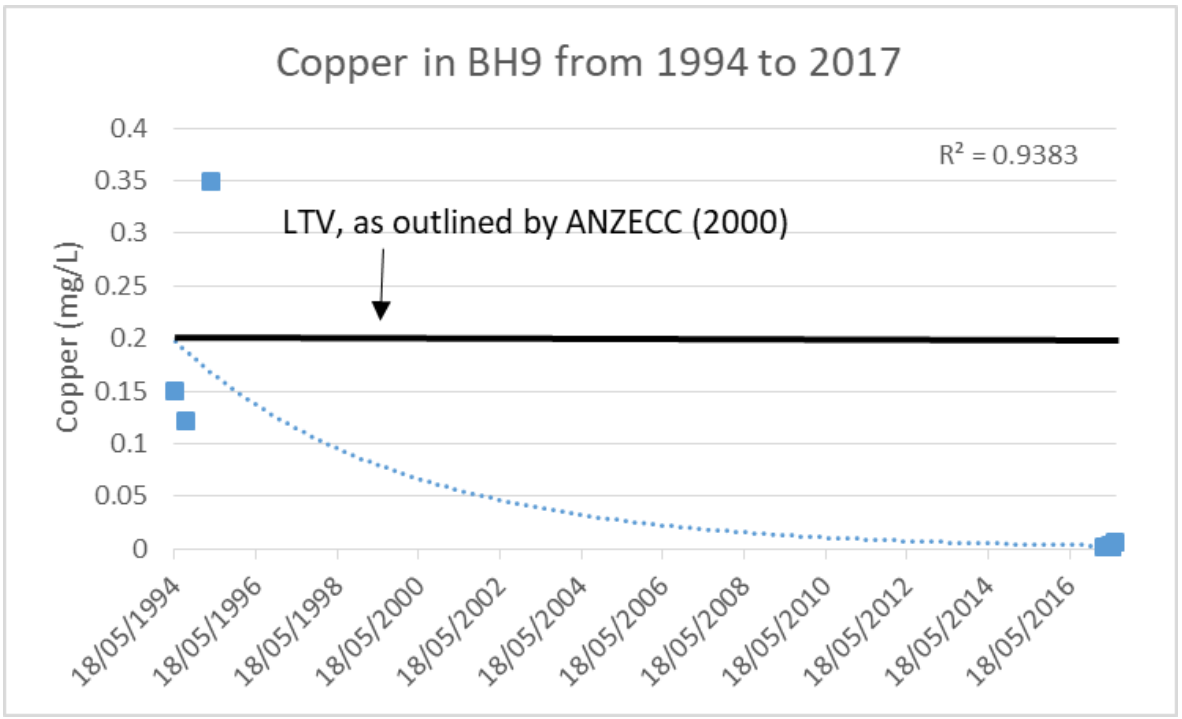

Figure 26: Changes in copper concentration in BH9 from 1994 to 2017

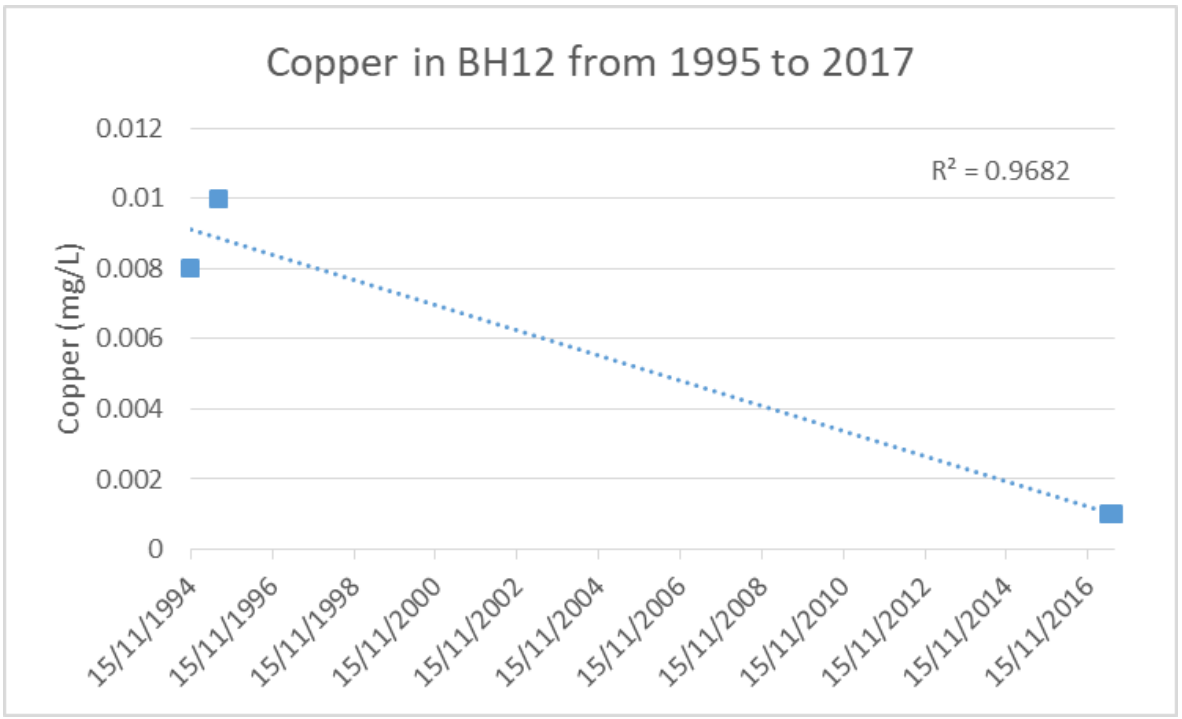

Figure 27: Changes in copper concentration in BH12 from 1995 to 2017

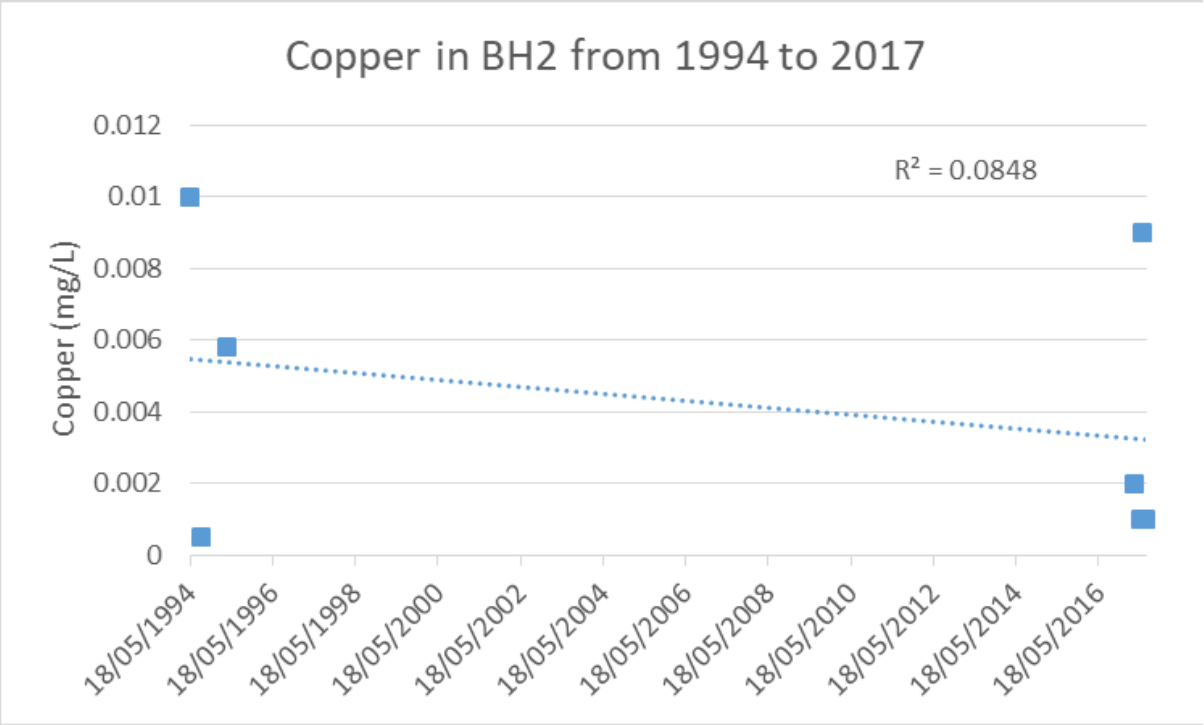

Figure 28: Changes in copper concentration in BH2 from 1994 to 2017

4.2.4.4. Cadmium

Concentrations of cadmium reported in papers from the mid 1990's contained levels up to 8X above the ANZECC LTV guidelines (Figure 29). This reduced in the sampling rounds conducted in this study, down to approximate background levels (Yassini, 1994). Unless an anomaly to this trend develops in the future due to altered weathering or mobilization of the remaining cadmium in the slag, it seems the metal will likely not be a major issue into the future.

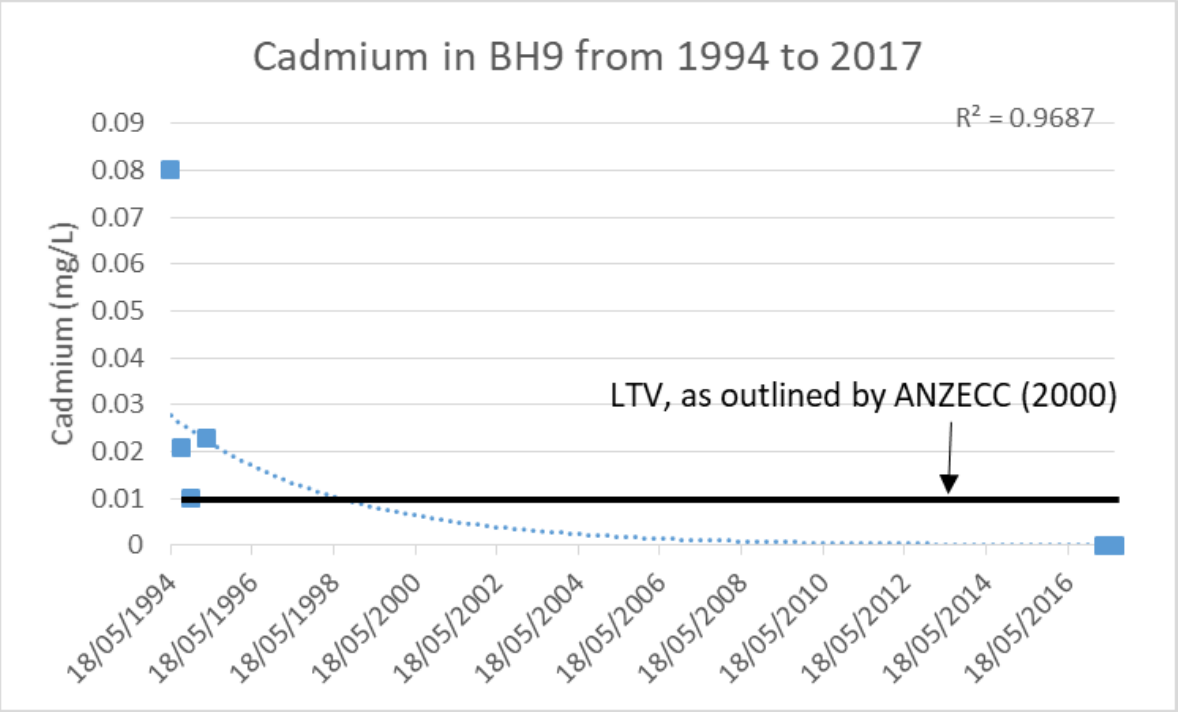

Figure 29: Changes in cadmium concentration in BH9 from 1994 to 2017

4.2.4.5. Lead

All concentrations of Lead reported in BH9 and BH2 (Figures 30 and 31) have been well below both the STV (5mg/L) and LTV (2mg/L) outlined by ANZECC (2000). The change between 1994 and 2017 also highlights a decrease in concentration over time, similar to copper and cadmium. Therefore seeing as concentrations were very low in the first place, and concentrations are trending down, it is likely that lead also does not pose a threat to the Windang aquifer and nearby Lake Illawarra.

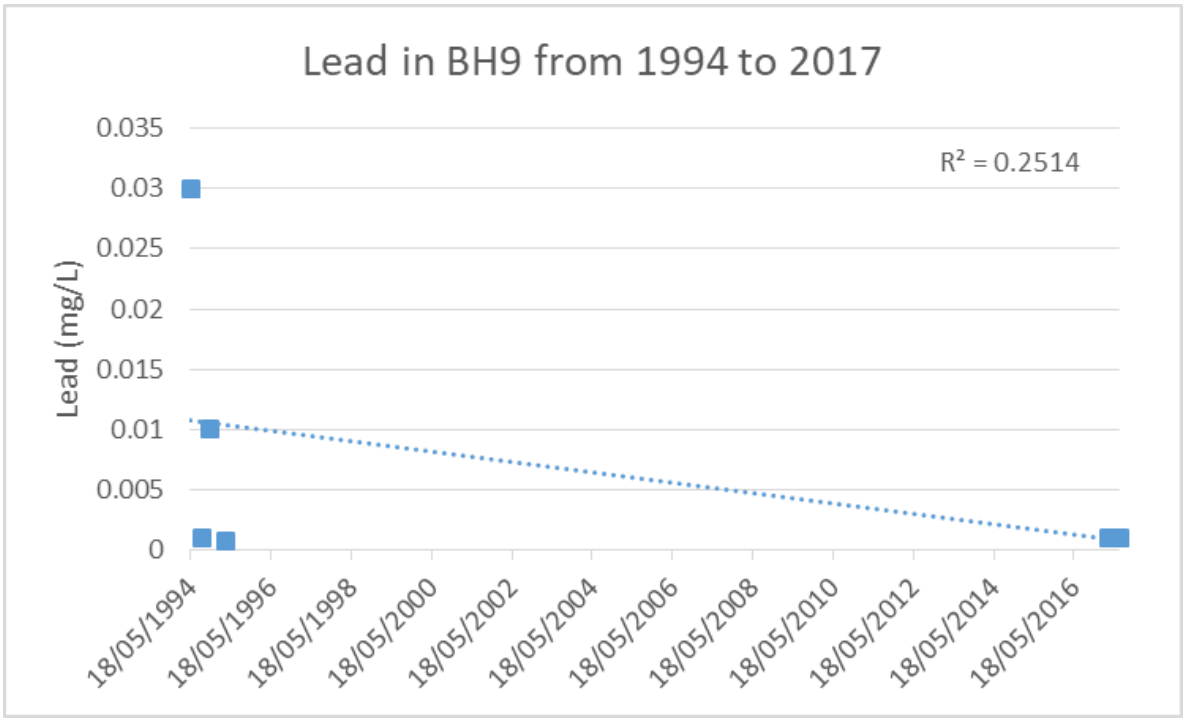

Figure 30: Changes in lead concentration in BH9 from 1994 to 2017

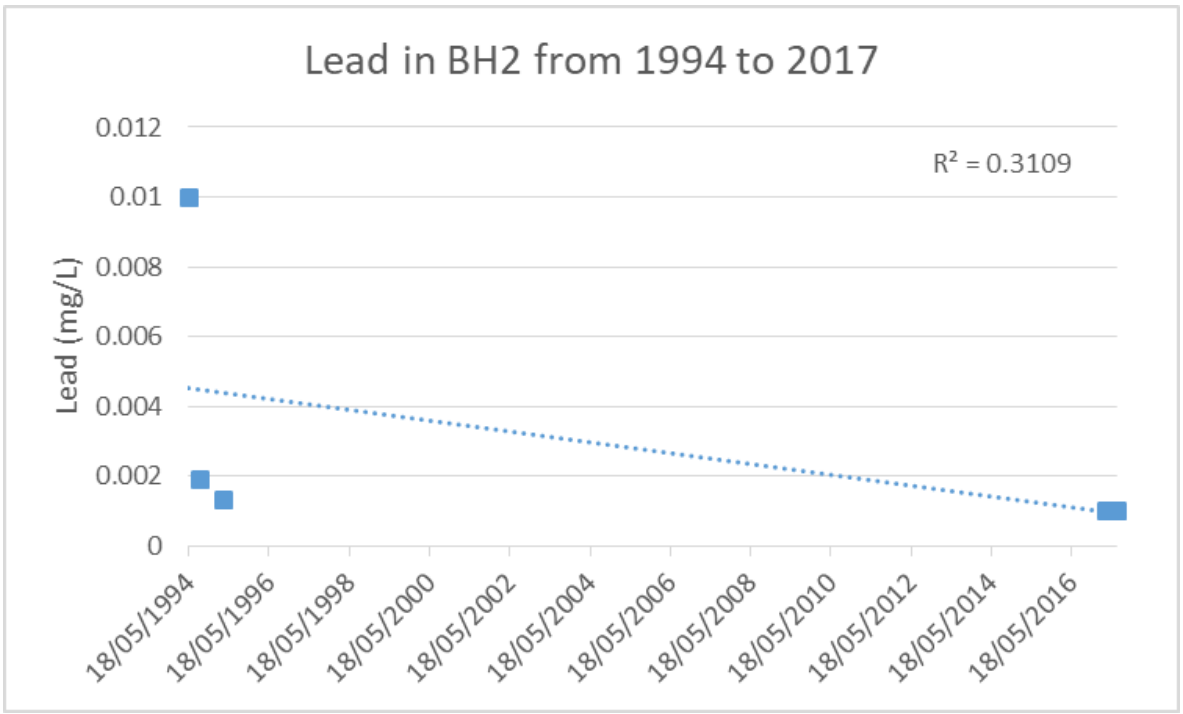

Figure 31: Changes in lead concentration in BH2 from 1994 to 2017

As only around half of the sampling rounds in all past reports on the Windang aquifer contain analyses of arsenic, manganese, nickel and selenium concentrations, there is significantly less data to work with in terms of developing a trend over time. Due to this, scatterplots with trendlines were not produced for these metals, as any trends formed from less than 2 previous sampling rounds would be considered

inconclusive. In addition to this, and perhaps the reason these metals were not analysed, was that most papers reported values for these metals significantly below the ANZECC guidelines, and near background levels. However, a written description of some changes over time have been noted below.

4.2.4.6. Arsenic

In addition to the small amount of data available for arsenic, the concentrations reported have all been either close to, or equal to the LOR (limit of reporting), and as the samples have been analysed over a 23 year time period, it is quite possible that LOR levels have decreased over time due to advancements in analysis technology. Therefore, older samples may have contained much lower concentrations of arsenic than what was reported in the papers. Nevertheless taking that factor into consideration, a reduction in arsenic concentration was experienced in BH2, BH9 and BH12, down to levels considered background for the Windang area (Yassini, 1994). As far as results in other bores not sampled in this study, there were no results in past papers with an arsenic concentration higher than 0.01mg/L, which is still 10 times less than the ANZECC (2000) LTV of 0.1mg/L. Therefore arsenic concentration in the Windang aquifer from copper slag leachate is low enough not to be considered a threat to nearby Lake Illawarra at present, and that is unlikely to change into the future.

4.2.4.7. Manganese

Manganese concentrations in BH2 appeared to have reduced over time, however once again due to higher LOR values in the earlier paper (Coffey, 1995) this trend is hard to confirm. Manganese concentrations in BH9 and BH12 were not analysed prior to the report by Yassini (1994). In both these bores, manganese concentrations increased marginally from 1994 to 2017, however even the highest values obtained were lower than the highest background concentration obtained by Yassini (1994). Out of all the past samples analysed from the bores at Windang, only two returned manganese concentrations higher than the ANZECC (2000) LTV of 0.2mg/L, with the highest value 0.5mg/L reported in the report by Coffey in 1994. Even when considering this breach, the 2 samples were still well below the ANZECC STV of 10mg/L. Considering the relatively low concentrations of manganese across the board, and especially in recent reports, the metal is unlikely to pose a threat to nearby Lake Illawarra, despite the slight increase in concentration between 1994 and 2017 in BH9 and BH12. In addition, manganese concentrations within the Windang aquifer shouldn't be a cause for concern, however long-term monitoring may be in order.

4.2.4.8. Nickel

Nickel concentrations in all 3 bores have reduced over time, by a factor of 3 in BH9, and a factor of 20 in BH2 and BH12. There was only one sample out of all the past reports on the Windang aquifer which was slightly higher than the ANZECC (2000) LTV of 0.2mg/L, reported by Yassini in 1994. Current concentrations of nickel are at near background levels in both BH2 and BH12, but slightly higher in

BH9 (approx. 0.15mg/L), however still consistently below ANZECC guidelines. Given current concentrations and the observed trend over time, it is unlikely that nickel in the Windang aquifer will pose a threat to nearby Lake Illawarra into the future.

4.2.4.9. Selenium

There is a very limited amount of data for selenium in the Windang aquifer groundwater, however all values obtained for all bores are equal to the LOR of 0.01mg/L, which also equate to the background values obtained for Windang aquifer by Yassini (1994).

4.2.5. Major anions and cations

The proportions of major anions and cations in the groundwater are displayed below in Figure 32 as a piper diagram, and Figure 33 and 34 as stiff diagrams. The ternary diagrams in Figure 32 display the relative abundance of cations and anions in separate graphs, while the stiff diagrams show abundance of cations to the left of the centrefold axis, and the abundance of anions to the right of the axis. Raw data is presented in Appendix 1b.

The three deeper bores BH12, DR_NEW_EAST and DR_NEW_WEST all have similar proportions of anions as indicated by the stiff diagrams (Figures 33 and 34). These bores appear to have higher concentrations of bicarbonate compared to the two shallower bores, most likely due to the presence of shelly fragments which were observed in core 3 at around 9m depth. BH2 had a significantly different composition compared to BH9 considering they are both at a similar depth, however due to the distance between them, this may indicate a different source of groundwater. The lake water was significantly different in composition compared to all groundwater.

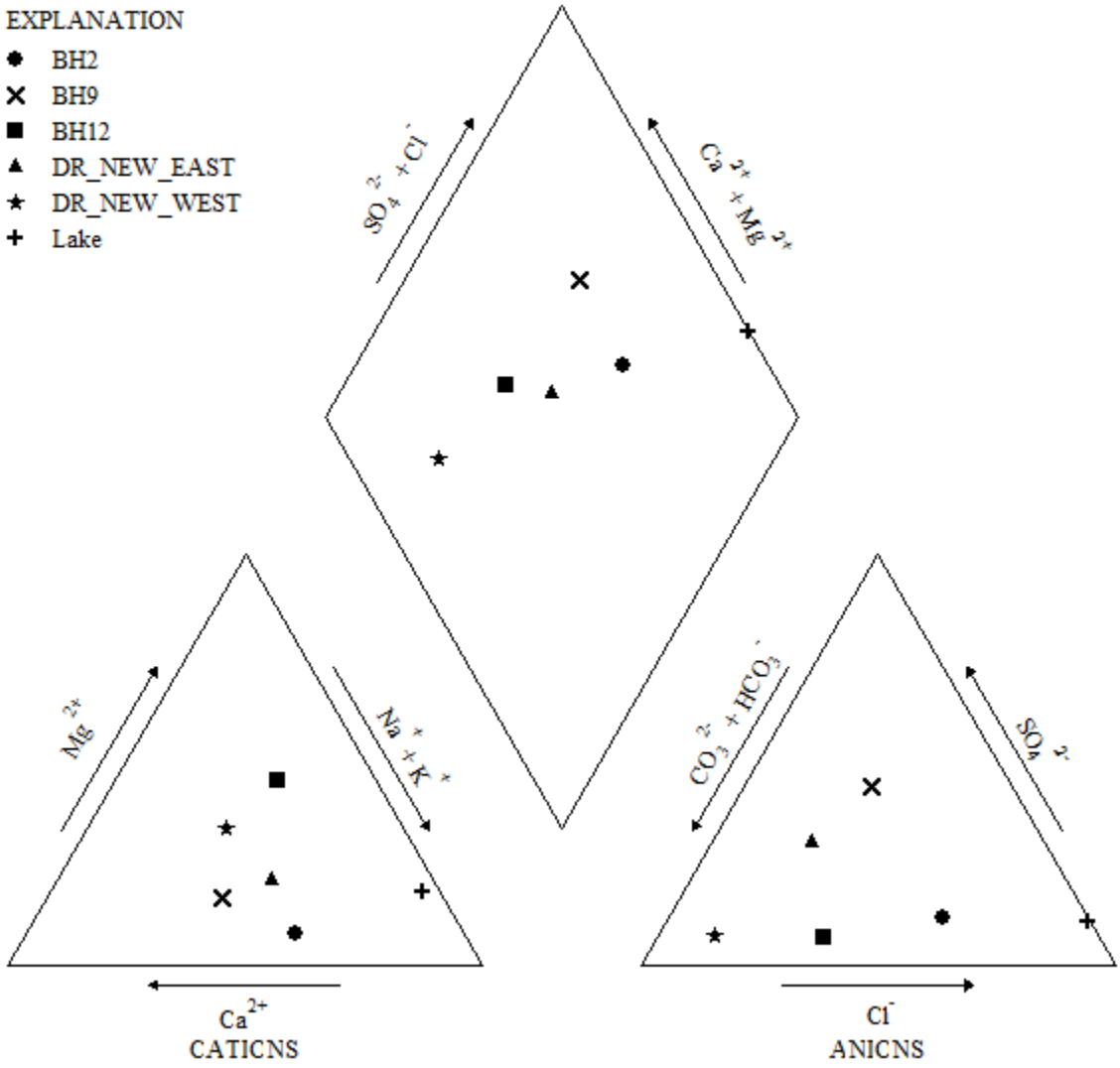

Figure 32: Piper Diagram showing a graphical representation of the chemistry of groundwater sampled from each bore, plus one sample from Lake Illawarra.

Figure 33: Stiff diagrams in relation to their corresponding bores

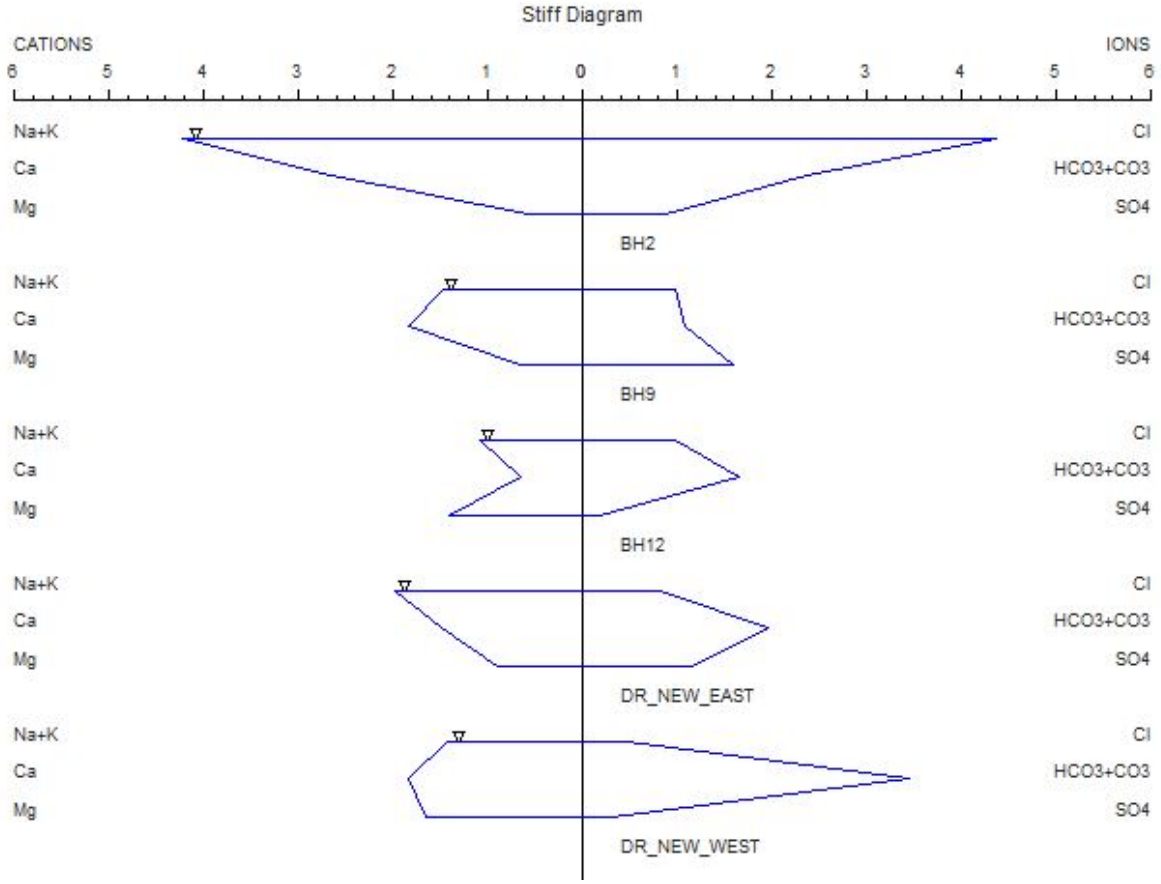

Figure 34: Stiff diagrams provide a graphical representation the different proportions of cations and anions for each bore

4.2.6. Water table fluctuations

Regular, quarter-daily fluctuations in water table level of around 0.02m to 0.04m were observed. This variation is shown in Figure 35, a small extract of the data obtained from BH2 and presented in the HOBOware software suite, from which the data was later exported to excel in order to add rainfall data. This variation is most likely due to tidal pumping, which is the response of groundwater level to the tidal variation of nearby water bodies. Taking into account the high hydraulic conductivity of the sandy Windang aquifer, and the close proximity of the bores to the lake, this result was expected. Despite the varying distances of the bores from the lake, the magnitude of fluctuation remained the same in data collected from all three bores.

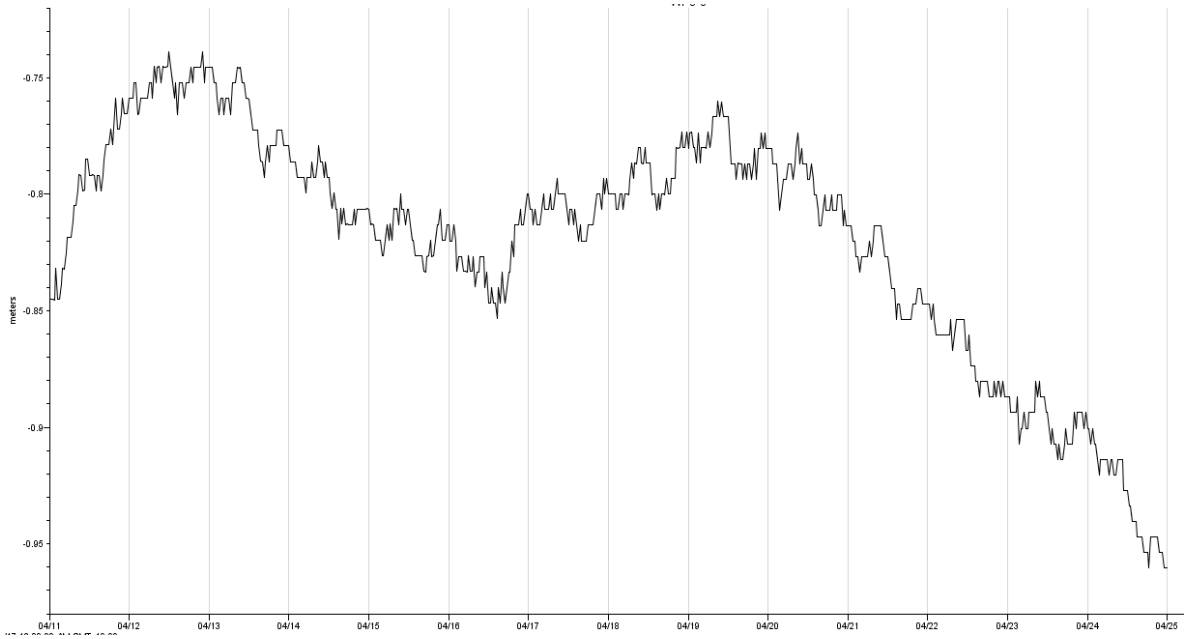

Figure 35: Water table level from 11/04/17 to 25/04/17 at the Boundary Road borehole (BH2), showing minor daily fluctuations most likely due to tidal pumping

The variation in depth to water table was plotted alongside with daily rainfall data in order to get an indication of the aquifer response to rainfall (Figures 36 to 38). Overall, it seems that there was a poor correlation between rainfall events and subsequent rises in the water table. In addition to this, it seems the magnitude of any response in water table level was not directly proportional to the rainfall received. This could be due to a high proportion of surface runoff for a number of reasons, such as layers of clay within the slag emplacement at BH9, features of the housing estate such as roads at BH2, and runoff into surface drains at DR_NEW_WEST. All of these features reduce surface water infiltration, and thus affect the extent and time delay that the aquifer is recharged following a rain event. If a high amount of rainfall is received in a short time frame, than the surface may get saturated quickly, increasing runoff. If rainfall ceases shortly after, than only a small amount of water infiltrates

into the water table. This could explain the poor water table response during the 24 hour period of significant rain on 20/5/17. When rainfall was sustained for a period longer than 48 hours, the water table response was much higher, as seen during the period from 7/6/17 to 10/6/17.

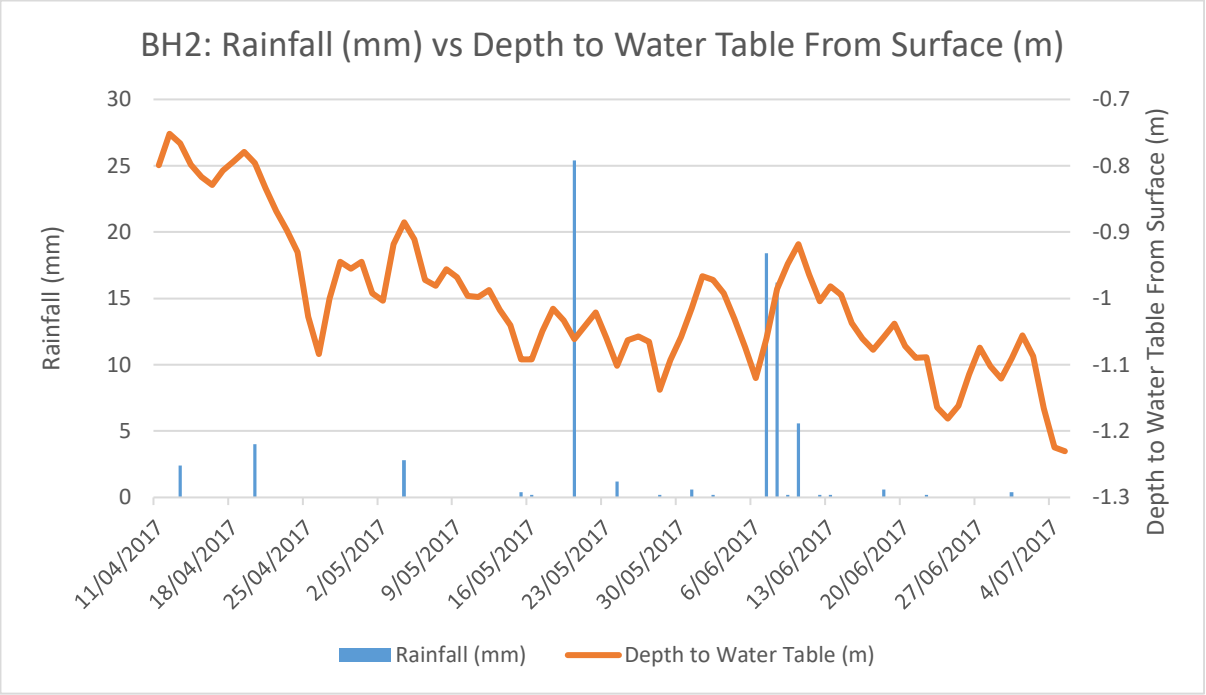

Figure 36: Rainfall vs Water Table Level over time at the Boundary Road borehole, BH2

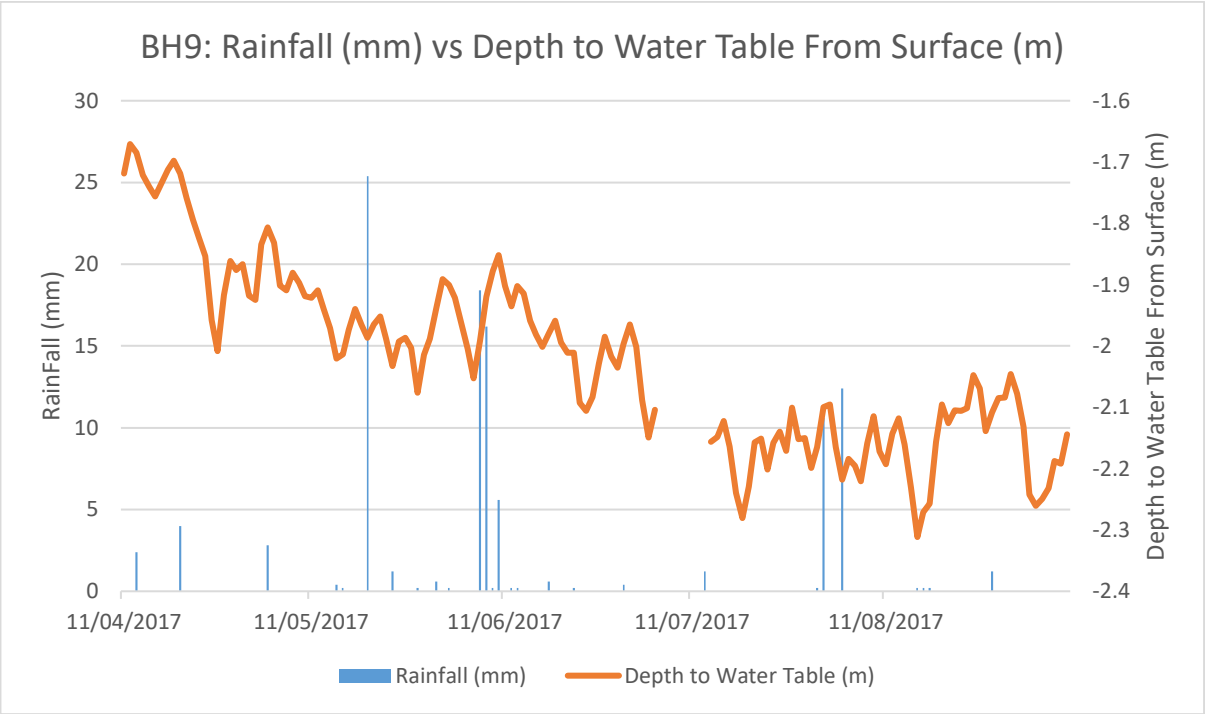

Figure 37: Rainfall vs Water Table Level over time at BH9

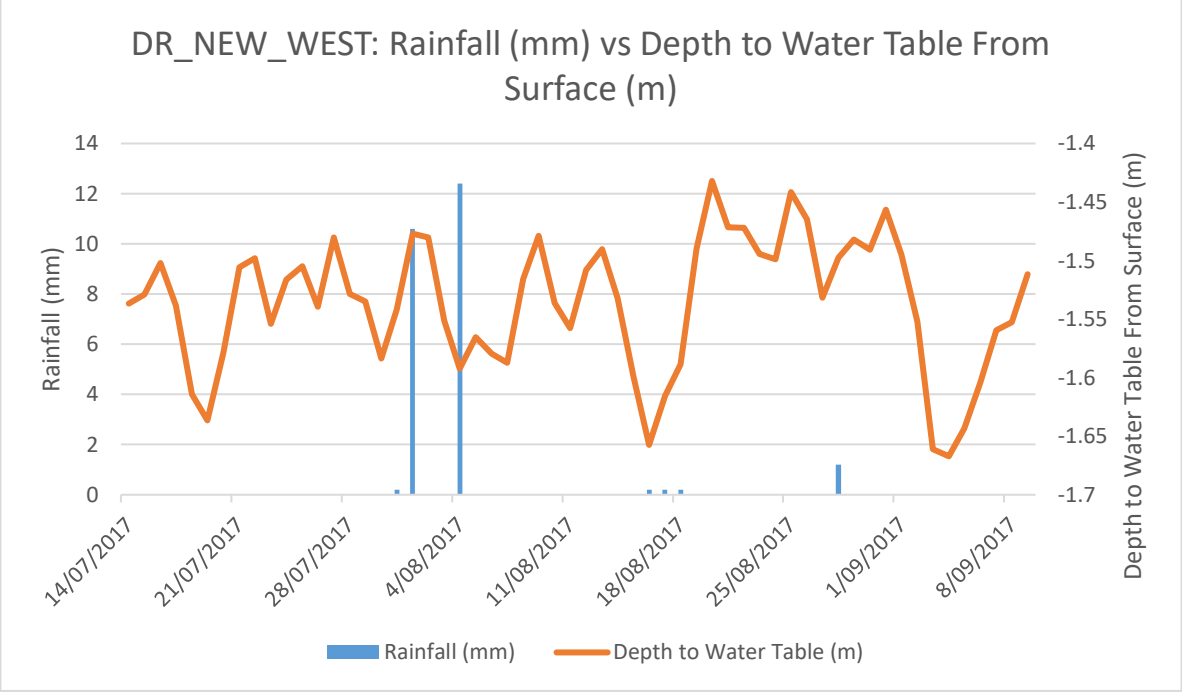

Figure 38: Rainfall vs Water Table Level over time at the DR_NEW_WEST bore

4.3. Soil/slag analysis

4.3.1. Grain size analysis

The top 0.05 to 0.1m of soil was the only portion which contained a considerable amount of silt and clay sized particles. As you go down from the surface to a depth of 0.6m, grain size seems to increase steadily. From 0.6m down to 1.55m and likely beyond, the spread of grain size seems to change very little. The majority of the soil found from 0.6m down to 1.5m seems to consist of an evenly spread mixture of grain sizes, however limited within the range of 2mm to 0.05mm in diameter, with the slag grains more prevalent towards the larger end of that range. There is a poor correlation between weathering status of the slag and grain size, as one of the most weathered slags found at 0.65m contained a higher proportion of smaller grains compared to fresh slag. This finding is not consistent with results obtained by Yassini (1994). The raw data is presented in Appendix 3.

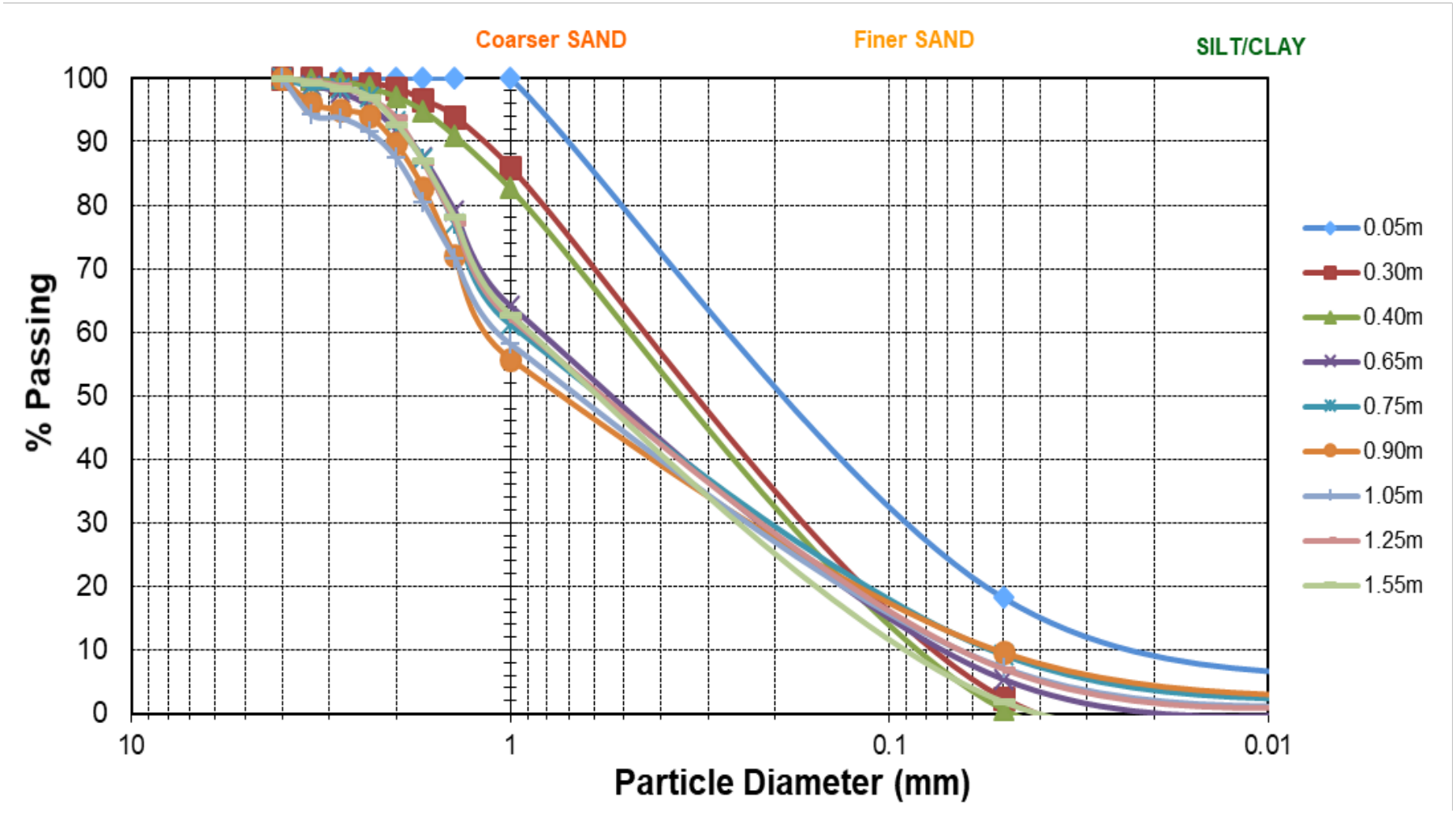

Figure 39: Grain size analysis of copper slag at various depths

4.3.2. XRF

Table 14 displays average elemental soil compositions of areas that represent baseline metal concentrations for the Windang area, and areas within the copper slag emplacement. Soil samples collected by Brian Jones in early 2017 were from a depth of approximately 0.1m. The raw data is displayed in Appendix 5.

Concentrations of zinc, lead, copper and nickel were around 50 to 100 times higher within the emplacement compared to background levels, with the main source being the slag granules present in the majority of emplacement soil samples analysed. This is to be expected, as it is known that the composition of copper slag comprises a notable amount of these metals, and although high compared to baseline soils, still make up a relatively small portion of the slag. Arsenic and cadmium concentrations were actually lower within the emplacement compared to background levels, indicating that the copper slag is not a major source of these elements in the area.

Table 14: Average concentration of metals in soils of unaffected areas (background levels) vs within the slag emplacement (Jones, 2017)

	Zn (%)	**Pb (%)**	**Cu (%)**	**Ni (%)**	**As (%)**	**Cd (%)**
Average background levels of soil (top 0.1m, Jones, 2017)	0.01	0.004	0.01	0.001	0.0004	0.0001
Average of Soil Within Slag Emplacement (top 0.1m; Jones, 2017)	1.36	0.26	0.20	0.01	0.002	0.0001
Average of Slag Emplacement (top 1.55m; Trajcevski, 2017)	3.07	0.48	0.30	0.02	0.001	0.0001

XRF analysis conducted in this study was performed on slag samples from a range of depths. Slag samples in this report were collected from sampling pit (b) at depths ranging from the surface to 1.55m. The raw data for all elements is displayed in Appendix 6. The graph below (Figure 40) displays the variation in zinc, copper and lead content (%) in the slag plotted against depth (metres below the surface) at which the slag was obtained. The sharp decrease in all metals at around 0.62m depth coincided with a layer of sand. Between depths of 0.8m and 1.2m, and again around 1.55m, the zinc concentration decreases by around 50%, and the copper concentration also decreases tenfold. This could be a result of weathering within this zone, and subsequent zinc and copper depletion into leachate, or it could be older slag with a different elemental composition. The latter explanation would make sense when related to the decreasing zinc content in older slag, however copper content was consistent between older and newer slag, and the depletion of copper in slag at this depth suggests

metal leaching due to weathering is a more likely explanation. As well as this, the depths of 0.8m and 1.2m coincide with a section of heavily weathered slag described in Table 5 and Figure 18. From depths of 0.8m and 1.55m, the lead content was fairly homogeneous, indicating a lower leaching potential.

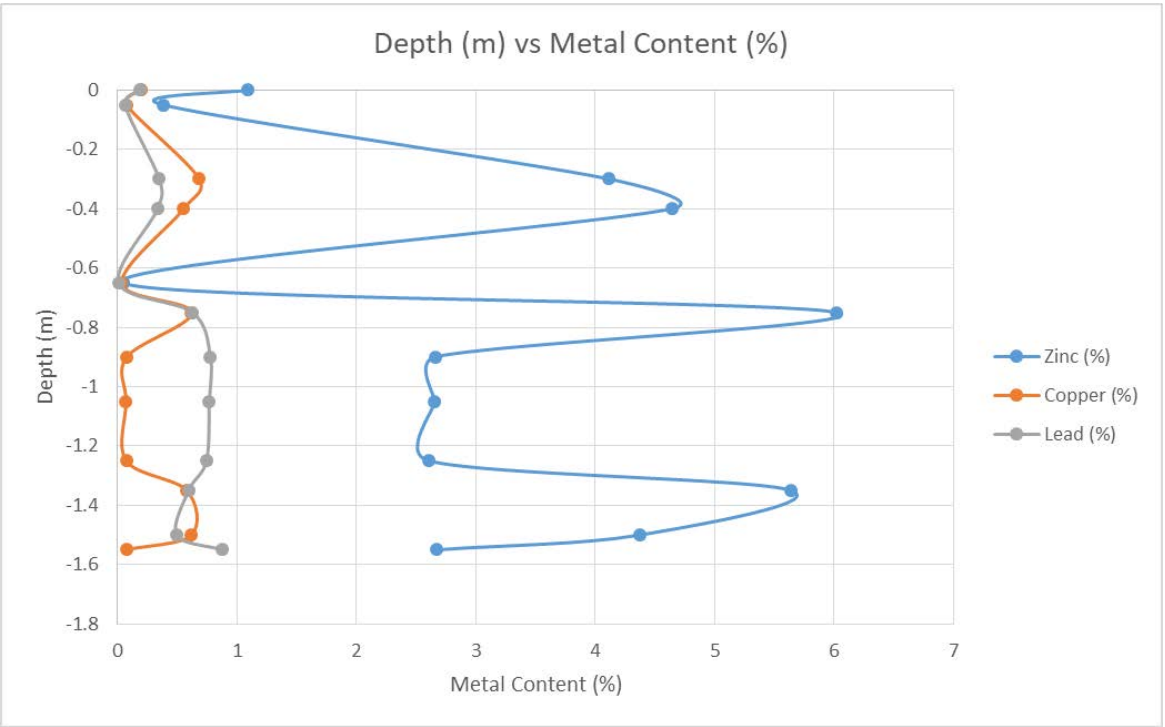

Figure 40: Results from XRF analysis on the percentage of each metal vs the depth below the surface that the slag originated

4.3.3. Microscopy and EDS analysis

4.3.3.1. Least weathered sample – MA

Under the microscope using reflected plane polarised light (Figure 41), sample MA seemed to show next to no signs of weathering, with the outer margins of individual slag granules looking intact and homogeneous with the rest of the particle. No “onion-peel” weathering structure seems to be present, and there are no obvious signs of metal oxidation occurring around the outer margins of slag.

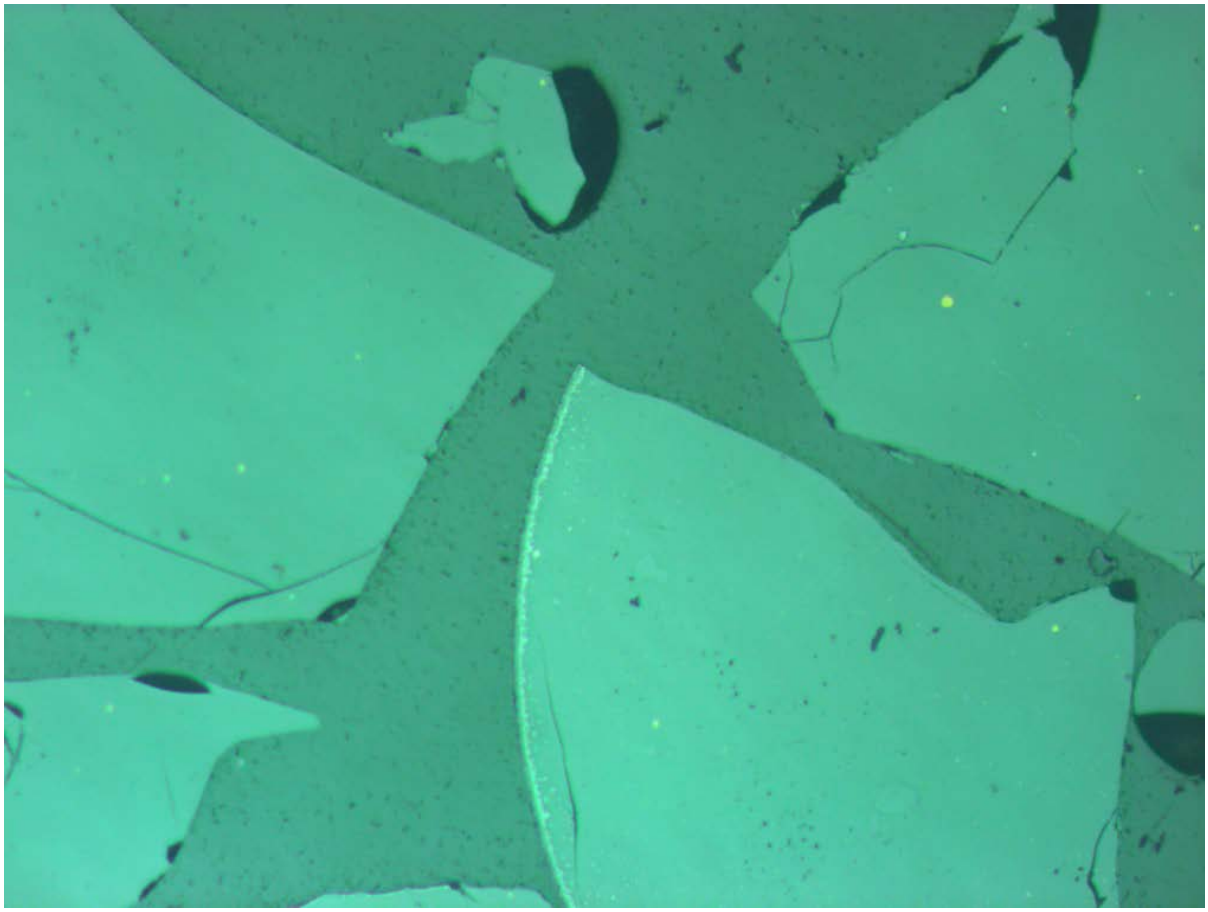

Figure 41: Sample MA under 100X magnification (10x Optical X 10x Eyepiece)

With closer examination under the scanning electron microscope (Figure 42), the perimeter of the slag granule tends to have jagged edges, however this is most likely due to the cooling process during slag production and not weathering. The structures near the margins with dark outlines are also most likely a product of fast cooling, causing elements to accumulate at the extremities that experience the fastest rate of cooling.

Table 15 shows the average elemental composition of the unweathered slag granule in sample MA (Appendix 7e). The main components are Carbon (26.81%), Oxygen (30.17%), and Iron (26.24%), with iron concentrations being the least homogeneous out of the three, as indicated by the larger standard deviation. Zinc (5.58%) was spread fairly homogeneously across the slag granule, with a standard deviation of 1.76. The majority of copper (2.83%) found in this sample comprises of the remaining unreacted copper ore and chalcopyrite, although most of the spectra centred on these particles were not counted in the average.

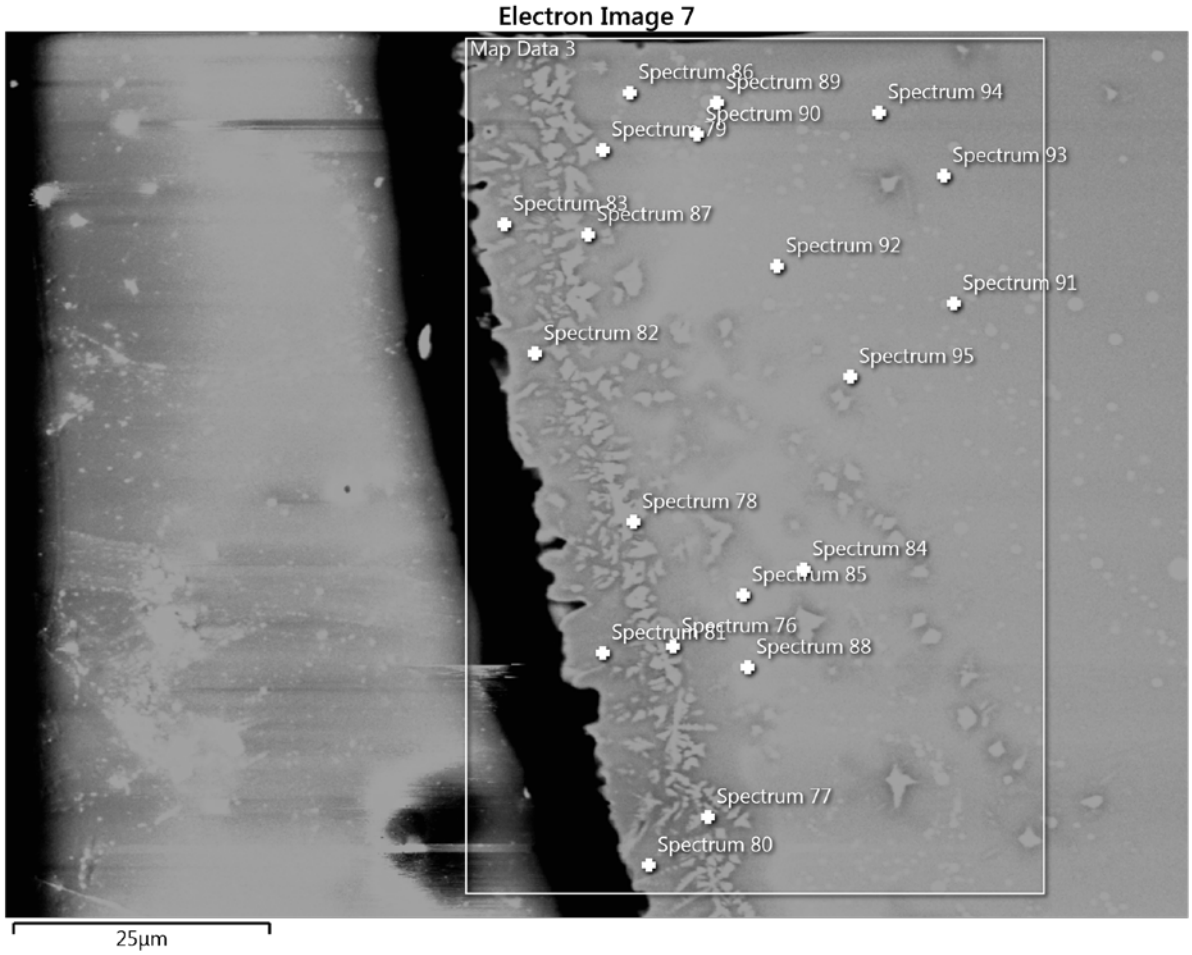

Figure 42: Image of sample MA obtained using a scanning electron microscope (SEM) showing locations of different spectra analysed using EDS

Table 15: Average elemental composition of unweathered slag granule in MA, shown in Figure 42

Element	% by weight (average)	Standard Deviation
C	26.81	2.28
O	30.17	1.24
Mg	0.62	0.11
Al	0.85	0.08
Si	8.18	2.10
S	0.91	1.10
K	0.10	0.01
Ca	0.20	0.05
Ti	0.20	0.01
Cr	0.22	0.07
Fe	26.24	6.09
Cu	2.83	3.05
Zn	5.58	1.76

A greater amount of zinc accumulates close to the edges of the slag granule during cooling, as shown in Figure 43. This can have implications for the leaching behaviour of the slag as the outer layer

weathers over time, because the area that will be weathered first (around the outer edge of the slag granule) is the most concentrated in zinc. This may result in a spike in zinc within groundwater as that outermost margin of the slag granule weathers, mobilising the zinc contained within that zone. Iron is slightly more concentrated near the edge of the slag than throughout the rest of the particle (Figure 44), but nowhere near to the extent that zinc is. Copper is low in abundance throughout the majority of the slag, and is most concentrated in remaining non-reacted copper ore or chalcopyrite, as shown in Figure 45. These remaining artefacts are of little significance in terms of leachability, due to the fact they make up a small portion of the total slag granule, and are encapsulated by the rest of the slag matrix. Only a small amount of the fragments are released from the matrix through weathering, and go on to oxidise through exposure to the elements. EDS maps of all other elements analysed are displayed in Appendix 7e.

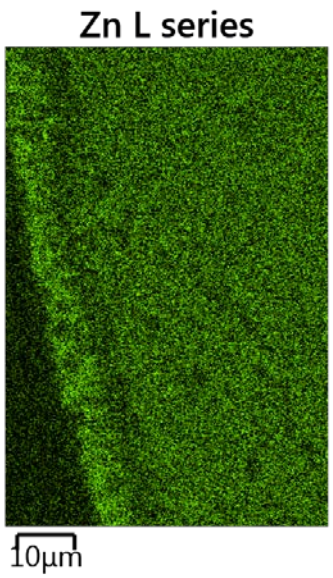

Figure 43: EDS map of zinc in sample MA

Figure 44: EDS map of iron in sample MA

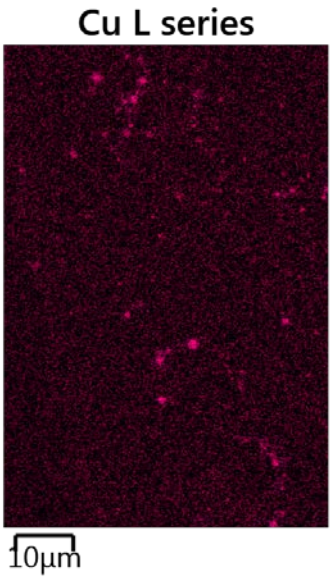

Figure 45: EDS map of copper in sample MA

The EDS layered map (Figure 46) shows the relative concentrations Cu/S, Zn, Fe and Si across the analysed surface. In areas with higher Iron concentrations, especially the outer margin on the left running top to bottom, it seems that Zinc and Silicon are deficient. By looking at the EDS map of iron and zinc, it is apparent that the concentrated strip of iron (Figure 44) also coincides with a decrease in zinc along the same strip (Figure 45), which is consistent with the observations from Figure 46.

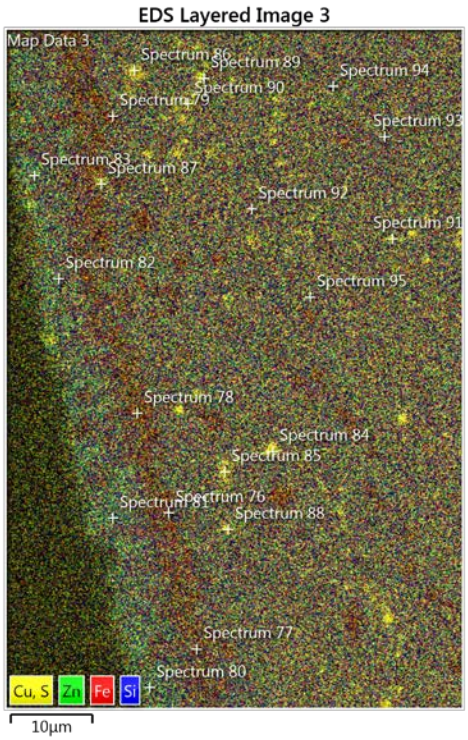

Figure 46: Layered EDS map showing the concentrations of copper/sulphur, zinc, iron and silicon in sample MA

4.3.3.2. Most weathered sample – MD

Observation of sample MD using reflected plane polarised light microscopy showed significantly greater signs of weathering than all other samples, as shown in Figure 47. A lot of fragmented remnants remained around the outer perimeters of the slag granules as a result of the extensive weathering. Ferric oxide/hydroxide, represented by a yellow-orange tinge, is present in the weathered zone (Figure 48). The weathering seems to follow an onion-peel weathering structure in some areas, and unstructured weathering in other areas. In the SEM image (Figure 49), the areas with the onion-peel weathering structure are well highlighted and distinguished, notably formed around the left slag granule.

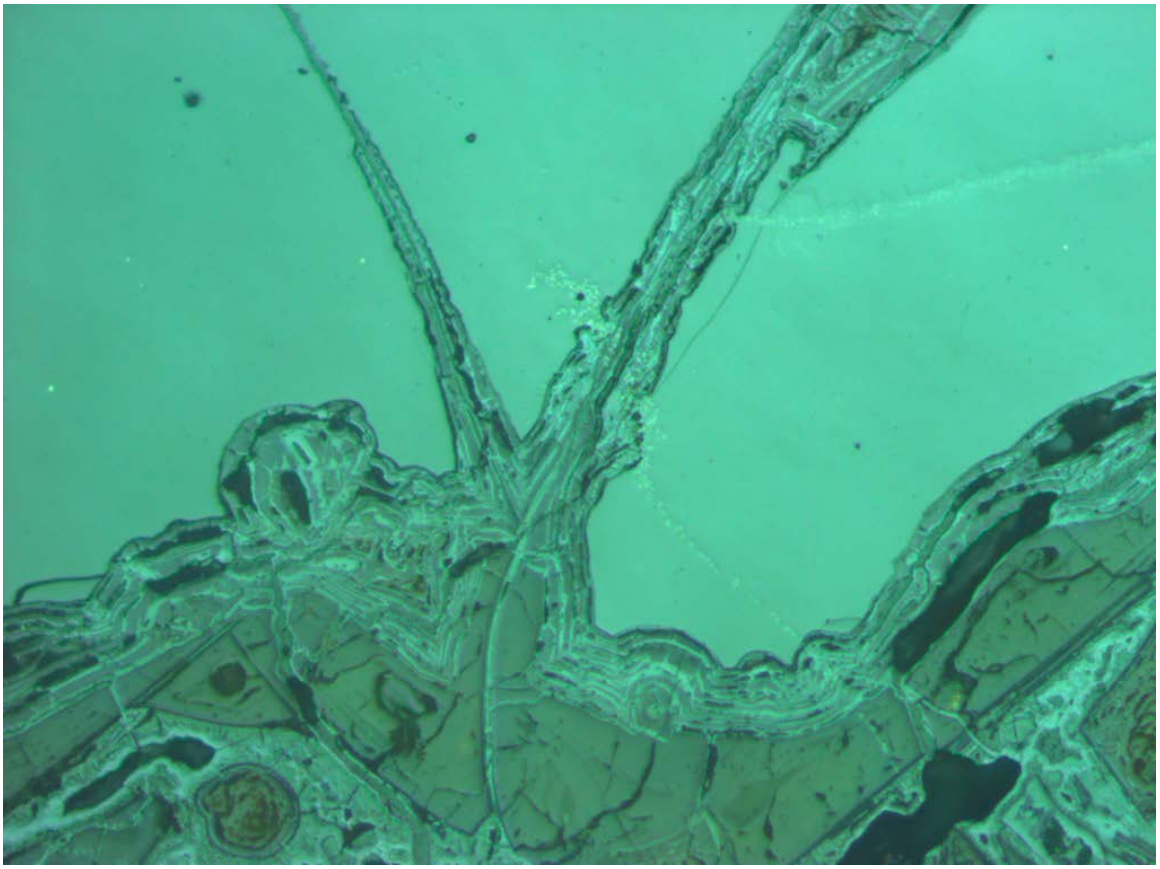

Figure 47: Sample MD under 100X magnification (10x Optical X 10x Eyepiece)

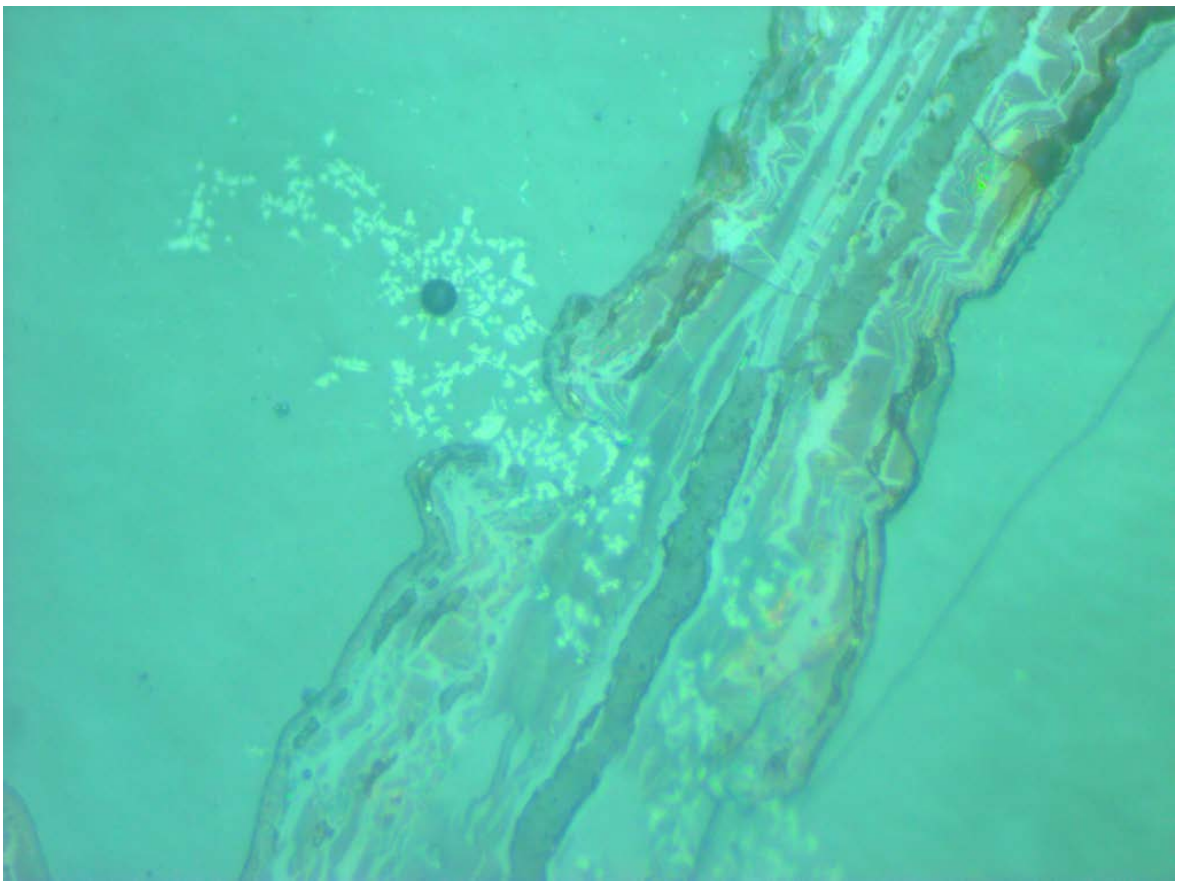

Figure 48: Sample MD under 500X magnification (50x Optical X 10x Eyepiece)

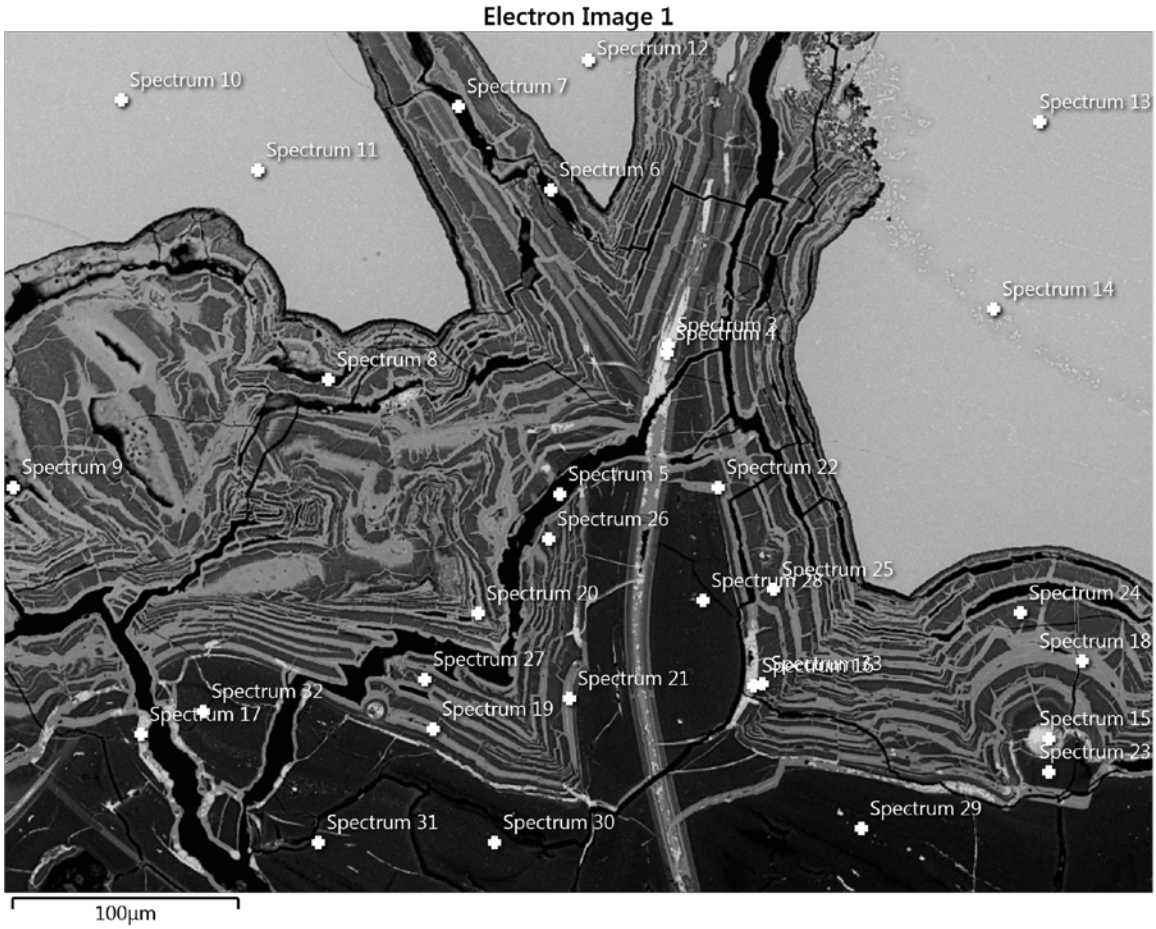

Figure 49: Image of sample MD obtained using a scanning electron microscope (SEM) showing locations of different spectra analysed using EDS

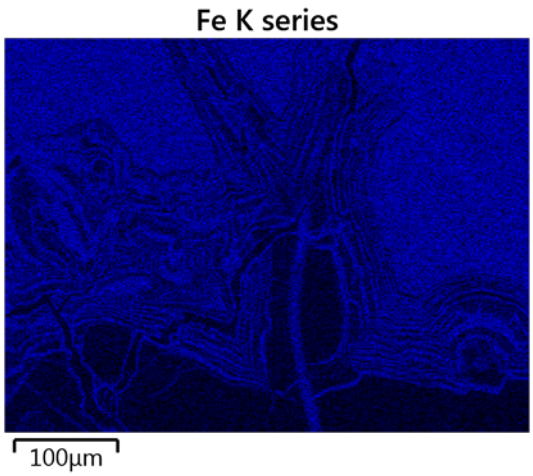

Figure 50: EDS map of iron in sample MD

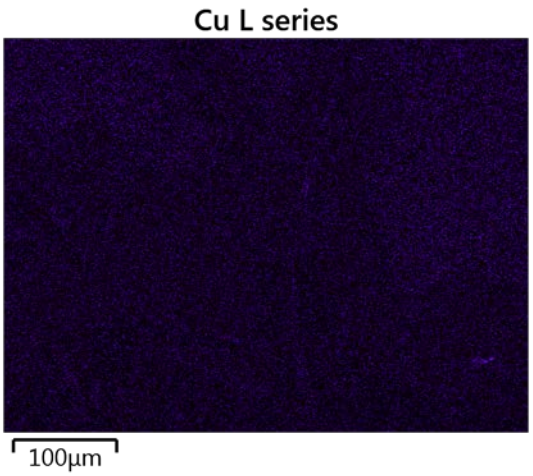

Figure 51: EDS map of copper in sample MD

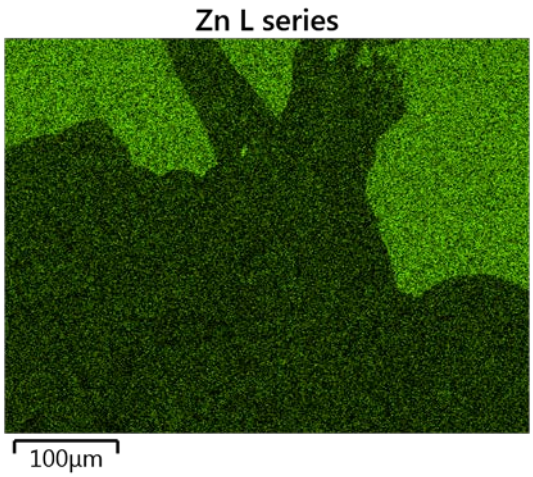

Figure 52: EDS map of zinc in sample MD

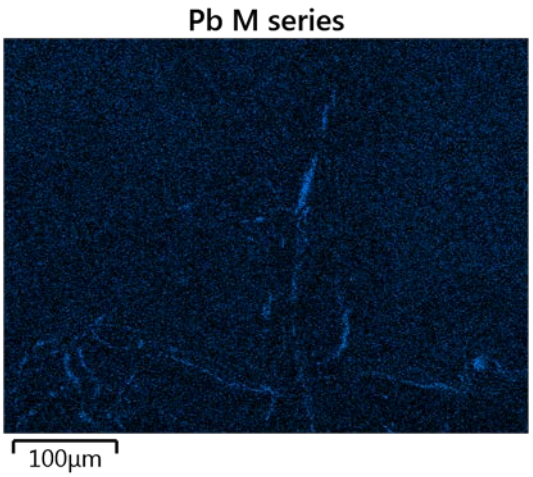

Figure 53: EDS map of lead in sample MD

Looking at spectrum 11 and 14 (Table 16), we can see that the slag granule has a zinc content of around 7.5% to 8% by weight. When comparing this to spectrum 15, 19 and 27 located within the weathered material, it is apparent that zinc is not present at all. To get a broader view of the distribution of zinc amongst the field of view, we can look at Figure 52, with the brighter green areas representing a higher concentration of zinc. It becomes clear that zinc is highly depleted within the weathered material.

Within the slag granule, the iron content is around 32%, as shown by spectrum 11 and 14 (Table 16). Spectrum 19 is located within the weathered zone, and has an iron content slightly higher than both spectrum 11 and 14. The distribution of iron within the unweathered zone can be observed in the EDS map (Figure 50). Iron seems to be present in similar concentrations consistently within the weathered zone compared to the unweathered zone, with the only difference being the absence of iron in the resin cracks throughout the weathered zone. This is to be expected, as the iron in the slag oxidises to

ferric oxide/hydroxide, which is highly immobile, hence why it is still in abundance throughout the weathered zone.

Based on this data, zinc from the weathered outer layers of the slag is leached and removed much quicker and to a higher degree than iron. When relating this to the trends of heavy metals in groundwater over time, this may be an explanation as to why zinc concentrations have been falling on average over time following initial spike after the last of the slag was deposited. It also is consistent with the rising iron concentrations over time, as much of the iron originating from the fresh slag still remains in the weathered section of the slag, due to slower leaching.

Copper is mostly devoid from the slag matrix (Figure 51), with the only amounts detected originating from fragments of remaining copper ore and chalcopyrite, as represented partly by spectrum 15 (Table 16). The same pattern was recognised in sample MA.

The distribution of lead seems to be fairly homogeneous across the weathered and unweathered sections of slag (Figure 53). Lead artefacts do seem to be present in the resin filled cracks, an example being spectrum 15 (Table 16). These concentrated areas of lead are not of interest.

Table 16: Elemental composition (% by weight) of slag at each spectrum (Appendix 7a)

Zone	Unweathered slag granule		Copper/ chalcopyrite	Weathered (light band)	Weathered (dark band)
Spectrum Label	Spectrum 11	Spectrum 14	Spectrum 15	Spectrum 19	Spectrum 27
C	7.19	5.32	7.39	9.28	12.42
O	34.22	33.21	37.87	40.85	45.51
Mg		0.71			
Al	1.79	1.65	1.04	2.15	1.83
Si	14.16	14.32	6.25	8.49	22.34
P					
S	0.82	0.81	6.81	1.43	0.64
Cl					
K			0.81		
Ca	0.35	0.45			
Ti					0.27
Fe	32.58	32.67	20.76	37.80	16.14
Co					
Ni					
Cu		0.98	3.70		
Zn	7.47	7.98			
In		0.42			
Sn					0.84
Pb	1.43	1.48	15.37		
Total	100.00	100.00	100.00	100.00	100.00

Table 17 shows a comparison of the elemental composition between the weathered vs unweathered zones within the slag granule. Cells highlighted in green represent the higher concentration of the two zones for each element. By observing the difference in standard deviation values between the two zones, it seems that the weathered zone contains far greater variability in composition between different spectra when compared to the unweathered zone, which is fairly homogeneous as indicated by the low standard deviation values. As to be expected, the unweathered zone contains a higher concentration of most heavy metals such as iron, nickel, copper, zinc. The weathered zone did contain a higher concentration of tin and lead, however the former was not of concern in regards to leachate. Lead artefacts were heavily concentrated in the resin cracks throughout the weathered zone, and are most likely traces of galena picked up from previously polished samples, thus not an important observation. The heavy metal with the most dramatic decrease in concentration between the unweathered zone and weathered zone was zinc, to be expected due to its high mobility and high leaching potential.

Table 17: Comparison of the average elemental composition (% by weight) of the unweathered zone vs the weathered zone (Appendix 7a)

Averages for each zone were calculated from the following spectra:

Unweathered – spectra 10, 11, 12, 13,14

Weathered – spectra 5, 6, 7, 8, 9, 16, 18, 19, 20, 21, 22, 24, 25, 26, 27, 28, 33

LOD = Limit of Detection

	Average (%) elemental composition of Unweathered Slag Granule	**Standard Deviation (Unweathered Slag Granule)**	**Average (%) elemental composition of Weathered Section**	**Standard Deviation (Weathered Section)**
C	6.95	0.87	17.89	14.93
O	33.23	1.24	39.17	7.56
Mg	0.65	0.07	Below LOD	
Al	1.7	0.06	1.58	0.69
Si	13.82	0.62	12.87	7.89
P	Below LOD		0.15	0
S	0.99	0.43	1.31	1.42
Cl	Below LOD		4.89	2.17
K	0.14	0.00	1.39	0
Ca	0.39	0.05	0.206	0.07

Ti	Below LOD		0.25	0.03
Fe	32.33	1.32	23.37	12.21
Ni	0.52	0	Below LOD	
Cu	3.06	2.08	2.11	0
Zn	7.26	0.46	1.06	0.56
In	0.42	0	Below LOD	
Sn	Below LOD		0.65	0.21
Pb	1.51	0.21	2.83	4.54

Table 18 compares the composition of lighter bands with darker bands which form part of the onion-peel weathering structure. Cells highlighted in green represent the higher concentration of the two bands for each element. The compositions of both bands varied quite a bit from spectrum to spectrum, indicated by the relatively high standard deviations. Concentrations of Iron were significantly higher in the light bands. All other heavy metals showed no significant difference in concentration between the bands, and combined with the high standard deviation values, indicate that there is not a strong enough correlation to associate a particular metal to a particular shade of weathered material, with the possible exception of iron.

Table 18: Comparison of the average elemental composition (% by weight) of the lighter bands vs darker bands within the weathered zone (Appendix 7a)

Averages for each zone were calculated from the following spectra:

Lighter bands – spectra 16, 17, 18, 19, 20, 21, 22

Darker bands – spectra 24, 25, 26, 27, 28

LOD = Limit of Detection

	Average (wt. %) elemental composition of Light Bands within weathered zone	**Standard Deviation (Light Bands)**	**Average (wt. %) elemental composition of Dark Bands within weathered zone**	**Standard Deviation (Dark Bands)**
C	9.61	2.12	9.35	1.62
O	38.78	6.08	46.39	1.34
Al	1.35	0.34	2.21	0.72
Si	7.75	1.25	22.65	3.57
S	2.95	2.41	0.87	0.24
Cl	0.11	0	Below LOD	

K	1.48	0.09	Below LOD	
Ca	0.15	0	Below LOD	
Ti	Below LOD		0.24	0.03
Fe	34.81	10.04	17.24	5.55
Cu	1.85	0.27	Below LOD	
Zn	0.65	0	0.85	0
Sn	0.71	0	0.71	0.17
Pb	6.25	5.53	1.16	0

4.3.3.3. Most weathered sample found beneath the surface – MB

Figures 54 and 55 are images of sample MB taken using plane polarised light microscopy. Sample MB was the most weathered slag encountered beneath the surface, and was found at a depth of 0.9m. Through examination under the microscope, sample MB seems to contain a significant amount of weathering compared to sample MA, however it is far less weathered than sample MD, according to the thickness of the weathered zone around the slag granule. Therefore it is likely that although all zinc has been leached from the weathered zone, overall the total amount of zinc leached from the slag in sample MB is less than the amount leached from sample MD, as the total area of the weathered zone surrounding the perimeter of the slag granule is less in MB than MD. Similar trends for iron and copper would be likely, although with a lesser extent of leaching in the weathered zone, as found in MD. The same yellowish iron oxide staining around the weathered zone is visible in MB.

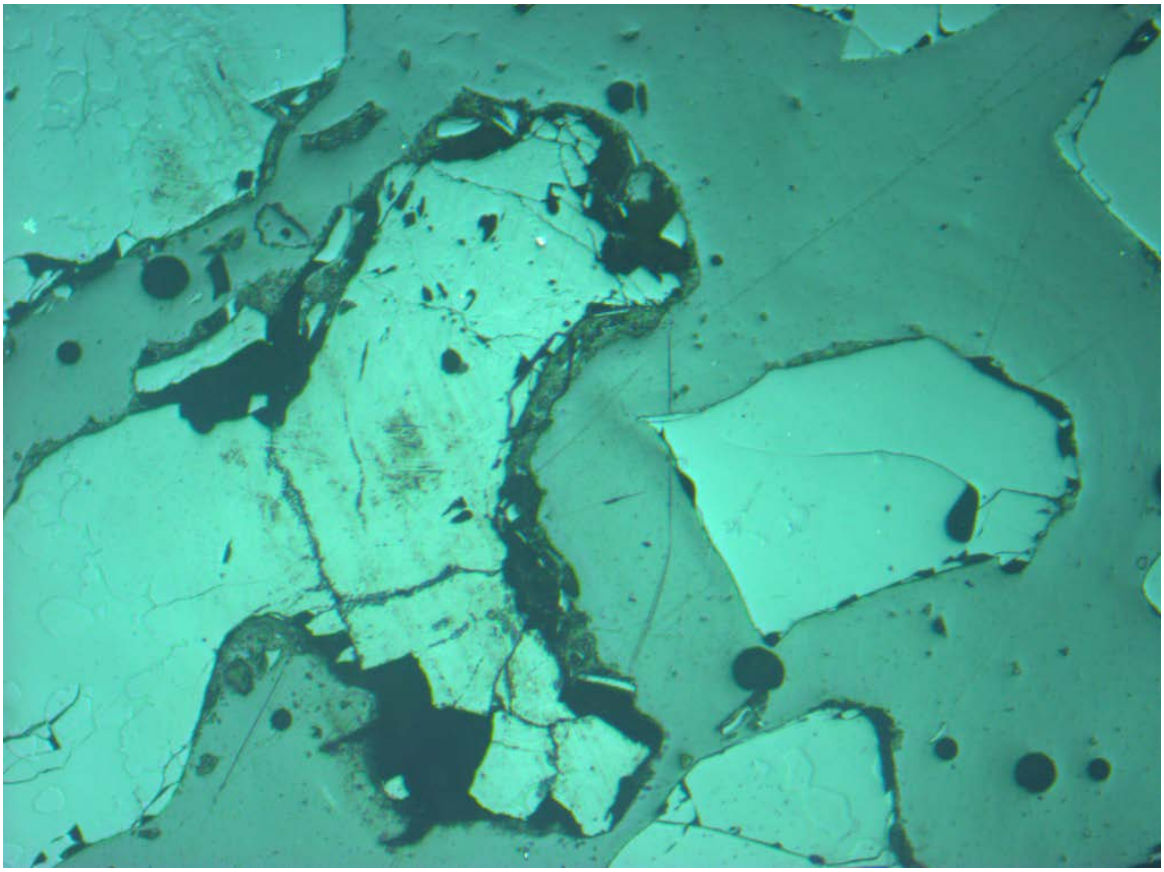

Figure 54: Sample MB under 40X magnification

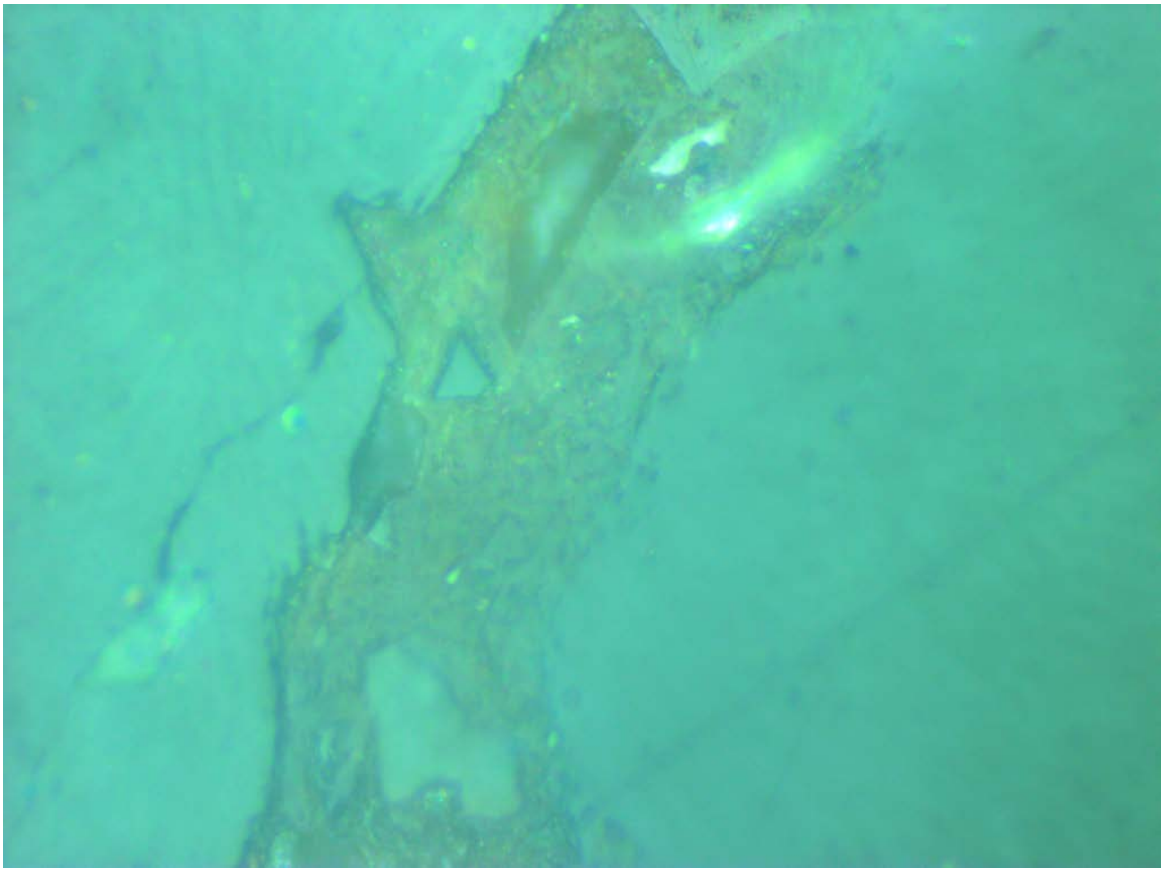

Figure 55: Sample MB under 500X magnification

4.3.4. Acid Neutralization Capacity/Acid Generation Capacity

Table 19 shows the actual acidity and the Net Acid Producing Potential (NAPP) in kilograms of sulfuric acid per tonne of slag. The NAPP takes into account the acid neutralizing potential of the slag. There is a clear trend for the more weathered slag to have less acid generating potential. It must be noted however that the actual acid generation occurring from the slag is much lower in reality, and was deemed below LOR in all samples. The raw data is displayed in Appendix 8.

Table 19: Potential Acid Generation Capacity of the four solid samples analysed, calculated as kilograms of sulfuric acid theoretically able to be produced per tonne of slag

Sample	**MA**	**MB**	**MC**	**MD**
NAPP (kg H_2SO_4 / t)	41.39	34.13	36.24	19.52
Actual Acidity (kg H_2SO_4 / t)	0.098	0.098	0.098	0.098

Chapter 5. Discussion

By observation of the side by side stratigraphic columns in Figure 18, correlating layers in the upper 0.9m could be identified between the drill core and pit (b), but not pit (c). Pit (b) and the drill core are located on the southern extremities of the driving range, and pit (c) is located at the northern extremity of the driving range, suggesting that the pattern of slag deposition amongst the site varied. Importantly, the uppermost slag encountered in pit (c) was oxidised, in contrast to the unoxidised upper layers in pit (b) and the drill core. This could indicate that the last of the slag deposition which happened in the late 1980's and early 1990's mainly occurred towards the southern bounds of the site, and perhaps the majority of the slag on the northern side of the site is considerably older.

Pugh and Yassini (2002) hypothesised that during a rainfall event following a long dry spell, a greater amount of zinc is leached into the groundwater system. This is due to the fact that sulphide decomposition proceeds at a higher rate during the dry spell, allowing leachable zinc to accumulate within the hydroxide deposits, and get mobilised once rainfall infiltrates. As groundwater sampling was separated into "dry" sampling events and "wet" sampling events, this theory was able to be tested. The majority of the metals did not show a definitive trend of either an increase or decrease in concentration between "wet" sampling events and "dry" sampling events. Zinc however did increase in four out of the five bores after rainfall, supporting the theory hypothesised by Pugh and Yassini (2002).

Although several heavy metals have been relatively high in concentration in the past groundwater analyses, zinc was the only metal with concentrations repeatedly above ANZECC (2000) guidelines throughout the sampling for this report. As well as this, most metals displayed trends of decreasing concentration over time, often down to values which were on par with or below background levels, as defined by Yassini (1994). Although iron concentrations exceeded the ANZECC LTV in a few samples, and were trending up over time in BH9 and BH2, they were still below or on par with the background values reported by Yassini (1994) for the Windang area, suggesting that any iron in the groundwater originating from the slag is not of great enough quantity to be concerned about.

There was a poor correlation between iron concentration and ORP values. BH9 consistently had a positive ORP value of around 200, indicating oxidation potential. Theoretically, this would lead to a lower iron concentration in groundwater, as an increased amount would be precipitated out of solution as ferric oxides and hydroxides. This is not what was observed, as BH9 had one of the highest concentrations of iron out of all bores. Groundwater from BH2 and BH12 had a slightly negative ORP values, but also contained low iron concentrations (below background). Groundwater from

DR_NEW_WEST and DR_NEW_EAST had ORP values similar to BH9, but much lower concentrations of iron, very similar to BH2 and BH12.

A history of notably high zinc concentrations have been identified in past papers on the Windang aquifer. As well as this, zinc was the only metal to breach the less stringent ANZECC STV guidelines on two occasions during sampling for this study. When including all of the bores sampled at Windang in the past, zinc accounted for the greatest number of ANZECC STV breaches. Further considering this across the various bores sampled, zinc concentrations obtained in this study only exceeded the ANZEC STV in groundwater from BH9. For context, the average zinc concentration in BH9 was fifty times higher than the averages found in BH2 and BH12.

BH2 is located around 350m to the south of BH9, and at around the same depth. This is still within the copper slag emplacement. BH12 is located only around 1m from BH9, but at a depth of 8m. This suggests that the abundance of zinc varies within the aquifer both horizontally and vertically. This was also supported by findings from Figure 19, which displayed a trend of decreasing zinc concentration with increasing bore depth, based on data from a number of bores.

The variation horizontally across the aquifer between BH2 and BH9 may be due to different source waters. This theory is supported by differences in ion composition between the bores, as shown by the piper plots and stiff diagrams in Figures 32 to 34. Groundwater from BH2 was significantly higher in sodium chloride compared to BH9. BH9 also contained considerably more calcium and sulphate.

The reason for the reduction in zinc concentration at depth may relate to differing groundwater flow characteristics. Groundwater data obtained by Longhurst (2015) from just north of the slag emplacement indicated that a higher volume of water passes through the sand from the dunes at depth compared to the shallow portion of the aquifer. This implies that there is a higher dilution factor of the groundwater at depth, resulting in lower concentrations of zinc. The shallow portion of the aquifer is hence only intermittently flushed during periods of rainfall, and not continuously by regional groundwater forcing, resulting in the accumulation of zinc in this zone.

Based on visual observation using reflected light microscopy and under the scanning electron microscope (SEM), along with the analysis of elemental distribution by energy dispersive spectroscopy (EDS), the weathering behaviour of copper slag within the emplacement was able to be investigated. The slag from the first half metre depth was unexpectedly one of the most unweathered samples encountered, which may have possibly been a lot younger than the rest of the emplacement. A sample from the unweathered section, sample MA, showed little to no signs of weathering around the outer perimeter of slag granules. It is therefore likely that little to no heavy metals are being leached out of

this unweathered slag, as the widespread notion that copper slag is chemically inert in groundwater systems was originally based on TCLP (toxicity characteristic leaching procedure) analysis on unweathered copper slag samples. However, based on examination of sample MD under the SEM (Figure 49) and analysis on the distribution of zinc using EDS (Figure 52), it is definitely evident that zinc in the groundwater is originating from the outer margins of weathered copper slag.

Zinc concentrations trended down consistently in bores with an initially high concentration. BH9 contained the highest amount of zinc in both the older studies and this study. Zinc concentrations were as high as 35mg/L in 1994 (Coffey Partners International Pty Ltd, 1995), which is 7 times higher than the LTV defined by ANZECC (2000). In 2017, this figure dropped to around 5mg/L. Following this trend, zinc concentrations can be expected to fall further in to the future, but the rate of decrease will start to slow, as the trend is not linear (Figure 20). However, concentrations have already reached a stage where they are near the ANZECC (2000) STV guideline, so zinc in the groundwater is not an issue requiring immediate action as long as the trend continues.

The reasoning for this trend has been hypothesised by myself and Brian Jones, relating to the leaching behaviour of Zinc specifically. As zinc has a high leaching potential, any amount of the metal released by the weathering of the copper slag granule was rapidly leached, causing the extremely high spikes in concentration seen in the mid 1990's. This was supported by observation of the EDS map (Figure 52) of zinc concentration across the weathered sample, MD. The weathered sections were almost completely devoid of any zinc (around 1% by weight), while the unweathered sections contained around 5.5% by weight.

As weathering happens relatively rapidly when the entire surface area of a slag granule is fully exposed to air and water, lots of zinc was released some time after the initial deposition of the slag. As more of the perimeter of the slag granule weathers away, a weathering rind forms around the perimeter of the slag granule. As the weathering process progresses, the thickness of this weathering rind around the slag granule increases. Iron hydroxide also accumulate within the weathering rind around the slag granule. It is certainly possible that the presence of this weathering rind and iron hydroxide hinders the rate of weathering of the fresh slag granule that remains. Ultimately this could be an explanation as to why zinc concentrations throughout the Windang aquifer have decreased over time, as a slower rate of fresh slag weathering means less zinc is released and mobilised from the slag granule, and when taking into consideration the depletion of zinc from the weathered zone due to its high mobility, the availability of mobile zinc decreases. As zinc disperses throughout the groundwater system, the source (unweathered copper slag) is not weathering fast enough to maintain the initially high concentration of zinc, hence the reduction in concentration.

An important consideration to take into account, is that BH9 is located underneath the slag emplacement. A reduction in zinc concentration here may not mean that the zinc concentration is decreasing elsewhere, as the zinc is dispersing away from beneath the slag emplacement at BH9. Although unlikely to require any form of action at the moment, it may be beneficial to monitor heavy metal concentrations in bores not located within the slag emplacement, and perhaps towards the path of groundwater flow, in order to determine if concentrations increase to significant levels over time. However, concentrations downstream from the slag emplacement are unlikely to be high enough to cause concern, especially as concentrations in the upper portion of groundwater closest to the emplacement have been found to be within a reasonable range, and dispersion that will occur with transport will result in further reduction of heavy metal concentrations as one moves away from the source.

As well as the dilution of metals in the groundwater away from the source, density differences between the highly saline lake water and the fresh groundwater at the saltwater wedge zone (SWZ) could act to partially inhibit some of the metal transport into the lake, as indicated by the significant differences in ionic composition between the two waters. The effectiveness of this barrier (i.e. the proportion of metals which would be blocked from entering the lake) would have to be determined through further investigation of waters directly either side of the barrier to determine how sharp the distinction in metal concentration is. It will be difficult however to determine how much of the reduction in metals will be solely due to the density barrier, or how much can be attributed to horizontal loss due to tidal pumping and horizontal advection on the estuarine side of the barrier (Longhurst, 2015). Longhurst (2015) also reported that increased freshwater advection rates across the SWZ were experienced during rainfall events due to a larger hydraulic gradient in the freshwater lens. Implications would likely be the increased transport of metals across the barrier during rainfall.

Chapter 6. Conclusions

Wollongong City Council have put forth an interest in this study because some environmental impact reports published within the past 25 years (Coffey Partners International Pty. Ltd. 1994, 1995, 1996; Pugh, 2002; Yassini, 1994; Forbes Rigby Pty Ltd, 1998; Gay, 1995; Southern Copper Pty Ltd, 1992) were claiming higher than background heavy metal concentrations in the Windang aquifer as a likely result of slag leachate. Other papers (Gee et al., 1997; Manz and Castro, 1997; Sobanska et al., 2000; Ettler et al., 2003; Piatak et al., 2004; Reuter et al., 2004; Ettler et al., 2009 Vitkova et al., 2010; Piatak and Seal, 2010; Kierczak et al., 2013; Ettler and Johan, 2014; Piatak et al., 2015) from global sources on copper slag also reported that it is indeed not stable once weathering takes place in the environment of deposition, and a leachate containing heavy metals of a notable concentration is produced. The heavy metals eventually infiltrate the soil and enter the groundwater system during and after rainfall.

This study aimed to investigate how significant the contamination of the Windang aquifer is, by determining the concentration of heavy metals in the groundwater, the trend of the heavy metal concentration in groundwater over time, and the rate at which the heavy metals are being leached out of the weathered section of slag.

Despite some areas within the Windang aquifer containing above-background concentrations of zinc, around BH9 in particular, overall the majority of groundwater sampled in this study contained concentrations equal to or less than background levels obtained for the Windang aquifer (Yassini, 1994). As well as this, the highest concentration of zinc experienced was still within close proximity of the ANZECC (2000) STV guidelines. Thus, any zinc-rich plumes which may be present within the Windang aquifer are likely to have negligible effect on a lake of 75000 megalitres capacity (Scanes et. al., 2011), once taking into account a relatively low concentration at the source, dilution of metals during transport, and possible partial barrier to metal transport at the saltwater wedge zone.

Due to an apparent slowing in the rate of weathering, along with an observed decrease in zinc concentrations over time, it is unlikely that weathering rates will be high enough in the future to substantially raise zinc concentrations within the groundwater, providing the landfill site is not agitated or excavated, and the emplacement stays as is.

6.1. Recommendations

Although results obtained in this paper suggest no action is required at the moment, groundwater monitoring into the future can help determine if there are any significant shifts in the trends obtained over time, especially for metals like iron, which were trending up, and found in the weathered outer rim of the slag.

As there was a significant decrease in zinc concentration with depth due to dilution, it may be useful to investigate contaminant transport at shallow depths by installing a series of shallow bores at the base of the slag emplacement, where there would likely be a much higher concentration of zinc in the groundwater. As well as this, horizontal transport of groundwater could be investigated by installing shallow bores west of the emplacement to determine if concentrations vary from deeper groundwater located outside the emplacement. The installation of new bores west of the emplacement could also be positioned in order to locate the saltwater wedge zone, and further investigate the behaviour of metal transport across this barrier.

If there is significant amounts of contaminant transport horizontally through the groundwater at a shallow depth, than action may need to be taken. At Korrongulla swamp, a reactive barrier made from steel furnace slag acts to precipitate heavy metals out of groundwater by increasing the pH of passing groundwater (Douglas Partners, 2012; Longhurst, 2015). A similar structure could be implemented to the west of the slag emplacement in the future if further investigations deem Lake Illawarra to be at risk from heavy metals in the Windang aquifer.

References

ANZECC & ARMCANZ 2000, 'Australian and New Zealand Guidelines for Fresh and Marine Water Quality', vol. 1.

Australian Groundwater Consultants 1983, 'Korrongulla Swamp Environmental Study'.

Australian Groundwater Consultants 1984, 'Windang hydrogeological study report 1052 for the Wollongong City Council'.

Bolland, M, Posner, AM & Quirk, JP 1977, *Zinc adsorption by goethite in the absence and presence of phosphate*, vol. 15.

Bureau of Meteorology 2017, *Albion Park, New South Wales 2017 Daily Weather Observations*, Australian Government, viewed 19th September 2017, http://www.bom.gov.au/climate/dwo/IDCJDW2001.latest.shtml

Boyle, M & Fuller, WH 1987, 'Effect of Municipal Solid Waste Leachate Composition on Zinc Migration through Soils', *Journal of Environmental Quality*, vol. 16, pp. 357-60.

Brown, J, Glynn, P & Bassett, R 1999, *Geochemistry and reactive transport of metal contaminants in ground water, Pinal Creek Basin, Arizona*.

Cavallaro, N 1982, 'Sorption And Fixation Of Cu And Zn, And Phosphate By Soil Clays As Influenced By The Oxide Fraction', Cornell University.

C.D. Mackie & Associates Pty Ltd 1984, *Groundwater Investigations At Korrongulla Swamp*.

Coffey Partners International Pty. Ltd. 1994, 'Windang groundwater assessment', *Report No. SC955/1-AE for Wollongong City Council. Coffey Partners International Pty Ltd, North Ryde, August 1994 (unpublished).*

Coffey Partners International Pty Ltd & Wollongong City Council 1995, *Windang Groundwater Assessment*.

Coffey Partners International Pty. Ltd. 1996, 'Preliminary assessment of the potential for contaminant migration within the shallow aquifer Lake Illawarra, Windang, NSW', *Report No. SC955/2-AC for Wollongong City Council & Southern Copper Ltd. Coffey Partners International Pty Ltd, North Ryde, August 1996 (unpublished).*

Domel, RU & Holden, PJ 1994, 'A Report To Wollongong City Council On Microbiological Examination Of Windang Estate Bore Hole Samples'.

Ettler, V & Johan, Z 2014, '12 years of leaching of contaminants from Pb smelter slags: Geochemical/mineralogical controls and slag recycling potential', *Applied Geochemistry*, vol. 40, no. Supplement C, pp. 97-103.

Ettler, V, Johan, Z, Kříbek, B, Šebek, O & Mihaljevič, M 2009, 'Mineralogy and environmental stability of slags from the Tsumeb smelter, Namibia', *Applied Geochemistry*, vol. 24, no. 1, pp. 1-15.

Ettler, V, Piantone, P & Touray, JC 2003, 'Mineralogical control on inorganic contaminant mobility in leachate from lead-zinc metallurgical slag: experimental approach and long-term assessment', *Mineralogical Magazine*, vol. 67, no. 6, p. 1269.

Forbes Rigby Pty Ltd 1998, *Site Contamination Assessment Proposed Windang Subdivision*.

Gay, J 1995, 'Bioleaching of Heavy Metals from Copper Slag', Bachelor of Science (Honours) thesis, University of Wollongong

Gee, C, Ramsey, MH, Maskall, J & Thornton, I 1997, 'Mineralogy and weathering processes in historical smelting slags and their effect on the mobilisation of lead', *J. Geochem. Exploration*, vol. 58, no. 2-3, pp. 249-57.

Gorai, B, Jana, RK & Premchand 2003, 'Characteristics and utilisation of copper slag—a review', *Resources, Conservation and Recycling*, vol. 39, no. 4, pp. 299-313.

Kaksonen, AH, Särkijärvi, S, Peuraniemi, E, Junnikkala, S, Puhakka, JA & Tuovinen, OH 2017, 'Metal biorecovery in acid solutions from a copper smelter slag', *Hydrometallurgy*, vol. 168, pp. 135-40.

Kelly, DP & Harrison, AP 1989, 'Genus Thiobacillus, in; Bergey's Manual of Systematic Bacteriology', in JT Staley, MP Bryant, N Pfenning & JG Holt (eds), vol. 3, pp. 1842-59.

Kierczak, J, Potysz, A, Pietranik, A, Tyszka, R, Modelska, M, Néel, C, Ettler, V & Mihaljevič, M 2013, 'Environmental impact of the historical Cu smelting in the Rudawy Janowickie Mountains (south-western Poland)', vol. 124.

Kuo, S & Baker, AS 1980, 'Sorption of Copper, Zinc, And Cadmium by some Acid Soils', *Soil Sci. Soc. Am. J.*, vol. 44, pp. 969-74.

Kuo, S & McNeal, BL 1984, 'Effect of pH and Phosphate on Cadmium Sorption by a Hydrous Ferric Oxide', *Soil Sci. Soc. Am. J.*, vol. 48, pp. 1040-4.

Kurdi, F & Doner, HE 1983, 'Zinc And Copper Sorption An Interaction In Soils', *Soil Sci. Soc. Am. J.*, vol. 47, pp. 873-6.

Larsson, L, Olsso, G, Hoist, O & Karlsson, HT 1993, 'Oxidation of Pyrite by Acidianus Brierleyi: Importance of Close Contact between the Pyrite and the Microorganisms', *Biotechnology Letters*, vol. 15, no. 1, pp. 99-104.

Longhurst, S 2015, 'Groundwater Monitoring and Water Quality in Lake Illawarra: Contamination and Migration from Night Soil Deposits in the Port Kembla Sand Dunes', Bachelor of Environmental Science thesis, University of Wollongong

Lottermoser, BG 2002, 'Mobilization of Heavy Metals From Historical Smelting Slag Dumps, North Queensland, Australia', *Mineralogical Magazine*, vol. 66, no. 4, pp. 475-90.

Lottermoser, BG 2010, 'Mine Wastes: Characterization, Treatment and Environmental Impact: [2.1]: Early Historical Observations on Sulfide Oxidation and Acid Mine Drainage, [2.7]: Acid generation prediction', *Springer 3rd Edition*.

Manz, M & Castro, LJ 1997, 'The environmental hazard caused by smelter slags from the Sta. Maria de la Paz mining district in Mexico', *Environmental Pollution*, vol. 98, no. 1, pp. 7-13.

McBride, MB & Blasiak, JJ 1979, 'Zinc and Copper Solubility as a Function of pH In an Acidic Soil', *Soil Sci. Soc. Am. J.*, vol. 43, pp. 866-70.

McKenzie, La 1983, *Evidence Prepared For Land and Environment Court Of NSW*.

McLean, JE & Bledsoe, BE 1992, 'Behavior of Metals in Soils', *Ground Water Issue*.

Palma, J 2016, 'Water Quality in Lake Illawarra, New South Wales: Groundwater Contamination and Migration from Septic and Nightsoil Waste Deposits in the Coastal Windang Unconfined Sandy Aquifer', Bachelor of Environmental Science thesis, University of Wollongong

Partners, D 2012, 'Annual Report on Reactive Barrier Water Quality Testing – Proposed Subdivision Golf Place, Primbee', *Report No. 40239.03 for Port Kembla Golf Club*.

Perez, A & De Anta, RC 1992, 'Soil pollution in copper sulphide mining areas in Galicia (N.W. Spain)', *Soil Technology*, vol. 5, no. 3, pp. 271-81.

Piatak, NM, Parsons, MB & Seal, RR 2015, 'Characteristics and environmental aspects of slag: A review', *Applied Geochemistry*, vol. 57, no. Supplement C, pp. 236-66.

Piatak, NM & Seal, RR 2010, 'Mineralogy and the release of trace elements from slag from the Hegeler Zinc smelter, Illinois (USA)', *Applied Geochemistry*, vol. 25, no. 2, pp. 302-20.

Piatak, NM, Seal, RR & Hammarstrom, JM 2004, 'Mineralogical and geochemical controls on the release of trace elements from slag produced by base- and precious-metal smelting at abandoned mine sites', *Applied Geochemistry*, vol. 19, no. 7, pp. 1039-64.

Potysz, A 2015, 'Copper metallurgical slags: mineralogy, bio/weathering processes and metal bioleaching', Université Paris-Est.

Potysz, A, Grybos, M, Kierczak, J, Guibaud, G, Lens, PNL & van Hullebusch, ED 2016, 'Bacterially-mediated weathering of crystalline and amorphous Cu-slags', *Applied Geochemistry*, vol. 64, pp. 92-106.

Potysz, A, Kierczak, J, Fuchs, Y, Grybos, M, Guibaud, G, Lens, PNL & van Hullebusch, ED 2016, 'Characterization and pH-dependent leaching behaviour of historical and modern copper slags', *Journal of Geochemical Exploration*, vol. 160, pp. 1-15.

Potysz, A, Lens, PNL, van de Vossenberg, J, Rene, ER, Grybos, M, Guibaud, G, Kierczak, J & van Hullebusch, ED 2016, 'Comparison of Cu, Zn and Fe bioleaching from Cu-metallurgical slags in the presence of Pseudomonas fluorescens and Acidithiobacillus thiooxidans', *Applied Geochemistry*, vol. 68, pp. 39-52.

Potysz, A, van Hullebusch, ED, Kierczak, J, Grybos, M, Lens, PNL & Guibaud, G 2015, 'Copper Metallurgical Slags – Current Knowledge and Fate: A Review', *Critical Reviews in Environmental Science and Technology*, vol. 45, no. 22, pp. 2424-88.

Pugh, M 2002, 'Analysis of Contaminant Transport Mechanisms within an Unconfined Coastal Sand Aquifer' *(unpublished)*.

Reedy, JH & Machin, JS 1923, 'The Oxidation of Ferrous Sulfate to Ferric Sulfate by Means of Air', *Industrial & Engineering Chemistry*, vol. 15, no. 12, pp. 1271-2.

Scanes, P 2011, *Assessing the condition of estuaries and coastal lake ecosystems in NSW*.

Shi, C & Qian, J 2000, 'High Performance Cementing Materials from Industrial Slags - A Review'.

Smith, LA, Means, JL, Chen, A, Alleman, B, C.C., C, Jr.Tixier, JS, Brauning, SE, Gavaskar, AR & Royer, MD 1995, 'Remedial Options for Metals-Contaminated Sites'.

Sobanska, S, Ledésert, B, Deneele, D & Laboudigue, A 2000, 'Alteration in soils of slag particles resulting from lead smelting', *Comptes Rendus de l'Académie des Sciences - Series IIA - Earth and Planetary Science*, vol. 331, no. 4, pp. 271-8.

Southern Copper Pty Ltd 1992, *Investigation of the Geochemistry of Slag, Sand and Groundwater at Windang*.

Stanton, DA & Burger, RDT 1970, 'Studies on Zinc Selected Orange Free State soils: V. Mechanisms for reaction of zinc with iron and aluminium oxides', *Agrochemophysica*, vol. 2, pp. 65-76.

Starkey, RL 1945, 'Transformation of Iron by Bacteria in Water'.

Talpos, E, Buzatu, M & Predescu, C 2013, 'Chemical and Structural Assays and Analysis of the Leaching Behaviour and Acid Draining', *U.P.B. Sci. Bull., Series B*, vol. 75, no. 2.

Tessier, A, Campbell, PGC & Bisson, M 1980, 'Trace metal speciation in the Yamaska and St. François Rivers (Quebec)', *Canadian Journal of Earth Sciences*, vol. 17, no. 1, pp. 90-105.

Vítková, M, Ettler, V, Johan, Z, Kříbek, B, Šebek, O & Mihaljevič, M 2010, 'Primary and secondary phases in copper-cobalt smelting slags from the Copperbelt Province, Zambia', *Mineralogical Magazine*, vol. 74, no. 4, p. 581.

Yassini, I 1994, 'Copper Slag - An Analysis of Weathering Behaviour and Environmental Impact'.

Yassini, I & Council, WC 2003, *Pulsative Discharge of Dissolved Metals from Copper Slag Emplacements Into the Windang Unconfined Sandy Aquifer Adjacent to Lake Illawarra*, Wetlands (Australia).

Appendices

Appendix 1. Groundwater data sampled during this study

1a. Trace Metals

Table 20: Concentration of dissolved metals in groundwater sampled after a significant rain event on 31/3/17

Bore Depth (m)	LOR	4.03	3.28
Bore I.D.		BH2	BH9
Arsenic (mg/L)	0.001	0.014	0.002
Cadmium (mg/L)	0.0001	0.0001	0.0001
Copper (mg/L)	0.001	0.002	0.002
Manganese (mg/L)	0.001	0.038	0.067
Nickel (mg/L)	0.001	0.01	0.133
Lead (mg/L)	0.001	0.001	0.001
Selenium (mg/L)	0.01	0.01	0.01
Zinc (mg/L)	0.005	0.042	4.69
Iron (mg/L)	0.05	0.18	0.91

Table 21: Concentration of dissolved metals in groundwater sampled during a dry spell on 17/5/17

Bore Depth (m)	LOR	4.03	3.28	8
Bore I.D.		BH2	BH9	BH12
Arsenic (mg/L)	0.001	0.002	0.002	0.001
Cadmium (mg/L)	0.0001	0.0001	0.0001	0.0001
Copper (mg/L)	0.001	0.001	0.003	0.001
Manganese (mg/L)	0.001	0.05	0.097	0.02
Nickel (mg/L)	0.001	0.004	0.17	0.003
Lead (mg/L)	0.001	0.001	0.001	0.01
Selenium (mg/L)	0.01	0.01	0.01	0.01
Zinc (mg/L)	0.005	0.038	5.46	0.1
Iron (mg/L)	0.05	0.5	1.12	0.13
Turbidity (NTU)		24.4	3.75	299

D.O. (% Sat)		58	147	54
D.O. (mg/L)		5.01	12.25	4.76
pH		6.8	7.23	6.9
ORP (mv)		-32	176	-30
Salinity (ppt)		0.32	0.24	0.14
TDS (g/L)		0.4	0.3	0.2
E.C. (µS/cm)		650	492	284

Table 22: Dissolved metals in groundwater sampled after a significant rain event on 9/6/17

Bore Depth (m)	LOR	4.03	3.28	8	8.2	9.08
Bore I.D.		BH2	BH9	BH12	DR_NEW_EAST	DR_NEW_WEST
Arsenic (mg/L)	0.001	0.019	0.002	0.001	0.002	0.003
Cadmium (mg/L)	0.0001	0.0001	0.0001	0.0001	0.0001	0.0001
Copper (mg/L)	0.001	0.009	0.002	0.001	0.002	0.005
Manganese (mg/L)	0.001	0.037	0.078	0.023	0.018	0.023
Nickel (mg/L)	0.001	0.009	0.162	0.002	0.003	0.001
Lead (mg/L)	0.001	0.001	0.001	0.006	0.001	0.001
Selenium (mg/L)	0.01	0.01	0.01	0.01	0.01	0.01
Zinc (mg/L)	0.005	0.044	5.28	0.1	0.051	0.064
Iron (mg/L)	0.05	0.21	1.24	0.05	0.05	0.09
Turbidity (NTU)		6.7	14.5	108	77.9	111
D.O. (% Sat)		85.2	42.7	45.6	14.4	90.9
D.O. (mg/L)		7.7	3.83	4.13	1.24	8.1
pH		6.95	6.9	6.89	8.28	8.11
ORP (mv)		6	158	-18	210	275
Salinity (ppt)		0.26	0.23	0.14	0.2	0.22
TDS (g/L)		0.3	0.3	0.2	0.3	0.3
E.C. (µS/cm)		548	481	304	422	464

Table 23: Concentration of dissolved metals in groundwater sampled during a dry spell on 7/7/17

Bore Depth (m)	LOR	4.03	3.28	8	8.2	9.08
Bore I.D.		BH2	BH9	BH12	DR_NEW_EAST	DR_NEW_WEST
Arsenic (mg/L)	0.001	0.002	0.002	0.001	0.001	0.003
Cadmium (mg/L)	0.0001	0.0001	0.0001	0.0001	0.0001	0.0001
Copper (mg/L)	0.001	0.001	0.007	0.001	0.001	0.004
Manganese (mg/L)	0.001	0.071	0.066	0.021	0.041	0.057
Nickel (mg/L)	0.001	0.006	0.13	0.001	0.001	0.001
Lead (mg/L)	0.001	0.001	0.001	0.001	0.001	0.001
Selenium (mg/L)	0.01	0.01	0.01	0.01	0.01	0.01
Zinc (mg/L)	0.005	0.019	4.88	0.013	0.014	0.01
Iron (mg/L)	0.05	0.62	0.72	0.05	0.1	0.24
Turbidity (NTU)		8.4	5	2.5	1.1	4
D.O. (% Sat)		6.97	45.8	42.8	23.6	34.9
D.O. (mg/L)		6.27	4.09	3.85	2.11	3.12
pH		6.3	6.59	6.5	7.61	7.48
ORP (mv)		3	207	-54	171	211
Salinity (ppt)		0.42	0.23	0.16	0.23	0.23
TDS (g/L)		0.5	0.3	0.2	0.3	0.3
E.C. (µS/cm)		870	485	343	472	511

1b. Major ions

Table 24: Concentration of major ions in groundwater and lake water sampled on 7/7/17

Bore Depth (m)	LOR	4.03	3.28	8	8.2	9.08	
Bore I.D.		BH2	BH9	BH12	DR_NEW_EAST	DR_NEW_WEST	Lake
Hydroxide Alkalinity as $CaCO_3$ (mg/L)	1	1	1	1	1	1	1
Carbonate Alkalinity as $CaCO_3$ (mg/L)	1	1	1	1	1	1	1
Bicarbonate Alkalinity as $CaCO_3$ (mg/L)	1	140	63	97	115	205	136
Total Alkalinity as $CaCO_3$ (mg/L)	1	140	63	97	115	205	136
ED041G: Sulfate (Turbidimetric) as SO_4^{2-} by DA							
Sulfate as SO_4 - Turbidimetric (mg/L)	1	42	76	9	56	15	2170
ED045G: Chloride by Discrete Analyser							
Chloride (mg/L)	1	155	35	35	29	17	13700
ED093F: Dissolved Major Cations							
Calcium (mg/L)	1	53	37	13	30	37	394
Magnesium (mg/L)	1	7	8	17	11	20	1160
Sodium (mg/L)	1	94	32	23	43	30	9550
Potassium (mg/L)	1	5	3	3	4	5	360

Appendix 2. Dissolved trace metals in groundwater (Sampled in past studies)

2a. Southern Copper Pty Ltd (1992)

Table 25: Groundwater data collected in 1992 by Southern Copper Pty Ltd

Sample Date	Bore Depth (m)	Bore I.D.	Cadmium (mg/L)	Copper (mg/L)	Lead (mg/L)	Zinc (mg/L)	Iron (mg/L)	pH	E.C. (dS/cm)
15/05/1992	2	EGI-1	0.02	0.082	0.032	1.52	0.002	6.9	1.17
15/05/1992	2	EGI-2	0.008	0.63	0.011	5.2	0.069	5.3	0.218
15/05/1992	2	EGI-3	0.004	0.28	0.001	7.9	0.026	6.3	0.176
15/06/1992	2.5	WCC1	0.057	0.22	0.002	14.7	3.9	6.2	1.68
15/06/1992	6	WCC2	0.002	0.002	0.001	14.1	43	6.2	1.05

2b. Yassini (1994)

Table 26: Groundwater data collected in 1994 by Yassini

Sample Date	Bore Depth (m)	Bore I.D.	Arsenic (mg/L)	Cadmium (mg/L)	Copper (mg/L)	Manganese (mg/L)	Nickel (mg/L)	Lead (mg/L)	Selenium (mg/L)	Zinc (mg/L)	Iron (mg/L)	pH	ORP (mv)	E.C. (µS/cm)
1994	4	BH1	0.01	0.005	0.02	0.02		0.01		0.02	0.45	5.3	-151	200
1994	4	E1	0.01	0.005	0.002	0.052	0.005	0.01	0.01	0.01	2.12	5.7	-217	398
1994	8	E2	0.01	0.005	0.002	0.064	0.005	0.01	0.01	0.2	2.15	5.7		266
1994	3.6	BH8	0.01	0.005	0.01	0.09		0.01		0.17	0.29	5.3	-137	100
1994	3.6	E6	0.05	0.005	0.013	0.19	0.092	0.01	0.01	2.93	3.97	5.9	30	520
1994	4	WS1		0.02	0.06			0.05		8.8	1.24	6.4	-126	885
1994	4.7	WS1		0.045	0.02			0.05		4		5.5		155
1994	4	BH9	0.01	0.01	2.17	0.023	0.28	0.01	0.01	12	0.02	6.2	194	246
1994	8	BH12	0.01	0.005	0.008	0.152	0.12	0.01	0.01	4.15	3.13	6.2	36	423
1994	4	BH11			0.0481			0.0119		1.074	21.62	6.6	-98	440
1994	4	WCC 3						0.0101		4.56	14.99	6.4	-119	683
1994	4	BH7	0.01	0.005	0.01	0.02		0.02		0.02	0.03	7.7		1100
1994	8.5	BH5	0.01	0.005	0.1	0.23		0.01		0.1	1.7	7.1		51000

1994	4	BH6	0.01	0.005	0.01	0.11		0.01		0.05	0.16	7.2		800
1994	4	BH10	0.01	0.005	0.01	0.06		0.01		0.05	0.06	7.3		620

2c. Coffey Partners International Pty Ltd (1995)

Table 27: Groundwater data collected in 1995 by Coffey Partners International Pty Ltd

Sample Date	Bore Depth (m)	Bore I.D.	Arsenic (mg/L)	Cadmium (mg/L)	Copper (mg/L)	Manganese (mg/L)	Lead (mg/L)	Zinc (mg/L)	Iron (mg/L)	pH	E.C. (µS/cm)
18/05/1994	3.5	BH1	0.01	0.005	0.02	0.02	0.01	0.02	0.45	5.2	200
18/05/1994	4	BH2	0.01	0.005	0.01	0.1	0.01	0.02	0.22	6.7	7010
18/05/1994	7.95	BH3	0.01	0.005	0.01	0.2	0.01	0.08	0.13	7.3	700
18/05/1994	4	BH4	0.01	0.005	0.01	0.5	0.01	0.01	0.42	6.9	1100
18/05/1994	8.7	BH5	0.01	0.005	0.1	0.23	0.01	0.1	1.7	7.1	19900
18/05/1994	4	BH6	0.01	0.005	0.01	0.11	0.01	0.05	0.16	7.2	800
18/05/1994	3.9	BH7	0.01	0.005	0.01	0.02	0.02	0.02	0.03	7.7	1100
18/05/1994	3.6	BH8	0.01	0.005	0.01	0.09	0.01	0.17	0.29	6.2	100
18/05/1994	4	BH9	0.01	0.08	0.15	0.23	0.03	34	0.14	6.6	1300
18/05/1994	4	BH10	0.01	0.005	0.01	0.06	0.01	0.05	0.06	7.3	700

2d. Gay (1995)

Table 28: Groundwater data collected in 1995 by Gay

Sample Date	Wet/Dry	Bore Depth (m)	Bore I.D.	Cadmium (mg/L)	Copper (mg/L)	Lead (mg/L)	Zinc (mg/L)	pH	TDS (g/L)	E.C. (µS/cm)
3/04/1995	Wet	4	BH2	0.0044	0.0058	0.0013	0.027	6.36	0.42	627
3/04/1995	Wet	4	BH9	0.023	0.35	0.0007	25	5.7	0.5	548
3/04/1995	Wet	3.6	BH8	0.0017	0.001	0.0029	0.27	4.4	0.14	628
3/04/1995	Wet	4	BH10	0.001	0.001	0.0005	0.005	7.09	0.41	515
27/08/1994	Dry	4	BH2	0.0001	0.0005	0.0019	0.01			
27/08/1994	Dry	4	BH9	0.021	0.122	0.001	18			

27/08/1994	Dry	3.6	BH8	0.0001	0.0005	0.0011	0.089			
27/08/1994	Dry	4	BH10	0.0001	0.004	0.0006	0.01			

2e. Coffey Partners International Pty Ltd (1996)

Table 29: Groundwater data collected in 1996 by Coffey Partners International Pty Ltd

Sample Date	Wet/Dry	Bore Depth (m)	Bore I.D.	Copper (mg/L)	Zinc (mg/L)
07/1995	Dry	4.5	BH11	0.01	1
07/1995	Dry	8.1	BH12	0.01	2.7
07/1995	Dry	6.3	BH13	0.01	0.03
07/1995	Dry	4.5	BH14	0.01	0.05

2f. Forbes Rigby Pty Ltd (1998)

Table 30: Groundwater data collected in 1998 by Forbes Rigby Pty Ltd

Sample Date	Bore Depth (m)	Bore I.D.	Cadmium (mg/L)	Copper (mg/L)	Lead (mg/L)	Zinc (mg/L)	pH	E.C. (µS/cm)
01/1998	3	WS1	0.02	0.06	0.05	8.8	6	885
01/1998	3	WS2	0.045	0.02	0.05	4	5.5	155
01/1998	3	WS3	0.02	0.02	0.05	0.15	7.1	1065
01/1998	3	WS4	0.02	0.02	0.05	0.1	6.7	800
01/1998	3	WS5	0.02	0.02	0.05	0.19	6.8	675
01/1998	3	WS6	0.02	0.02	0.05	0.11	6.1	690

2g. Longhurst (2015)

Table 31: Groundwater data collected in 2015 by Longhurst

Sample Date	Wet/Dry	Bore Depth (m)	Bore I.D.	Cadmium (mg/L)	Copper (mg/L)	Lead (mg/L)	Zinc (mg/L)	Iron (mg/L)	D.O. (% Sat)	D.O. (mg/L)	pH	ORP (mv)	Salinity (ppt)	E.C. (µS/cm)
20/07/2015		4	WP1-4	0.0001	0.006	0.001	0.02		82.8	8.27	6	-62	0.15	337
20/07/2015		12	WP1-12	0.0001	0.001	0.002	0.005		62	5.75	8	-8	0.52	1079

20/07/2015			BH10	0.0001	0.001	0.001	0.012	0.29					
20/07/2015			BH4	0.0001	0.001	0.001	0.005	9.1					
13/08/2015	Dry	4	WP1-4	0.0001	0.001	0.001	0.052	0.64	42.9	4.33	6.3	-10	0.13	253
13/08/2015	Dry	8	WP1-8						21.2	2.05	8.1	-12	0.4	760
13/08/2015	Dry	12	WP1-12	0.0001	0.001	0.001	0.026	4.68	23.5	2.26	7.7	-22	0.54	1032
13/08/2015	Dry	4	WP2-4	0.0001	0.009	0.001	0.129	3.19	45.2	4.44	7.2	161	0.44	857
13/08/2015	Dry	8	WP2-8	0.0001	0.002	0.001	0.034	5.41	7.9	0.75	7.2	32	0.45	879
13/08/2015	Dry	12	WP2-12	0.0001	0.001	0.001	0.023	0.74	13	1.24	8	-29	0.88	1622
13/08/2015	Dry	4	WP3-4	0.0001	0.003	0.001	0.023	1.02	18	1.77	6.1	35	0.09	164
13/08/2015	Dry	8	WP3-8	0.0001	0.004	0.001	0.012	0.68	16.5	1.6	6.5	50	0.12	251
13/08/2015	Dry	12	WP3-12	0.0001	0.001	0.001	0.008	0.18	8.5	0.82	8.4	-118	0.78	1448
13/08/2015	Dry	4	WP4-4	0.0001	0.004	0.002	0.027	0.24	21.2	2.06	8.6	209	0.32	617
13/08/2015	Dry	8	WP4-8	0.0001	0.012	0.001	0.005	0.1	27.6	1.94	8	263		8000
13/08/2015	Dry	12	WP4-12	0.0001	0.01	0.001	0.005	0.1	47.9	3.21	7.8	234	57.28	8000
13/08/2015	Dry		BH10	0.0001	0.001	0.001	0.012	0.29	49.4	4.78	7.4	-141	1.21	2200
13/08/2015	Dry		BH4	0.0001	0.001	0.001	0.005	9.1	13.4	1.21	7	54		1294
27/08/2015	Wet	4	WP1-4						0.8	0.08	5.3		0.14	318
27/08/2015	Wet	8	WP1-8	0.0001	0.002	0.001	0.023	0.37	0.7	0.07	8.2		0.42	858
27/08/2015	Wet	12	WP1-12	0.0001	0.001	0.001	0.006	4.72	0.9	0.09	7.9		0.52	1051
27/08/2015	Wet	4	WP2-4						6.4	0.65	7.8		0.31	621
27/08/2015	Wet	8	WP2-8	0.0001	0.002	0.001	0.028	5.06	1.5	0.13	8.2		0.39	829
27/08/2015	Wet	12	WP2-12						4.7	0.44	8.6		0.79	1527
27/08/2015	Wet	4	WP3-4	0.0001	0.001	0.001	0.006	0.99	2.6	0.25	6.8		0.1	201
27/08/2015	Wet	8	WP3-8						8.5	0.81	7.6		0.13	280
27/08/2015	Wet	12	WP3-12						2.8	0.26	9		0.75	1474
27/08/2015	Wet	4	WP4-4	0.0001	0.001	0.001	0.014	0.29	6.2	0.58	8.6		0.3	623
27/08/2015	Wet	8	WP4-8						2.5	0.17	9.4		52.21	8000
27/08/2015	Wet	12	WP4-12						1.2	0.08	9.3		55.88	8000
27/08/2015	Wet		BH10	0.0001	0.001	0.001	0.005	0.05	3.6	0.31	8.9		1.29	2474
27/08/2015	Wet		BH4	0.0001	0.001	0.001	0.008	9.5	11	1.02	7.8		0.66	1303

Appendix 3. Grain size analysis

Table 32: Grain size analysis by depth performed by slag obtained from sample pit (b)

Percent passing		Depth									
		0.05m	0.30m	0.40m	0.65m	0.75m	0.90m	1.05m	1.25m	1.35m	1.50-1.55m
Particle Size	4mm	100.00	100.00	100.00	100.00	100.00	100.00	100.00	100.00	100.00	100.00
	3.35mm	100.00	100.00	99.65	98.87	98.69	96.02	94.21	99.48	98.75	99.41
	2.8mm	100.00	99.16	99.47	97.73	98.50	94.99	93.72	98.76	97.79	98.46
	2.36mm	100.00	99.16	98.51	95.61	97.09	94.02	91.56	96.82	96.28	97.14
	2mm	100.00	98.44	97.06	91.92	93.22	89.68	87.43	93.79	93.20	92.81
	1.7mm	100.00	96.62	94.86	87.59	87.24	82.84	80.45	86.90	86.71	87.05
	1.4mm	100.00	93.96	90.87	79.15	77.09	72.04	71.63	77.40	77.51	78.12
	1mm	100.00	86.00	82.64	64.18	61.21	55.83	58.17	62.17	61.88	62.81
	0.05mm	18.20	2.43	0.66	5.39	9.21	9.57	7.19	7.00	7.81	1.83
	0.002mm	3.55	0.00	0.00	0.57	1.01	1.22	0.68	0.86	0.93	0.03

Appendix 4. Typical chemical composition of slag (Gorai et al., 2003)

Table 33: Typical chemical composition of slag, based on analysis performed on slag from various sources (see bottom of table)

	Fe (%)	SiO_2 (%)	CaO (%)	MgO (%)	Al_2O_3 (%)	S (%)	Cu (%)	Co (%)	Mn (%)	Ni (%)	Zn (%)
1	44.78	40.97	5.24	1.16	3.78	1.06					
2	39.65	31.94	3.95	2.82	2.4		1.01	0.104	0.042	0.015	0.722
3	41.53	37.13				0.11	0.79				
4	47.8	29.9					0.7				
5	46.2	30.25	2.75			0.6	0.725			0.0017	0.2275
6	47.13					1.47	0.68	0.22	0.03	0.05	0.05
7	44	28					0.6	0.13		0.06	
8	47.8	26.1	0.7	1	6.8	1.5	0.82	0.4			0.15
9	44.8	24.7	10.9	1.7	15.6	0.28	2.1		0.4		
10	34.62	27.16	17.42	3.51	14.7	0.33	1.64		0.49		
Minimum	34.62	24.7	0.7	1	2.4	0.11	0.6	0.104	0.03	0.0017	0.05
Maximum	47.8	40.97	17.42	3.51	15.6	1.5	2.1	0.4	0.49	0.06	0.722
Range	13.18	16.27	16.72	2.51	13.2	1.39	1.5	0.296	0.46	0.0583	0.672
Average	43.83	30.6833	6.82667	2.038	8.656	0.76	1.0072	0.2135	0.2405	0.031675	0.287375

(1) Iranian National Copper Industries Co, (Marghussian and Maghsoodipoor, 1999)
(2) Etibank Ergani Copper Plant, Elazig-Turkey (Kiyak et al., 1999).
(3) Caletone Smelter Chile (Imris et al., 2000)
(4-7) Indian Copper Plants (Agrawal et al., 2000)
(8) Kure Copper Slag (Yucel et al., 1992)
(9-10) Copper Queen, Prince, USA (Mobasher et al., 1996).

Appendix 5. Elemental composition of soil within the Windang copper slag emplacement and surrounding areas outside the emplacement (Jones, 2017)

Table 34: XRF analysis performed on soil within the Windang copper slag emplacement, and in areas surrounding the emplacement

	W1	W2	W3	W4	W5	W6	MT1	W7	W8
Easting	304635	304786	304909	304556	304748	304875	304868	304558	304778
Northing	6178302	6178278	6178260	6178059	6178018	6177979	6177977	6177818	6177901
Cl (ppm)	346.6	179.4	90.9	734.4	269.7	74.7	53.3	380.8	162.5
V (ppm)	77.2	14	37.2	50.7	133.8	38.5	39.5	40.1	56.1
Cr (ppm)	128.1	262.6	370.3	47.3	367.4	341.2	402.6	236.7	573.7
Co (ppm)	16.4	15.6	12.2	3	14.4	18.1	29.5	81.7	51.2
Ni (ppm)	14.3	12.3	41.8	6.9	117.9	59.2	63.1	21.6	309
Cu (ppm)	82.7	267.1	1487	77.3	3440	2223	1929	538.4	2913
Zn (ppm)	371.3	1988	12530	219.9	28210	15060	10900	4120	22520
Ga (ppm)	13.3	0.7	16	2.6	31.5	8.6	7.1	4.3	16.1
Ge (ppm)	2.4	2.2	0.3	0.5	0.5	0.5	0.5	1.2	0.5
As (ppm)	6.3	0.5	0.5	4.9	17.7	2	7	33	11.1
Se (ppm)	0.4	0.5	2.3	0.2	2.5	3	2.7	1.6	3.8
Br (ppm)	8.8	5.1	1.2	170.4	6.8	2.2	3	19.7	4
Rb (ppm)	48.3	13.6	23.7	12.1	37.7	18.3	19.1	14.6	26.1
Sr (ppm)	155	25.6	57.3	300.5	253.4	54	69.8	76.5	127.8
Y (ppm)	23.8	4.3	10.8	2.9	19.5	9.3	11.6	4.5	14.7
Zr (ppm)	202.4	49.3	91.4	21.3	208.3	89.2	135	179.7	273.9
Nb (ppm)	7	1.9	3	1.1	4.7	2.6	3.5	3.6	5.6
Mo (ppm)	1	1	24.2	1	39.8	1	1	1	84.6
Cd (ppm)	0.4	0.3	0.2	0.9	0.4	0.4	0.1	1.5	1.4
Sn (ppm)	19.1	94.9	272	26	967.9	432.8	294	300.4	588.6
Sb (ppm)	0.2	1.9	3	10.7	33.9	3	3	14.8	3
Cs (ppm)	12.2	0.5	4	37.1	4	4	4	4	4
Ba (ppm)	337.6	96.4	154.4	87.5	334.7	180.7	172.6	131.7	518.8
La (ppm)	36.7	26.5	20.5	33.3	2	2	10	8.2	2
Ce (ppm)	154	2	2	2	55.8	2	2	2	2

Hf (ppm)	5.2	1	0.2	0.9	9.7	0.8	3.1	1.1	3.7
Ta (ppm)	1.2	3.4	1	5.5	1.4	1	1	1	1
W (ppm)	1	1	32.8	1	137.6	59.6	41.5	12.4	90.6
Hg (ppm)	1.8	2.7	0.9	1	1.8	1.3	1.1	0.5	1.6
Pb (ppm)	65.3	131.7	1357	45.1	3602	2509	1844	733.1	2952
Bi (ppm)	0.4	0.5	9.5	0.2	28.1	15.7	13.3	10.4	17.6
Th (ppm)	9.8	1	4	1	7.2	3	4.4	1.8	5.1
U (ppm)	1.9	1	4.2	5.3	6	2.9	2.7	2.4	6.9

	W9	**W10**	**W11**	**W12**	**W13**	**W14**	**W15**	**W16**	**S22**	**S23**
Easting	304964	304706	304600	304733	304459	304717	304844	305036	305137	304777
Northing	6177749	6177682	6177509	6177511	6177525	6177297	6177480	6178233	6178465	6178545
Cl (ppm)	262	334.7	178.7	164.7	214.9	166.2	222.9	126.2	145.2	249
V (ppm)	46.4	90.1	28.2	44.8	42.9	17	19.7	8.6	5.1	166
Cr (ppm)	140.5	325.2	233.6	342.8	256	269.7	277.5	273.5	189.3	70.9
Co (ppm)	12.5	699.4	13.4	159.1	11.6	6.9	12.8	8.9	1.5	21.7
Ni (ppm)	12.3	258.1	10.2	44.5	10.5	6.1	11.4	5.9	4.4	17.1
Cu (ppm)	68.1	2930	64.4	811.3	78.7	24.4	46.8	20.6	30.6	120.8
Zn (ppm)	136.4	13440	128.3	3708	140.3	80	124.5	30.2	68.6	167.5
Ga (ppm)	13	0.5	2.9	0.5	5.7	0.2	2.9	0.2	0.8	13
Ge (ppm)	1.6	0.5	2.1	0.2	1.4	1.7	1.4	0.3	1	1.7
As (ppm)	5.4	106.1	5.4	37.9	3.5	1.8	2.8	1.3	0.7	2.2
Se (ppm)	0.3	6.3	0.3	2	0.5	0.2	0.2	0.2	0.5	0.5
Br (ppm)	5.2	14.6	6	8.9	20.6	9.3	7.4	4.9	4.1	29.6
Rb (ppm)	39.8	31.2	19.3	20.6	23.6	13	16.3	12.4	8.6	56.3
Sr (ppm)	89.1	173.1	50.8	82.2	89.1	38.8	47.2	23.7	25.3	451.2
Y (ppm)	16.6	14.3	7.7	8.2	7.4	3.8	5.1	4.1	3	28.6
Zr (ppm)	219.1	298.9	162.1	136.1	77.5	122.1	78.9	101.2	39	163.1
Nb (ppm)	6.8	6.4	3.8	3.8	2.6	3.4	2.3	2.5	1.3	5.6
Mo (ppm)	1	1	1	1	1	1	1	1	0.5	0.5
Cd (ppm)	1.2	0.2	0.3	2	0.4	0.9	1.2	1.1	1	1

Sn (ppm)	31.4	711.1	17.4	169.7	16.9	22.9	32.2	28.2	8.7	6.7
Sb (ppm)	8.9	97.3	1.8	24.3	2.1	7.4	8.5	7.9	1.5	1.5
Cs (ppm)	24.7	4	2.9	4	4	25	23.7	22.6		
Ba (ppm)	410.7	537.8	117.7	173.4	140.8	81.8	110.6	91.9	71.7	569.4
La (ppm)	35	2	20.8	21.1	11.6	2	2	20.7		
Ce (ppm)	2	2	2	48.7	2	2	2	2		
Hf (ppm)	4.3	14.8	1.5	2	1.1	1.6	1.2	0.8	0.5	5.8
Ta (ppm)	2.1	5.1	1.9	1	0.7	2.6	3.3	1.2		
W (ppm)	1	70.3	1	8.4	1	1	1	1	0.5	0.5
Hg (ppm)	1.1	1.8	0.5	0.8	1.1	1.3	1.8	0.5	0.5	0.5
Pb (ppm)	47.1	7544	46.4	2893	96.3	15.3	60.1	12.3	14.8	43.3
Bi (ppm)	0.2	52.3	0.2	22.1	1.4	0.2	0.2	0.2	1.2	0.5
Th (ppm)	7.1	8	0.4	3.7	0.6	1	1	1	0.5	6.7
U (ppm)	0.6	55.7	1	17.7	1	1	1	1	0.5	3

Appendix 6. Windang copper slag emplacement - elemental composition by depth

Table 35: XRF analysis performed on copper slag obtained at various depths from sample pit (b)

Depth	0m	0.05m	0.3m	0.4m	0.65m	0.75m	0.9m	1.05m	1.25m	1.35m	1.5m	1.55m
Cl (ppm)	53	75	24	78	30	2				2	53	
V (ppm)	40	27	49	48	4	42	1	1	1	47	72	1
Cr (ppm)	403	317	1037	1189	291	782	3079	3467	2812	766	666	3540
Co (ppm)	30	21	20	21	8	3	32	32	42	3	86	60
Ni (ppm)	63	24	65	51	9	205	397	370	378	185	175	440
Cu (ppm)	1929	734	6811	5522	321	6181	739	695	710	5774	6157	714
Zn (ppm)	10900	3794	41150	46400	496	60200	26600	26560	26060	56390	43700	26700
Ga (ppm)	7	3	28	41	1	86	112	124	125	75	26	124
Ge (ppm)	0.5	1	0.5	0.5	1	0.5	4	3.9	4	0.5	0.5	4.1
As (ppm)	7	1	0.5	0.5	1	15	37	27	33	20	0.5	24
Se (ppm)	3	1	0.8	0.8	0.2	0.8	0.9	1	1	0.9	0.8	1
Br (ppm)	3	2	0.5	0.5	1	0.6	0.6	0.6	0.6	0.6	0.5	0.6
Rb (ppm)	19	14	31	27	11	17	23	23	22	18	25	20
Sr (ppm)	70	53	107	74	16	141	187	190	191	141	146	196
Y (ppm)	12	5	18	19	4	10	12	12	12	8	31	10
Zr (ppm)	135	83	163	170	65		283	287	279		184	332
Nb (ppm)	4	2	4	1	2		0.4	0.4	0.4		1	0.4
Mo (ppm)	1	1	417	258	1		223	162	214		124	152
Cd (ppm)	0.1	1	1	1	0	2	1	1	2	1	3	2
Sn (ppm)	294	192	568	632	40	1834	1427	1478	1410	1631	1298	1686
Sb (ppm)	3	9	3	3	5	32	87	91	90	24	33	139
Cs (ppm)	4	4	4	4	17	4	18	18	18	4	4	19
Ba (ppm)	173	137	344	238	89	205	424	407	456	299	328	372
La (ppm)	10	2	2	2	40	2	39	102	38	2	2	39
Ce (ppm)	2	2	2	2	2	2	34	65	35	2	2	34
Hf (ppm)	3	2	12	0.7	1	1	39	19	32	1	3.3	30
Ta (ppm)	1	1	2.3	1	7	7	44	22	18	1	16	31
W (ppm)	42	6	232	254	1	363	515	518	507	332	251	539

Hg (ppm)	1.1	1	3.4	3.5	1	4.4	4.1	4.1	4	4.2	3.9	4.4
Pb (ppm)	1844	620	3464	3337	72	6259	7756	7666	7422	5927	4936	8725
Bi (ppm)	13	5	2	7	0.2	33	24	30	29	30	16	34
Th (ppm)	4	1	7	6	1		28	25	23		4	26
U (ppm)	3	1	2	1	1		3	2.6	2		4	4

Appendix 7. SEM/EDS analysis

7a. Sample MD – site 1

Figure 56: Locations of various spectra obtained at Site 1 of sample MD

Table 36: Elemental composition of material at each spectrum (wt. %)

Spectrum Label	C	O	Mg	Al	Si	P	S	Cl	K	Ca	Ti	Fe	Co	Ni	Cu	Zn	In	Sn	Pb
Spectrum 3	7.33	36.1		1.35	5.21		6.17					15.78	0		6.55	2.36			19.14
Spectrum 4	9.01	36.24		1.39	4.95		6.11		0.22			16.24			5.68	1.65			18.52
Spectrum 5	52.99	26.95		0.71	4.33		0.45	5.71				8.21				0.42		0.23	
Spectrum 6	40.4	30.87		1.26	6.34		0.58	5.19		0.2		13.98				1.19			
Spectrum 7	22.52	34.99		1.31	9.38		0.81	6.2		0.34		22.18				2.27			
Spectrum 8	47.64	28.28		0.72	4.63	0.15	0.51	5.81		0.16		10.82				0.76			0.54
Spectrum 9	31.4	34.11		1	7.28		0.74	6.3		0.18		17.02				1.25			0.71
Spectrum 10	7.08	34.02	0.69	1.75	14.07		0.74			0.33		32.52				7.25			1.55
Spectrum 11	7.19	34.22		1.79	14.16		0.82			0.35		32.58				7.47			1.43
Spectrum 12	7.21	33.84		1.69	13.92		0.73			0.43		33.98				6.99			1.21
Spectrum 13	7.94	30.85	0.55	1.62	12.61		1.84		0.14	0.39		29.92		0.52	5.14	6.6			1.87
Spectrum 14	5.32	33.21	0.71	1.65	14.32		0.81			0.45		32.67			0.98	7.98	0.42		1.48
Spectrum 15	7.39	37.87		1.04	6.25		6.81		0.81			20.76			3.7				15.37
Spectrum 16	7.85	40.97		1.15	6.09		6.78		1.39			20.66			2.11				12.98

Spectrum 17	12.86	39.76		1.05	5.68		6.73		1.56			20.36			1.58				10.42
Spectrum 18	9.5	42.33		1.24	7.6		1.53					36.32				0.65			0.84
Spectrum 19	9.28	40.85		2.15	8.49		1.43					37.8							
Spectrum 20	12.64	24.19		1.23	8.94		1.07	0.11				50.36						0.71	0.75
Spectrum 21	7.48	43.45		1.35	8.72		1.83					37.18							
Spectrum 22	7.65	39.89		1.28	8.7		1.3			0.15		41.02							
Spectrum 23	7.53	49.18		3.63	27.72		1.18				0.3	9.87						0.6	
Spectrum 24	9.15	46.49		1.9	23.97		0.63				0.21	15.96				0.85		0.84	
Spectrum 25	8.49	45.89		2.1	23.42		0.8					18.56						0.73	
Spectrum 26	9.03	45.14		1.59	16.29		1.01				0.21	26.38						0.37	
Spectrum 27	12.42	45.51		1.83	22.34		0.64				0.27	16.14						0.84	
Spectrum 28	7.68	48.91		3.62	27.22		1.27				0.26	9.14						0.74	1.16
Spectrum 29	7.96	49.98		3.31	29.05		0.5				0.24	8.31						0.65	
Spectrum 30	8.5	49.48		3.51	27.65		1.66				0.19	8.39						0.63	
Spectrum 31	10.15	51.57		2.74	27.19		1.14					7.2							
Spectrum 32	11.88	45.44		3.48	24.92		1.15				0.23	12.39						0.52	

Spectrum 33	8.06	47.14		2.38	24.98		0.94				0.28	15.51						0.72	

Table 37: Overview of the elemental composition at site 1 in Sample MD, based on data from all spectra (wt. %)

Statistics	C	O	Mg	Al	Si	P	S	Cl	K	Ca	Ti	Fe	Co	Ni	Cu	Zn	In	Sn	Pb
Max	52.99	51.57	0.71	3.63	29.05	0.15	6.81	6.3	1.56	0.45	0.3	50.36	0	0.52	6.55	7.98	0.42	0.84	19.14
Min	5.32	24.19	0.55	0.71	4.33	0.15	0.45	0.11	0.14	0.15	0.19	7.2	0	0.52	0.98	0.42	0.42	0.23	0.54
Average	13.6	39.6		1.83	14.4		1.89					21.88							
Standard Deviation	12.3	7.5		0.87	8.68		2.1					11.57							

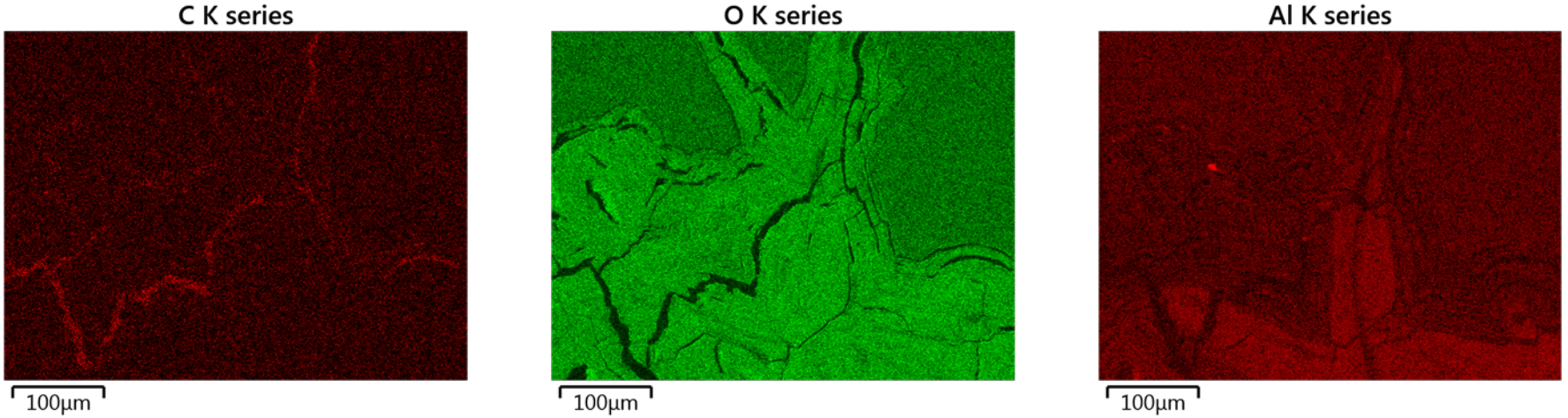

Si K series

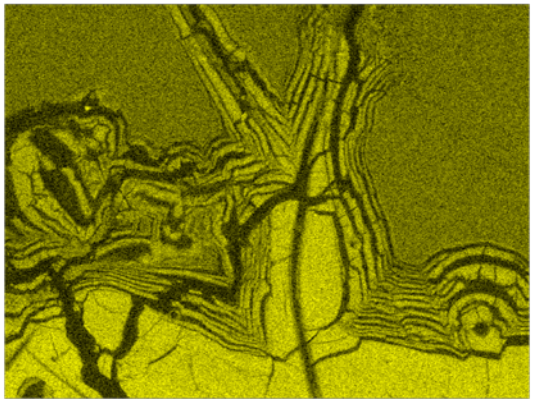

S K series

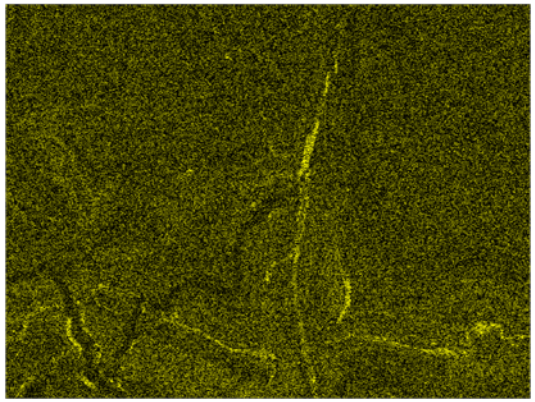

Cl K series

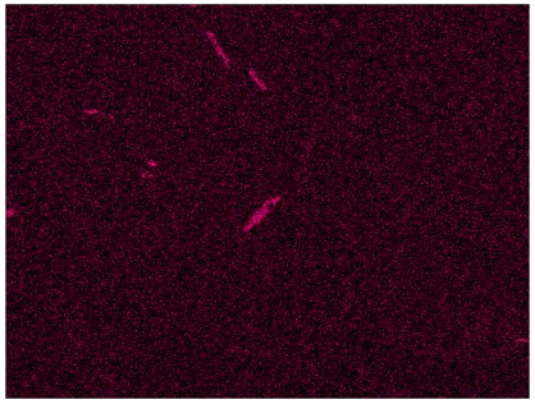

Ca K series

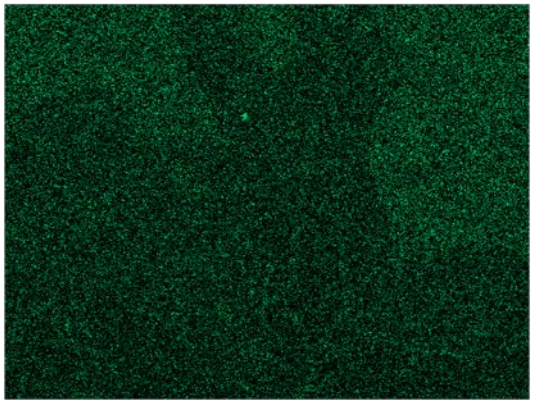

Ti K series

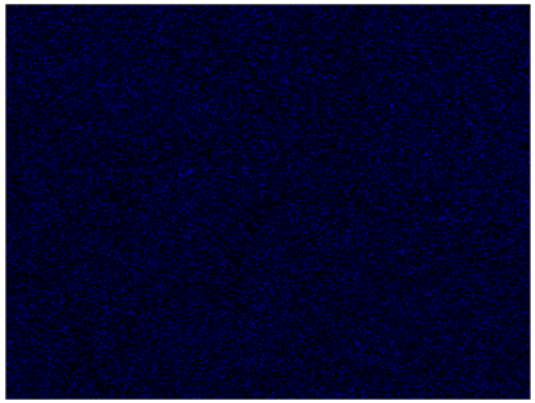

Fe K series

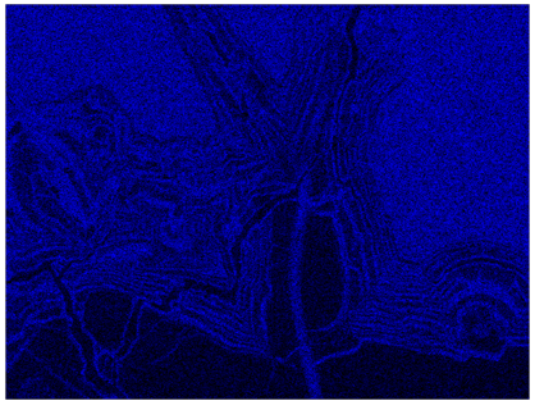

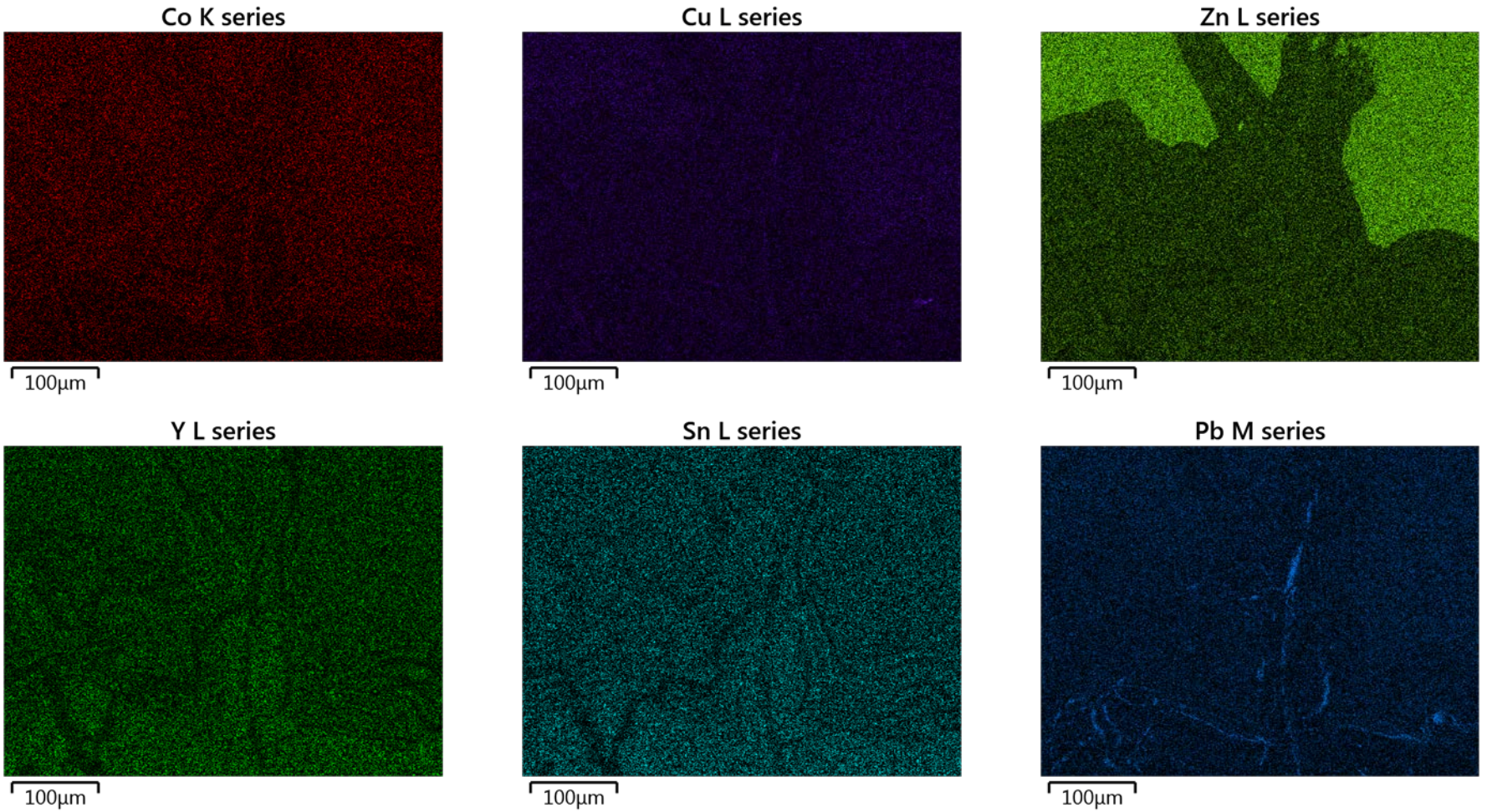

Figure 57: Element maps showing the spatial distribution of various elements at site 1 in sample MD

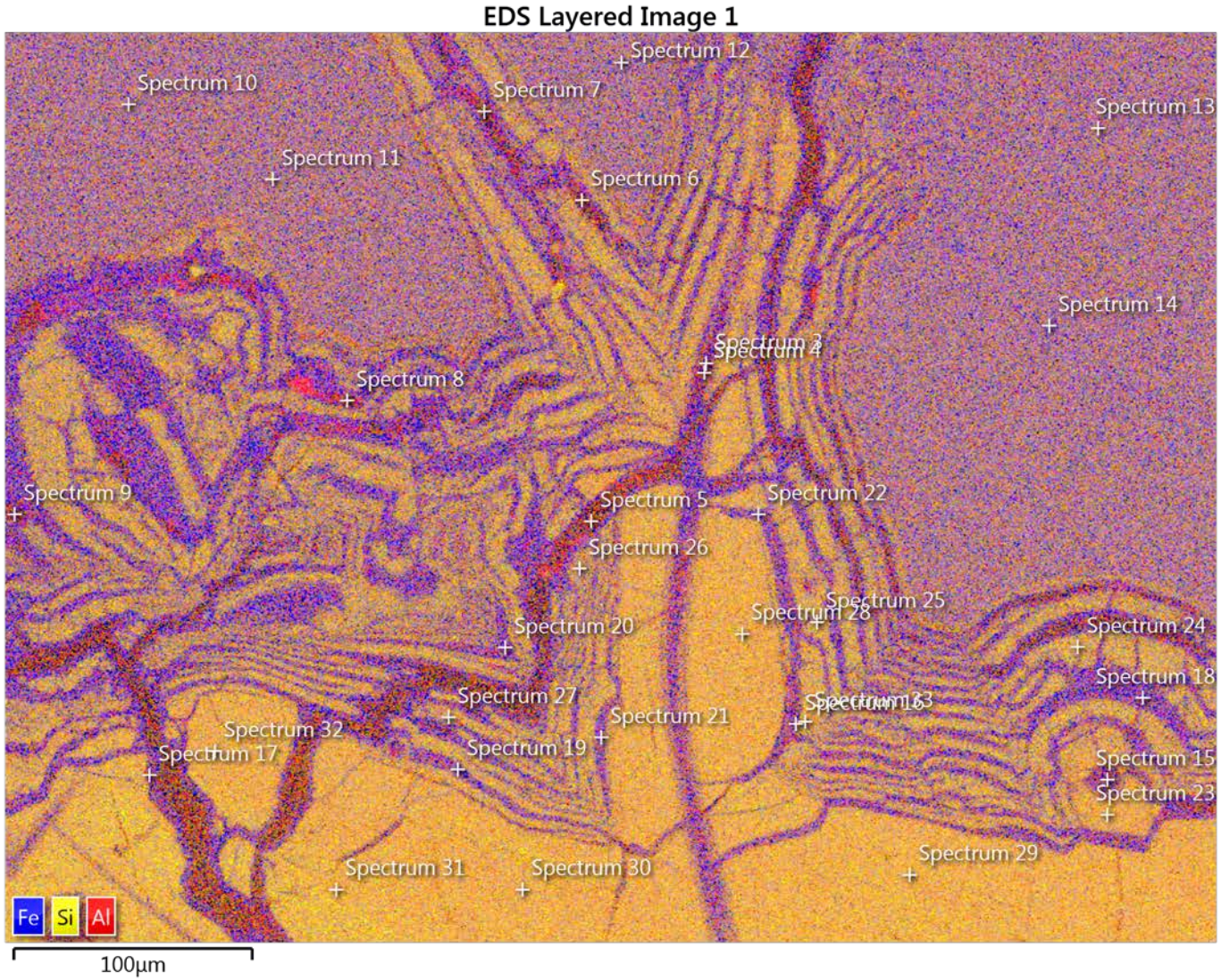

Figure 58: Layered element map showing the spatial distribution of iron, silicon and aluminium at site 1 in sample MD

7b. Sample MD – site 2

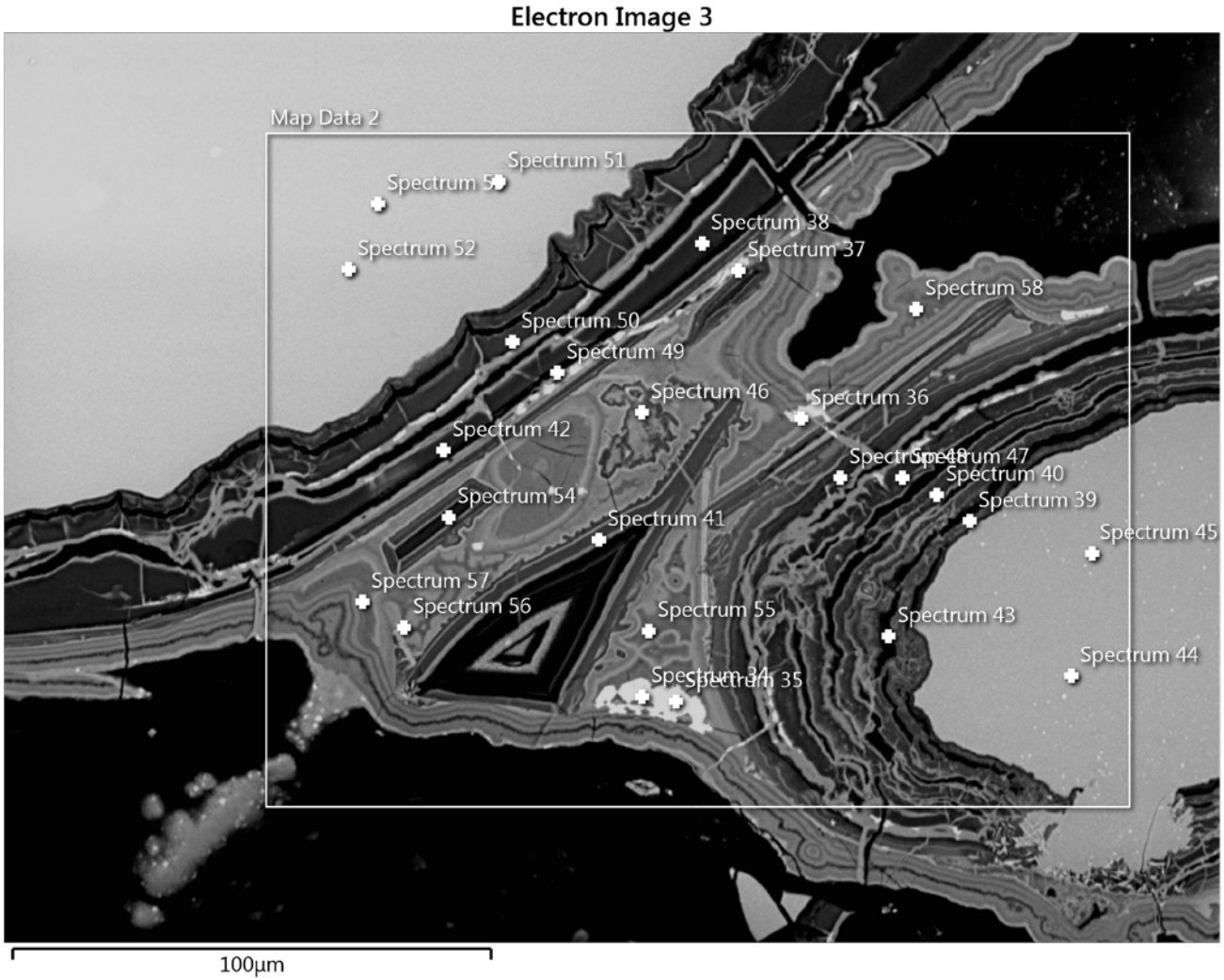

Figure 59: Locations of various spectra obtained at Site 2 of sample MD

Table 38: Elemental composition of material at each spectrum (wt. %)

Spectrum Label	C	O	Mg	Al	Si	S	Cl	K	Ca	Ti	Fe	Cu	Zn	Sn	Pb
Spectrum 34	18.94	33.25		1.19	2.57	5.32		0.28			14.46	6.31	1.33		16.34
Spectrum 35	16.34	33.13		1.2	2.7	5.62					15.03	6.66	1.35		17.98
Spectrum 36	14.25	35.46		1.33	3.33	5.19					17.2	5.59	1.75		15.92
Spectrum 37	15.09	36.13		1.71	7.75	1.92					31.26		1.12		5.03
Spectrum 38	18	44.11		2.88	23.64	0.46			0.21		9.84		0.87		
Spectrum 39	16.83	45.1		3.81	12.99	0.49			0.17	0.23	19.02			0.45	0.9
Spectrum 40	18.15	43.68		2.71	17.03	0.53			0.15		16.41		0.77	0.57	
Spectrum 41	17.86	39.27		2.92	12.44	0.73			0.28		25.4		1.1		
Spectrum 42	16.57	44.93		2.85	22.41	0.45			0.2	0.16	10.67		0.92		0.85
Spectrum 43	48.24	26.82		1.32	5.06	0.44	3.47		0.19		13.17		0.65		0.64
Spectrum 44	19.04	35.22	0.62	1.53	11.39	0.58		0.15	1.09		23.86		5.58		0.94
Spectrum 45	16.58	35.19	0.66	1.58	12.05	0.68			1.13		26.03		6.11		
Spectrum 46	13.33	41.22	0.99	2.22	13.8	0.36			6.79		19.66		1.61		
Spectrum 47	18.62	43.9		2.38	20.75	0.39					12.51		0.77	0.7	
Spectrum 48	18.06	43.23		2.78	19.16	0.64			0.22		15.24		0.66		
Spectrum 49	18.85	42.31		2.72	20.55	0.64			0.22	0.17	13.66		0.87		
Spectrum 50	16.27	44.29		2.82	21.23	0.4					12.92		0.98		1.08
Spectrum 51	15.2	36.97		1.78	13.12	0.58		0.18	0.52		22.62		7.43		1.61
Spectrum 52	15.08	36.95	0.69	1.69	12.96	0.54		0.18	0.48		22.43		7.37		1.65
Spectrum 53	13.73	35.84	0.67	1.74	13.14	0.56		0.24	0.51		22.89	1.1	7.97		1.59
Spectrum 54	17.17	45.67		2.76	21.9	0.61			0.21		11.02		0.66		
Spectrum 55	15.56	41.33		2.91	4.9	2.57					32.73				
Spectrum 56	14.82	38.52		1.25	7.89	0.81					35.28				1.42
Spectrum 57	14.97	41.12		2.75	4.81	2.52					32.97		0.85		
Spectrum 58	17.77	40.24		2.23	5.94	2.22					30.92		0.69		

Table 39: Overview of the elemental composition at site 2 in Sample MD, based on data from all spectra (wt. %)

Statistics	C	O	Mg	Al	Si	S	Cl	K	Ca	Ti	Fe	Cu	Zn	Sn	Pb
Max	48.24	45.67	0.99	3.81	23.64	5.62	3.47	0.28	6.79	0.23	35.28	6.66	7.97	0.7	17.98
Min	13.33	26.82	0.62	1.19	2.57	0.36	3.47	0.15	0.15	0.16	9.84	1.1	0.65	0.45	0.64
Average	17.81	39.36		2.2	12.54	1.41					20.29				
Standard Deviation	6.56	4.76		0.72	6.85	1.64					7.83				

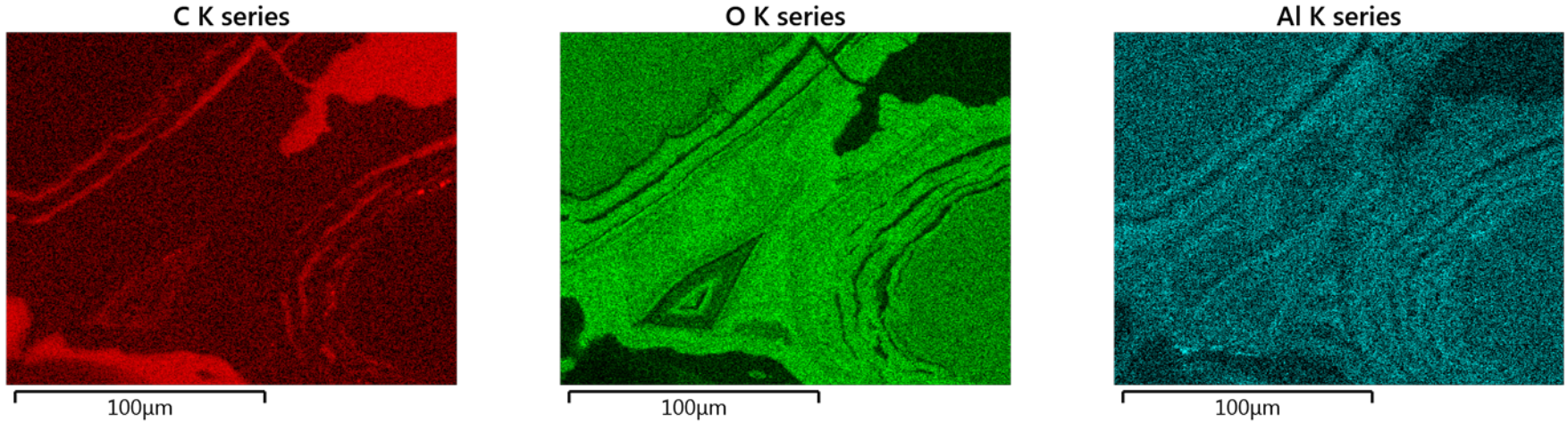

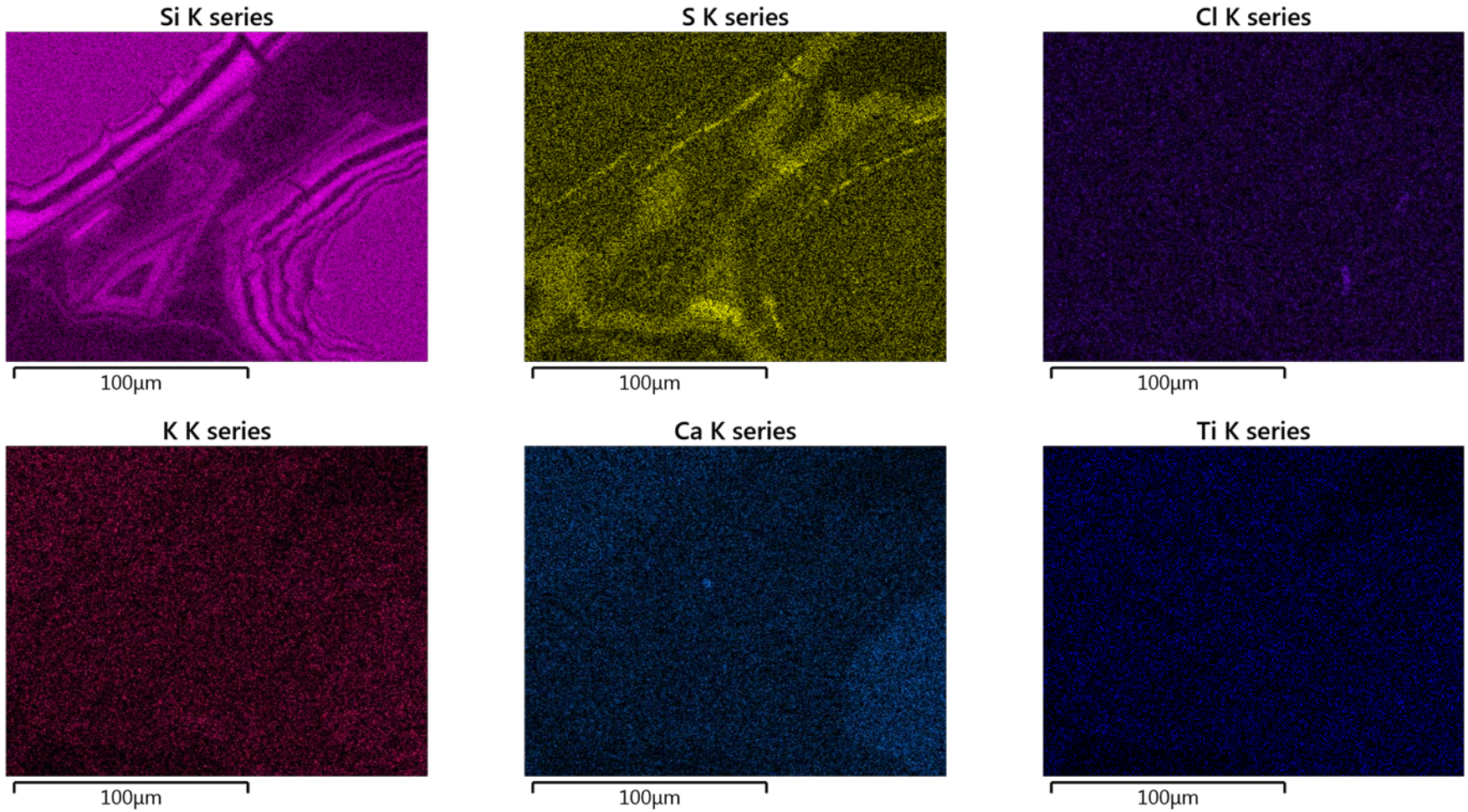
Si K series
100µm
S K series
100µm
Cl K series
100µm
K K series
100µm
Ca K series
100µm
Ti K series
100µm

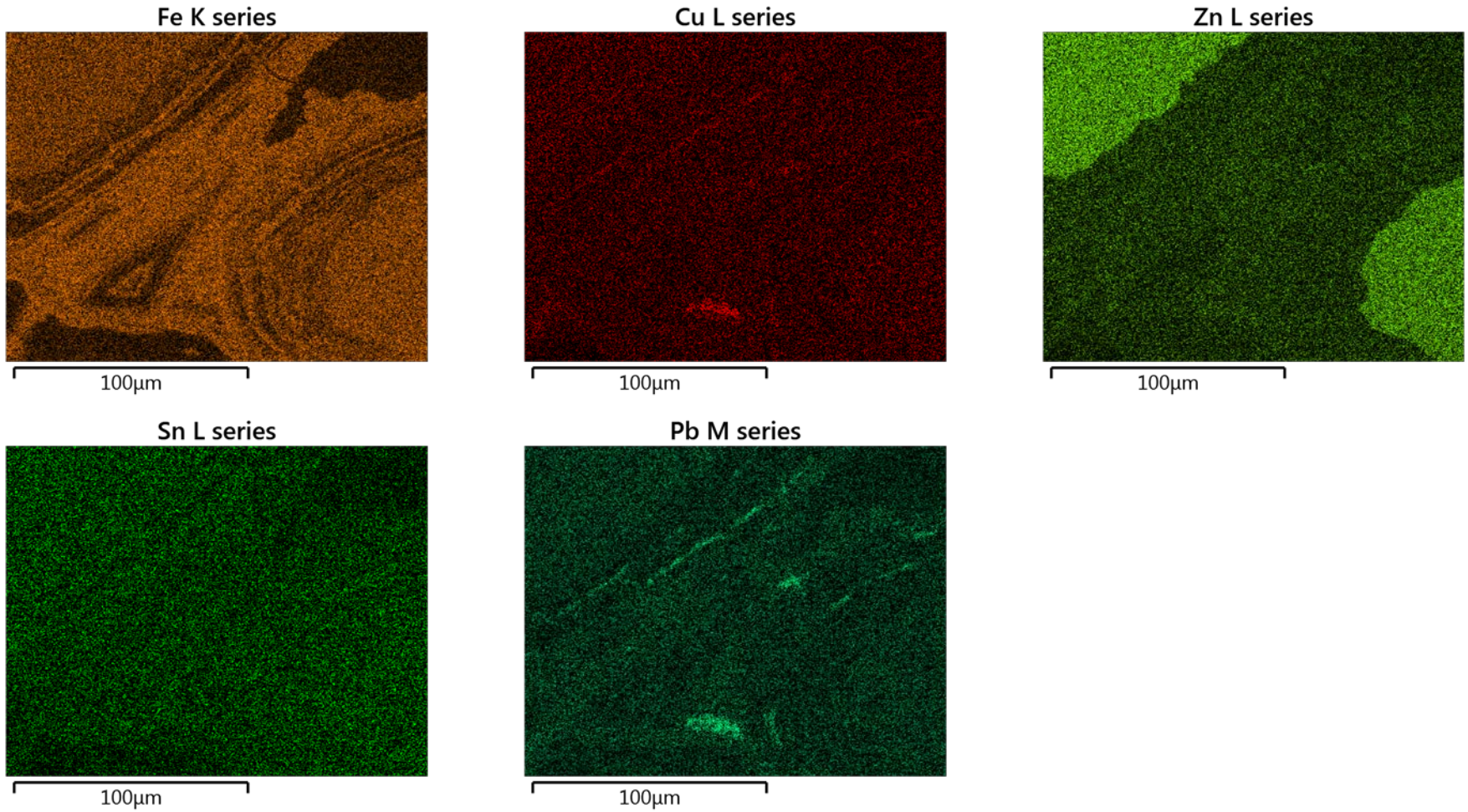

Figure 60: Element maps showing the spatial distribution of various elements at site 2 in sample MD

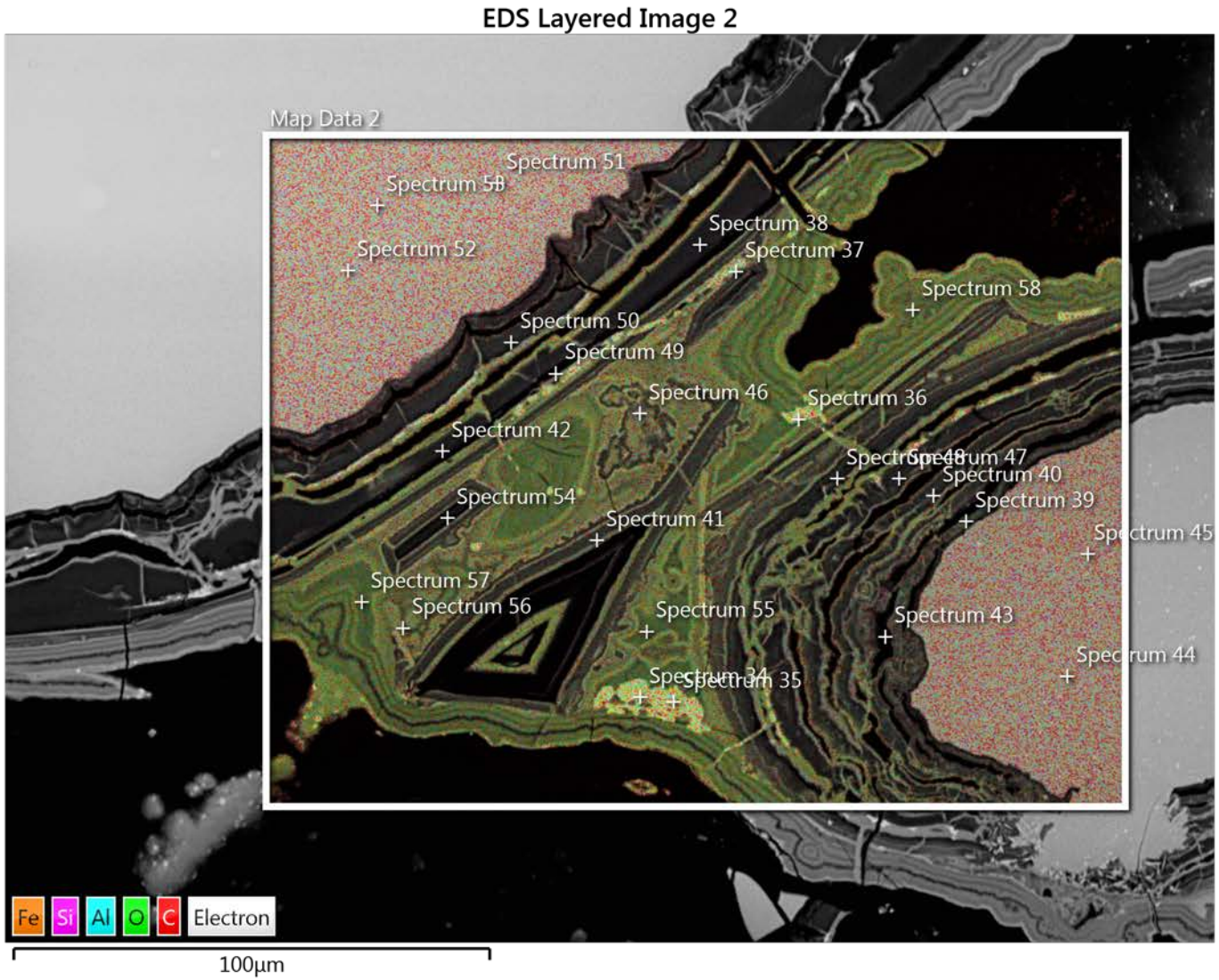

Figure 61: Layered element map showing the spatial distribution of iron, silicon, aluminium, oxygen and carbon at site 2 in sample MD

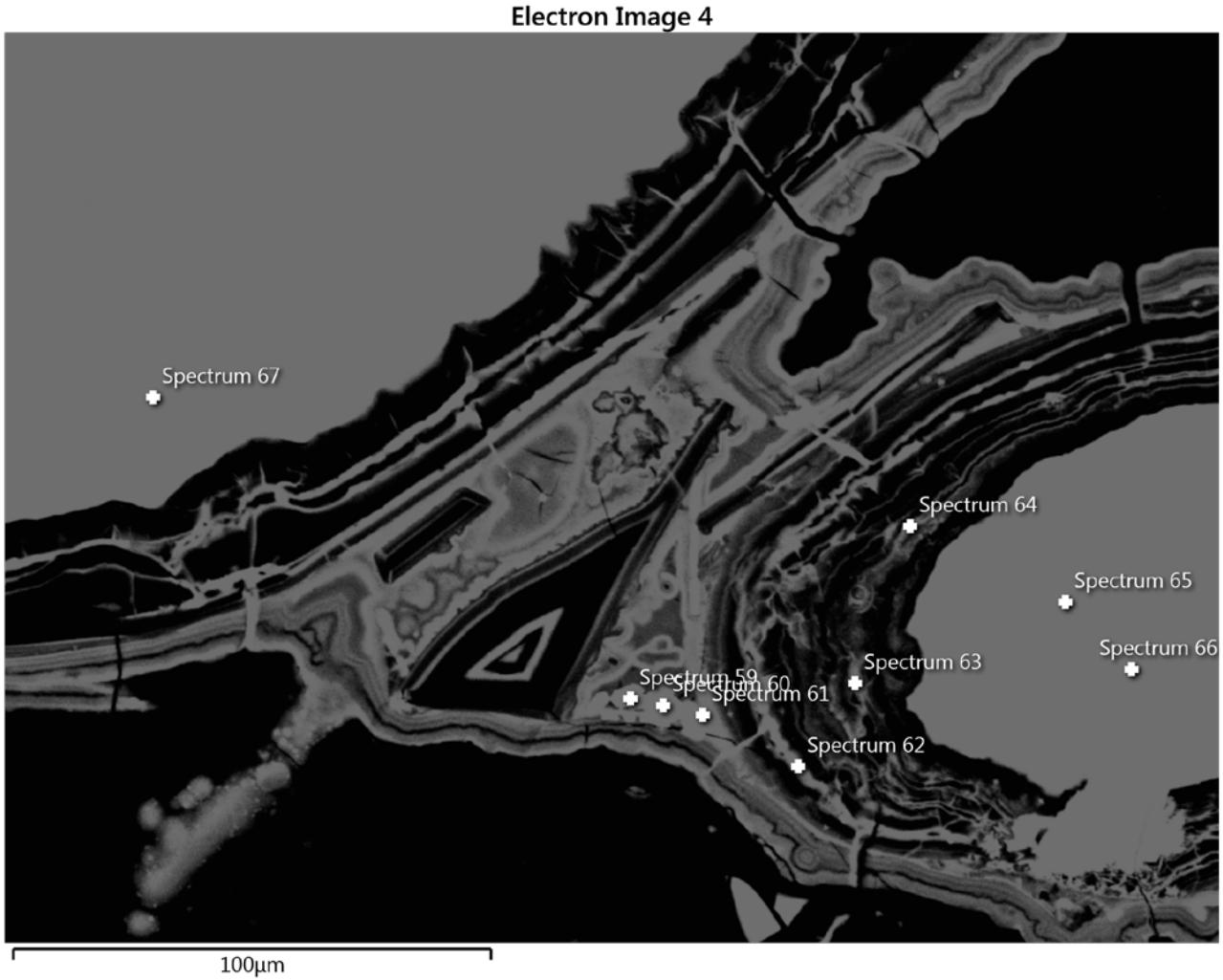

Figure 62: Locations of various spectra obtained at Site 2 of sample MD

Table 40: Elemental composition of material at each spectrum (wt. %)

Spectrum Label	C	O	Mg	Al	Si	S	Cl	K	Ca	Ti	Cr	Fe	Cu	Zn	Pb
Spectrum 59	18.06	37.53		1.49	2.13	4.94		0.31				23.22	2.89	0.69	8.74
Spectrum 60	17.57	35.06		1.15	1.74	6.08		0.26				17.97	4.7	0.92	14.54
Spectrum 61	16.15	41.85		1.63	3.27	2.91		0.09				26.16	1.78	0.7	5.45
Spectrum 62	15.94	43.92		2.12	9.93	0.94			0.09		0.08	26.3	0.19	0.49	
Spectrum 63	18.73	43.04		2.13	9.65	0.57				0.14		24.63	0.23	0.42	0.46
Spectrum 64	37.38	35.07		1.14	5.69	0.49	0.06		0.21	0.06		17.31	0.28	1.87	0.44
Spectrum 65	16.37	33.99	0.7	1.47	11.03	0.55		0.13	1.1			28.29	0.22	5.21	0.93
Spectrum 66	15.65	34.24	0.69	1.48	10.84	0.54		0.13	1.14	0.06		28.76	0.29	5.41	0.76
Spectrum 67	12.68	36.69	0.78	1.59	12.77	0.49		0.16	0.57	0.11		26.15	0.39	6.31	1.3

Table 41: Overview of the elemental composition at site 2 in Sample MD, based on data from all spectra (wt. %)

Statistics	C	O	Mg	Al	Si	S	Cl	K	Ca	Ti	Cr	Fe	Cu	Zn	Pb
Max	37.38	43.92	0.78	2.13	12.77	6.08	0.06	0.31	1.14	0.14	0.08	28.76	4.7	6.31	14.54
Min	12.68	33.99	0.69	1.14	1.74	0.49	0.06	0.09	0.09	0.06	0.08	17.31	0.19	0.42	0.44
Average	18.73	37.93		1.58	7.45	1.95						24.31	1.22	2.45	
Standard Deviation	7.21	3.94		0.36	4.26	2.18						4.14	1.61	2.45	

7c. Sample MD – site 3

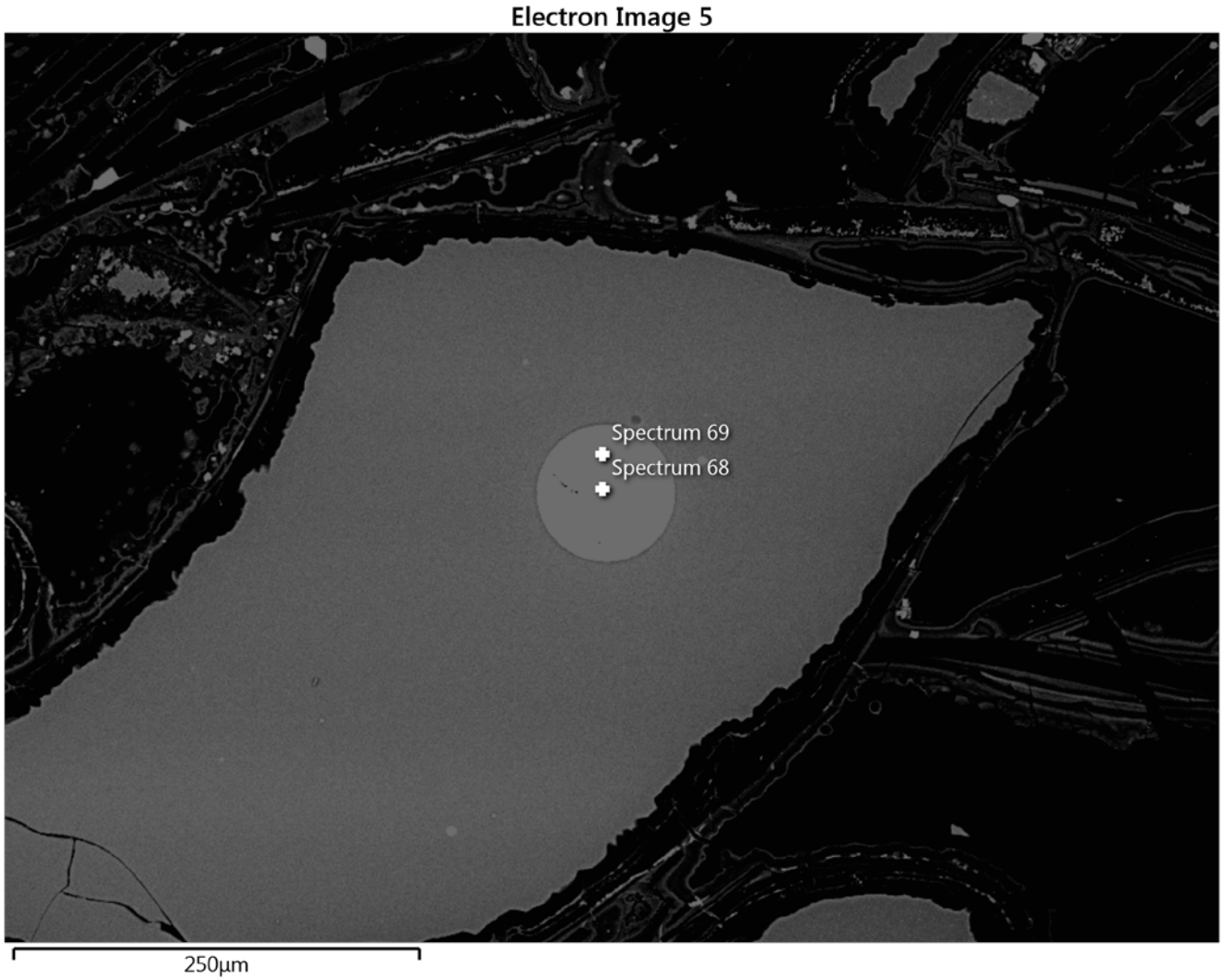

Figure 63: Locations of various spectra obtained at Site 3 of sample MD

Table 42: Elemental composition of material at each spectrum (wt. %)

Spectrum Label	C	O	Al	Si	S	Ca	Fe	Ni	Cu	Zn	As	Br	Sn	Sb	Pb
Spectrum 68	13.99	8.22	0.48	2.01	11.04	0.11	7.04	4.05	41.46	1.71	0.78		0.62	1.48	7.01
Spectrum 69	12.97	8.02		2.14	13.52	0.1	7.58	3.01	44.51	1.53		0	0.38	0.8	5.45

Table 43: Overview of the elemental composition at site 3 in Sample MD, based on data from all spectra (wt. %)

Statistics	C	O	Al	Si	S	Ca	Fe	Ni	Cu	Zn	As	Br	Sn	Sb	Pb
Max	13.99	8.22	0.48	2.14	13.52	0.11	7.58	4.05	44.51	1.71	0.78	0	0.62	1.48	7.01
Min	12.97	8.02	0.48	2.01	11.04	0.1	7.04	3.01	41.46	1.53	0.78	0	0.38	0.8	5.45
Average	13.48	8.12		2.08	12.28	0.1	7.31	3.53	42.99	1.62			0.5	1.14	6.23
Standard Deviation	0.72	0.15		0.09	1.75	0.01	0.38	0.74	2.16	0.12			0.17	0.48	1.1

7d. Sample MD – site 4

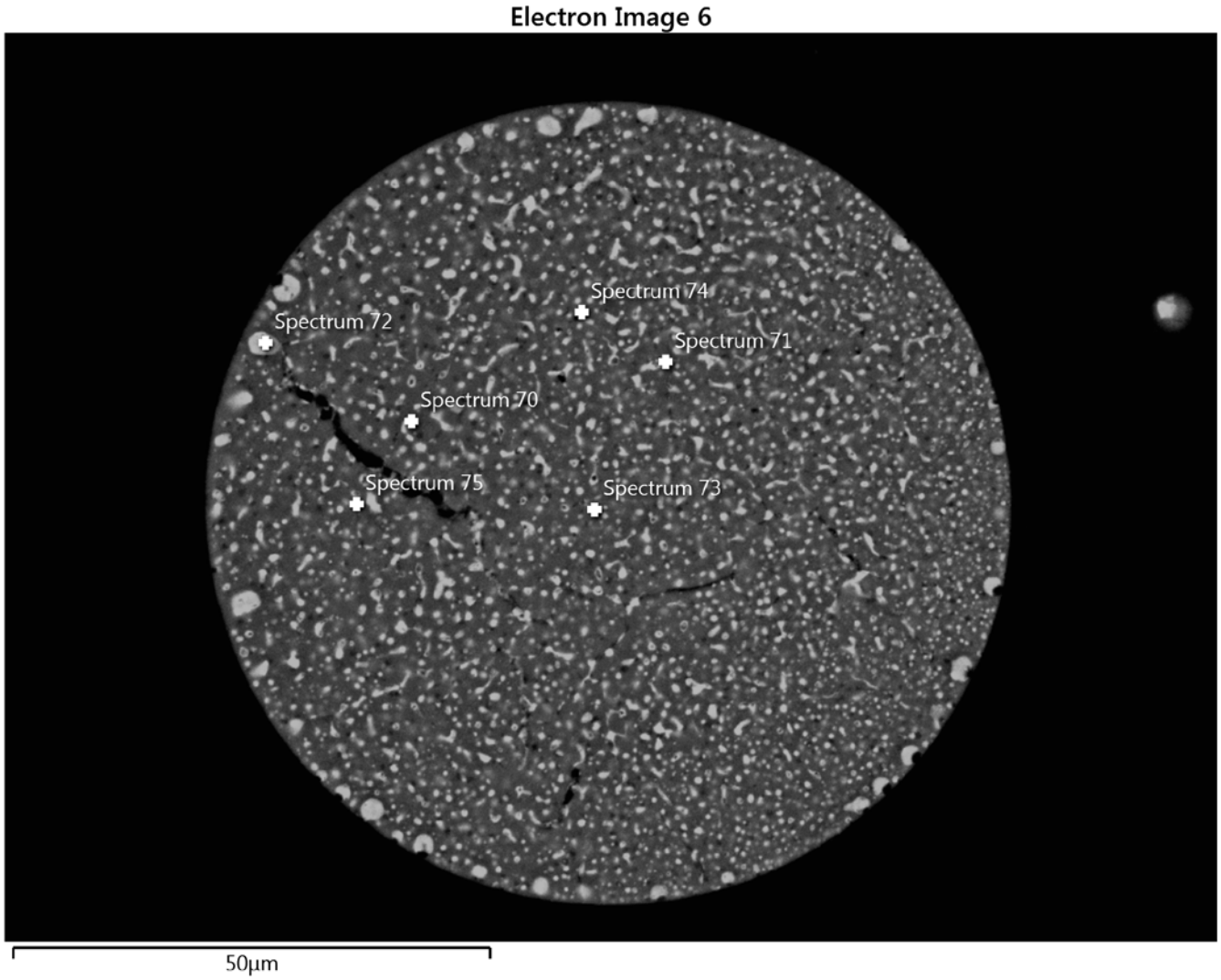

Figure 64: Locations of various spectra obtained at Site 4 of sample MD

Table 44: Elemental composition of material at each spectrum (wt. %)

Spectrum Label	C	O	Al	Si	S	Ca	Fe	Ni	Cu	Zn	As	Sn	Sb	Pb
Spectrum 70	12.81	7.26	0.35	2.02	8.48		6.09	11.22	27	1.21	1.99	1.72	3.65	16.2
Spectrum 71	13.54	7.76	0.34	1.72	8.91		5.8	7.31	24.98	1.41		0.66	1.33	26.24
Spectrum 72	10.88	7.75	0.39	2.63	4.71		7.59	18.37	21.88	1.38	3.05	3.59	7.81	9.97
Spectrum 73	13.43	7.56	0.38	1.98	14.7	0.14	7.06	1.9	47.57	1.17			0.38	3.72
Spectrum 74	13.49	7.75	0.41	2.04	14.3		7.04	2.33	46.63	1.82		0.31	0.54	3.33
Spectrum 75	13.58	8.38	0.36	2.19	13.73		7.64	2.32	46.57	1.15			0.35	3.73

Table 45: Overview of the elemental composition at site 4 in Sample MD, based on data from all spectra (wt. %)

Statistics	C	O	Al	Si	S	Ca	Fe	Ni	Cu	Zn	As	Sn	Sb	Pb
Max	13.58	8.38	0.41	2.63	14.7	0.14	7.64	18.37	47.57	1.82	3.05	3.59	7.81	26.24
Min	10.88	7.26	0.34	1.72	4.71	0.14	5.8	1.9	21.88	1.15	1.99	0.31	0.35	3.33
Average	12.95	7.74	0.37	2.1	10.81		6.87	7.24	35.77	1.36			2.34	10.53
Standard Deviation	1.06	0.37	0.03	0.3	4.05		0.77	6.58	12.33	0.25			2.96	9.2

7e. Sample MA – site 1

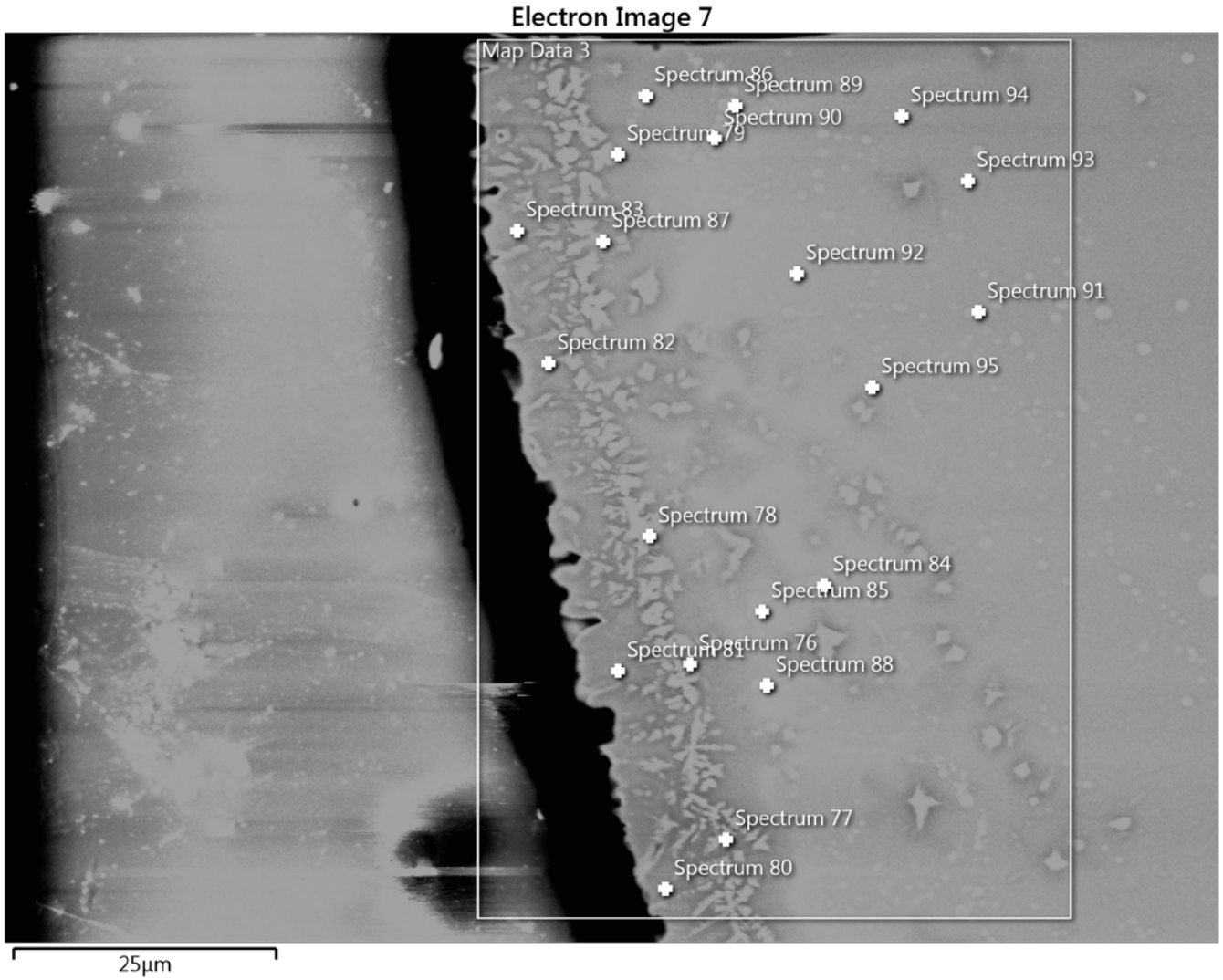

Figure 65: Locations of various spectra obtained at Site 1 of sample MA

Table 46: Elemental composition of material at each spectrum (wt. %)

Spectrum Label	C	O	Mg	Al	Si	S	K	Ca	Ti	Cr	Fe	Ni	Cu	Zn	Pb
Spectrum 76	22.91	30.18		0.92	6.24	0.36			0.18	0.24	34.98			4	
Spectrum 77	24.95	29.97		0.83	5.27	0.28	0.1	0.1		0.2	34.3			4	
Spectrum 78	26.19	30.23		0.85	5.39	0.32	0.12		0.2	0.18	33.17			3.36	
Spectrum 79	24.81	29.32		0.9	4.78	0.35			0.21	0.35	35.81			3.47	
Spectrum 80	29.47	31.19	0.75	0.75	9.28	0.32		0.24			19.45			8.55	
Spectrum 81	27.17	31.29	0.75	0.82	10.55	0.44		0.24			19.27		0.8	8.67	
Spectrum 82	30.61	30.92	0.54	0.8	9.36	0.52	0.09	0.16			20.72			6.28	
Spectrum 83	29.17	31.64	0.69	0.84	10.3	0.71		0.27			18.62			7.76	
Spectrum 84	26.3	13.96		0.41	4.1	9.69		0.1			15.34		26.17	3.92	
Spectrum 85	26.22	15.14		0.43	4.57	8.33		0.1			15.34		22.36	7.51	
Spectrum 86	32.08	15.49		0.37	3.37	9.68		0.09			14.35		15.97	8.6	
Spectrum 87	28.04	26.44		0.66	6.51	4.59					22.43		7.15	4.18	
Spectrum 88	25.27	17.78		0.59	5.77	6.14		0.14			17.02		23.51	3.79	
Spectrum 89	28.62	19.59		0.65	6.24	4.61		0.11			19.2		16.91	4.07	
Spectrum 90	29.93	14.39		0.41	3.93	8.61		0.09			14.12		24.54	3.97	
Spectrum 91	24.06	19.73		0.6	6.37	5.76		0.14			18.94	0.26	18.2	4.87	1.08
Spectrum 92	27.08	29.82	0.45	0.88	9.35	0.93	0.08	0.18			25.1		0.55	5.58	
Spectrum 93	26.68	30.21		0.94	9.48	1	0.09	0.21		0.13	25.93			5.35	
Spectrum 94	28.33	30.33		0.87	9.16	0.97	0.1	0.17			24.83			5.22	
Spectrum 95	23.16	30.71	0.56	0.95	10.67	1.09		0.23			26.54			6.1	

Table 47: Overview of the elemental composition at site 1 in Sample MA, based on data from all spectra (wt. %)

Statistics	C	O	Mg	Al	Si	S	K	Ca	Ti	Cr	Fe	Ni	Cu	Zn	Pb
Max	32.08	31.64	0.75	0.95	10.67	9.69	0.12	0.27	0.21	0.35	35.81	0.26	26.17	8.67	1.08
Min	22.91	13.96	0.45	0.37	3.37	0.28	0.08	0.09	0.18	0.13	14.12	0.26	0.55	3.36	1.08

Average	27.05	25.41		0.72	7.03	3.24					22.77			5.46	
Standard Deviation	2.49	6.87		0.19	2.46	3.56					7.09			1.84	

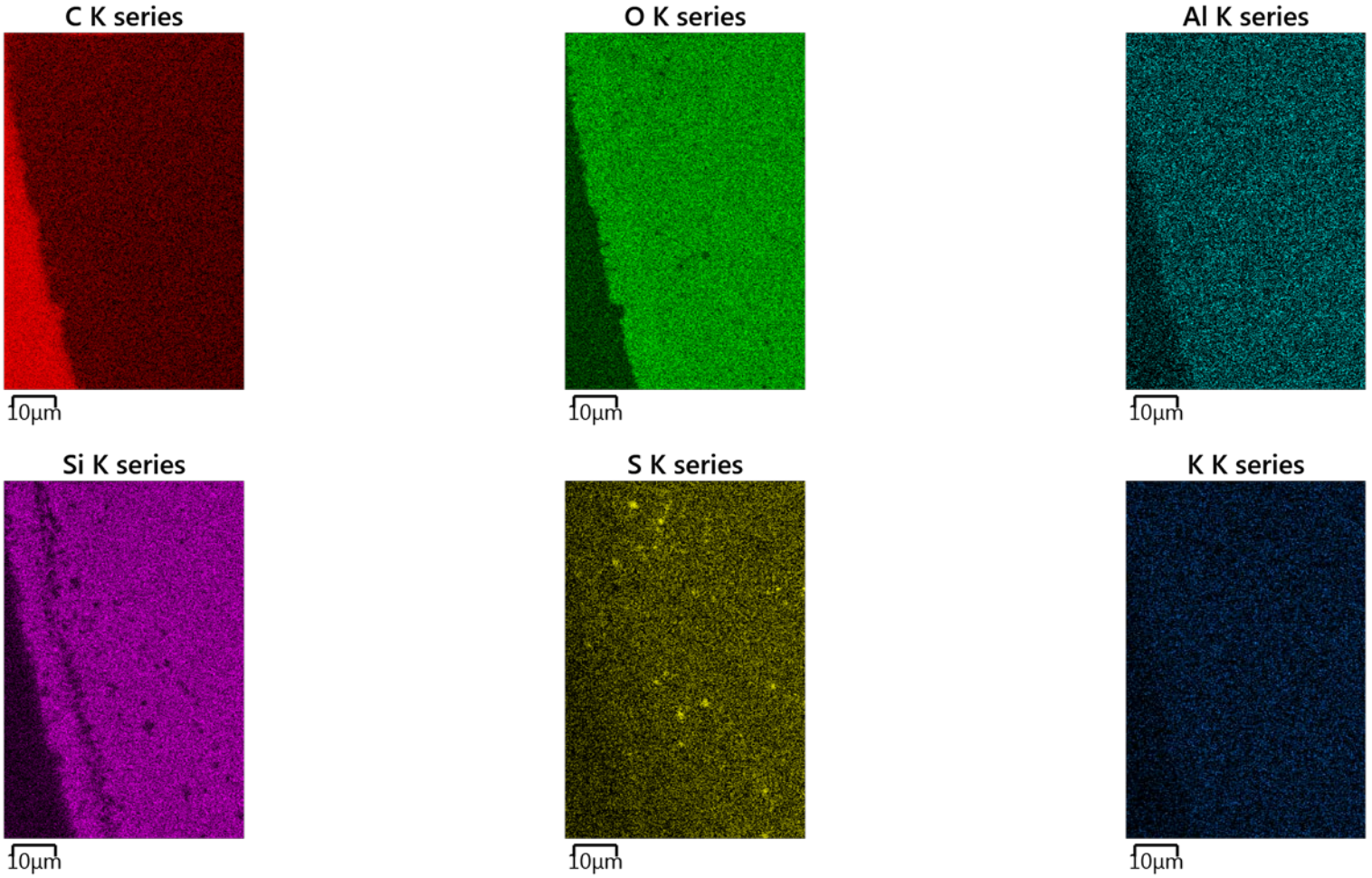

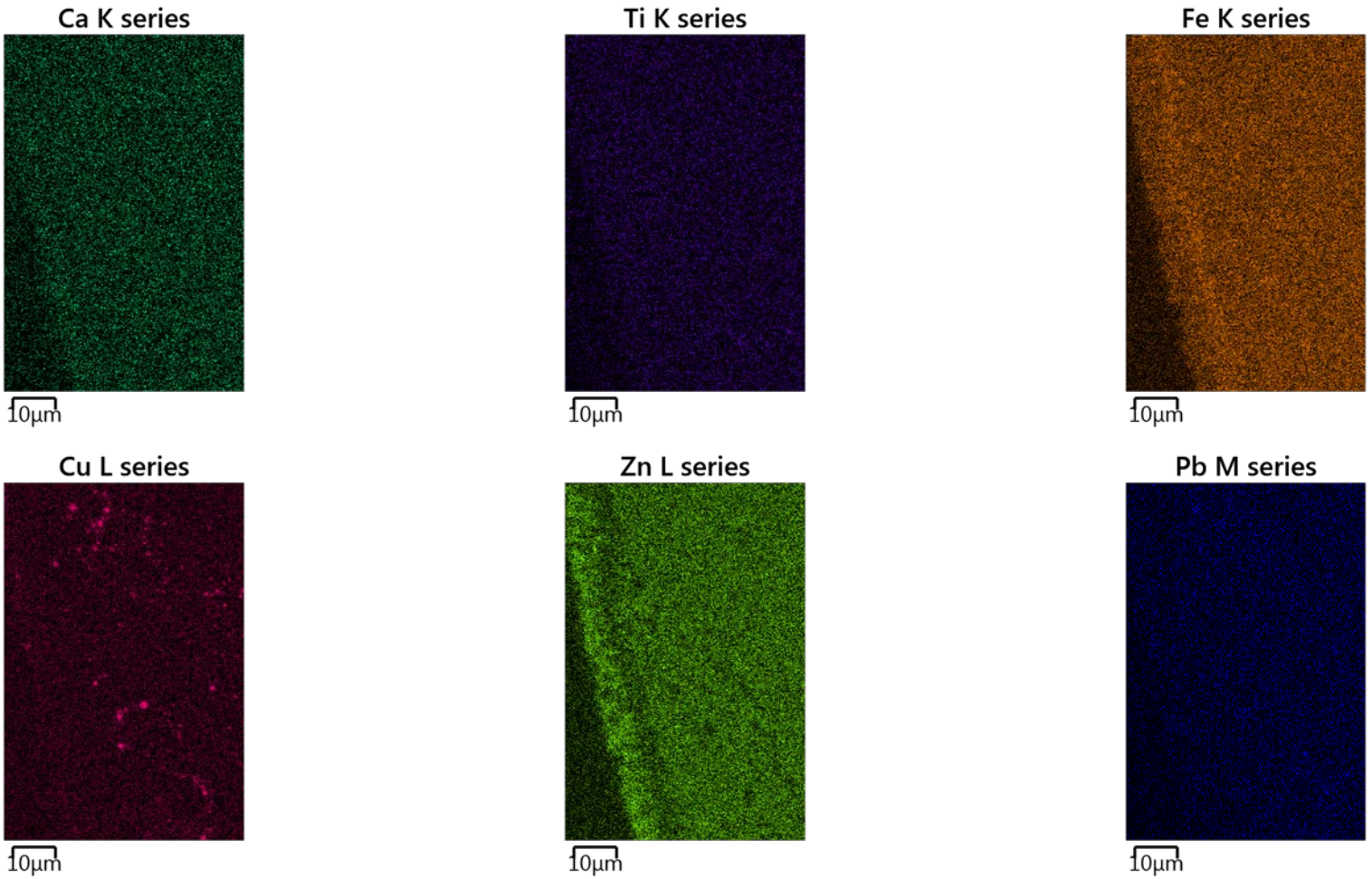

Figure 66: Element maps showing the spatial distribution of various elements at site 1 in sample MA

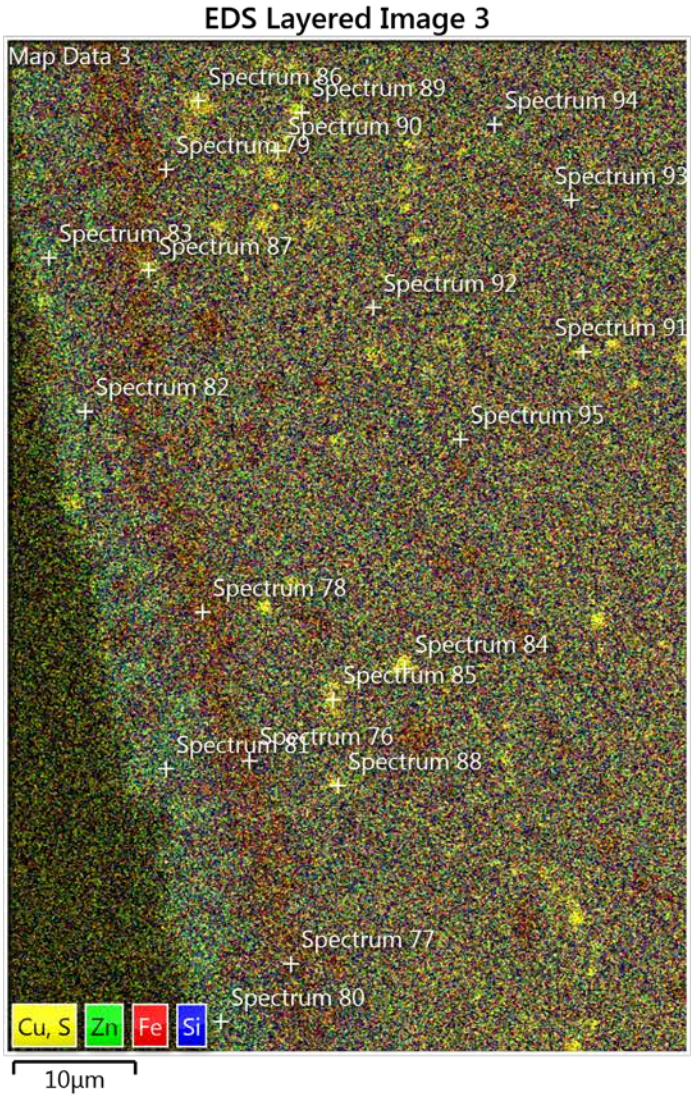

Figure 67: Layered element map showing the spatial distribution of copper/sulphur, zinc, iron and silicon at site 1 in sample MA

7f. Sample MA – site 2

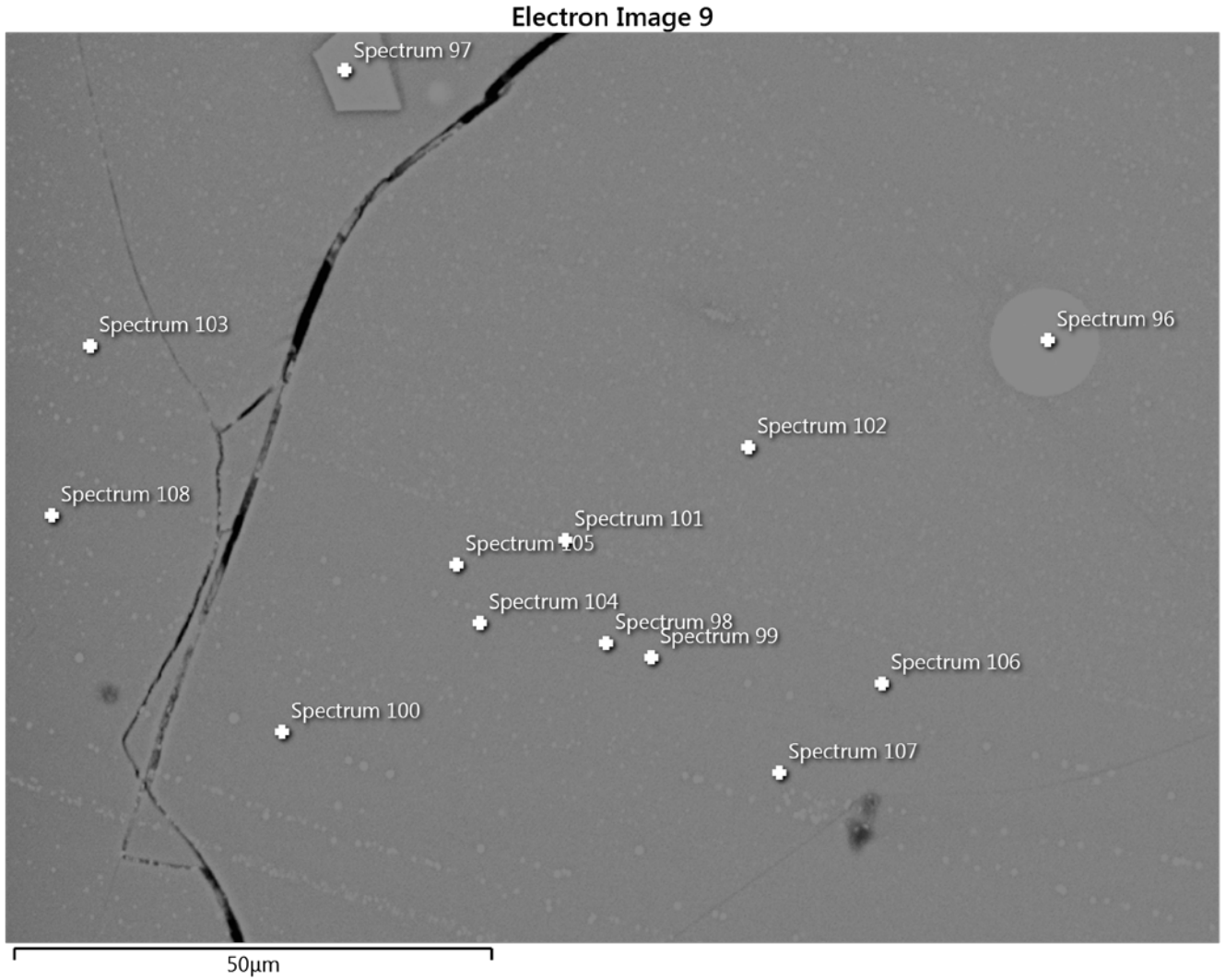

Figure 68: Locations of various spectra obtained at Site 2 of sample MA

Table 48: Elemental composition of material at each spectrum (wt. %)

Spectrum Label	C	O	Mg	Al	Si	P	S	K	Ca	Ti	Cr	Fe	Ni	Cu	Zn	Br	Pb
Spectrum 96	20.07	12.66			3.34		13.84					19.46	0.73	24.81	2.55	0.95	1.59
Spectrum 97	16.82	32.61		4.54	3.84		0.4			0.3	12.31	21.61			7.57		
Spectrum 98	21.28	29.16	0.59	1.38	9.66		2.69	0.12	0.28			23.71		6.56	4.56		
Spectrum 99	19.28	24	0.48	1.16	7.51		5.96		0.22			19.81		17.1	4.48		
Spectrum 100	21.21	19.84		0.87	5.86		7.88				0.16	17.6		20.38	5.24		0.96
Spectrum 101	20.75	30.1		1.47	9.64		2.41	0.13	0.29			23.3		6.66	5.25		
Spectrum 102	20.03	32.38	0.61	1.56	10.66	0.09	1.4	0.17	0.3			25.45		2.03	5.32		
Spectrum 103	22.39	33.53	0.58	1.87	8.85		0.91	0.16	0.28	0.41	1.61	24.72			4.69		
Spectrum 104	20.6	33.96	0.64	1.62	10.77		1.14	0.15	0.31	0.17		25.72			4.93		
Spectrum 105	20.87	33.44	0.63	1.54	10.54		1.15	0.14	0.32	0.12		25.15		0.9	5.2		
Spectrum 106	19.4	33.99	0.63	1.63	11.11		1.19	0.14	0.33	0.23		26.36			4.99		
Spectrum 107	20.05	34.18	0.61	1.61	10.97		1.19	0.12	0.32	0.12		25.86			4.98		
Spectrum 108	22.99	33.93	0.59	1.46	10.3		1.19	0.15	0.27	0.16		24.31			4.66		

Table 49: Overview of the elemental composition at site 2 in Sample MA, based on data from all spectra (wt. %)

Statistics	C	O	Mg	Al	Si	P	S	K	Ca	Ti	Cr	Fe	Ni	Cu	Zn	Br	Pb
Max	22.99	34.18	0.64	4.54	11.11	0.09	13.84	0.17	0.33	0.41	12.31	26.36	0.73	24.81	7.57	0.95	1.59
Min	16.82	12.66	0.48	0.87	3.34	0.09	0.4	0.12	0.22	0.12	0.16	17.6	0.73	0.9	2.55	0.95	0.96
Average	20.44	29.52			8.7		3.18					23.31			4.96		
Standard Deviation	1.52	6.7			2.72		3.88					2.82			1.06		

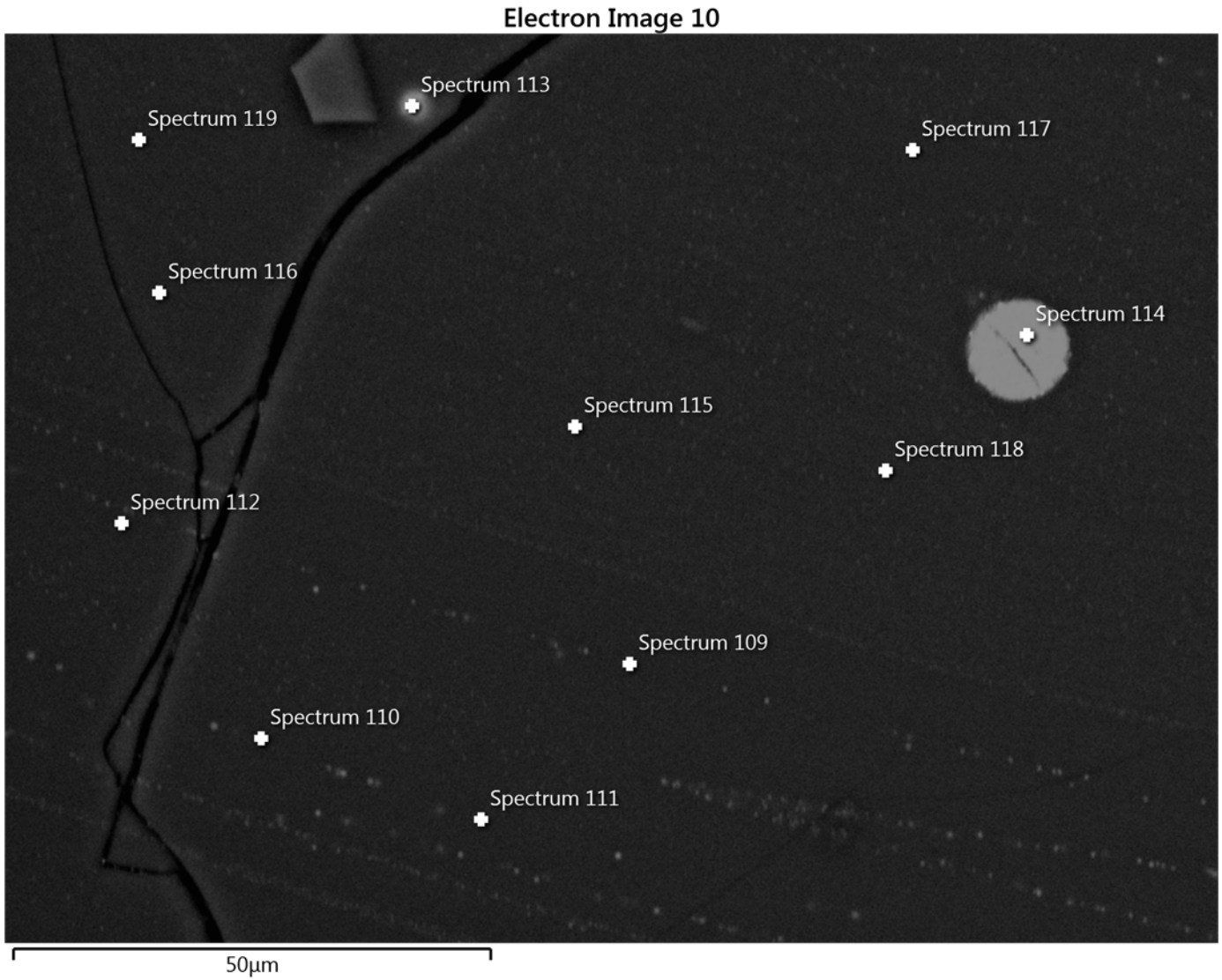

Figure 69: Locations of various spectra obtained at Site 2 of sample MA

Table 50: Elemental composition of material at each spectrum (wt. %)

Spectrum Label	C	O	Na	Mg	Al	Si	P	S	K	Ca	Ti	Cr	Mn	Fe	Ni	Cu	Zn	Br	W	Pb
Spectrum 109	18.19	28.76		0.57		9.24		4.3	0.16	0.31	0.16	0.1		27.97		6.1	4.14	0		
Spectrum 110	21.26	28.39			1.31	8.2		4.13	0.14	0.28	0.15			25.36	0.18	6.37	3.68			0.55
Spectrum 111	18.53	31.61		0.57	1.42	9.19		3.15	0.13	0.3	0.14		0.12	26.07		4.82	3.97			0
Spectrum 112	20.4	30.13				9.22		3.27	0.14	0.32	0.16			28.09		4.08	4.17	0		
Spectrum 113	16.06	25.95				5.53		8.57		0.17				18.97	0.6	21.06	2.27	0		0.82
Spectrum 114	19.55	10.11			0.45	2.28		17.45						21.27	0.95	23.54	2.91			1.47
Spectrum 115	16.51	33.4		0.6	1.66	10.76		1.12	0.17	0.34	0.19	0.1		30.54		0.33	4.27			
Spectrum 116	18.76	32.84	1.12	0.58	1.61	9.83		1.1	0.13	0.32	0.13	0.12		28.94		0.29	4.24		0	
Spectrum 117	15.35	33.91		0.63	1.71	10.79	0.12	1.12	0.18	0.35	0.17			30.99		0.27	4.4		0	
Spectrum 118	15.72	32.55		0.63	1.66	10.98		1.28	0.17	0.35	0.17	0.09	0.17	31.36		0.46	4.4			
Spectrum 119	18.17	32.89	0.99	0.58	1.54	10.07		1.19	0.13	0.35	0.13	0.12	0.12	29.27		0.43	4.02		0	

Table 51: Overview of the elemental composition at site 2 in Sample MA, based on data from all spectra (wt. %)

Statistics	C	O	Na	Mg	Al	Si	P	S	K	Ca	Ti	Cr	Mn	Fe	Ni	Cu	Zn	Br	W	Pb
Max	21.26	33.91	1.12	0.63	1.71	10.98	0.12	17.45	0.18	0.35	0.19	0.12	0.17	31.36	0.95	23.54	4.4	0	0	1.47
Min	15.35	10.11	0.99	0.57	0.45	2.28	0.12	1.1	0.13	0.17	0.13	0.09	0.12	18.97	0.18	0.27	2.27	0	0	0
Average	18.05	29.14				8.74		4.24						27.17		6.16	3.86			
Standard Deviation	1.95	6.78				2.63		4.93						3.99		8.36	0.68			

7g. Sample MA – site 3

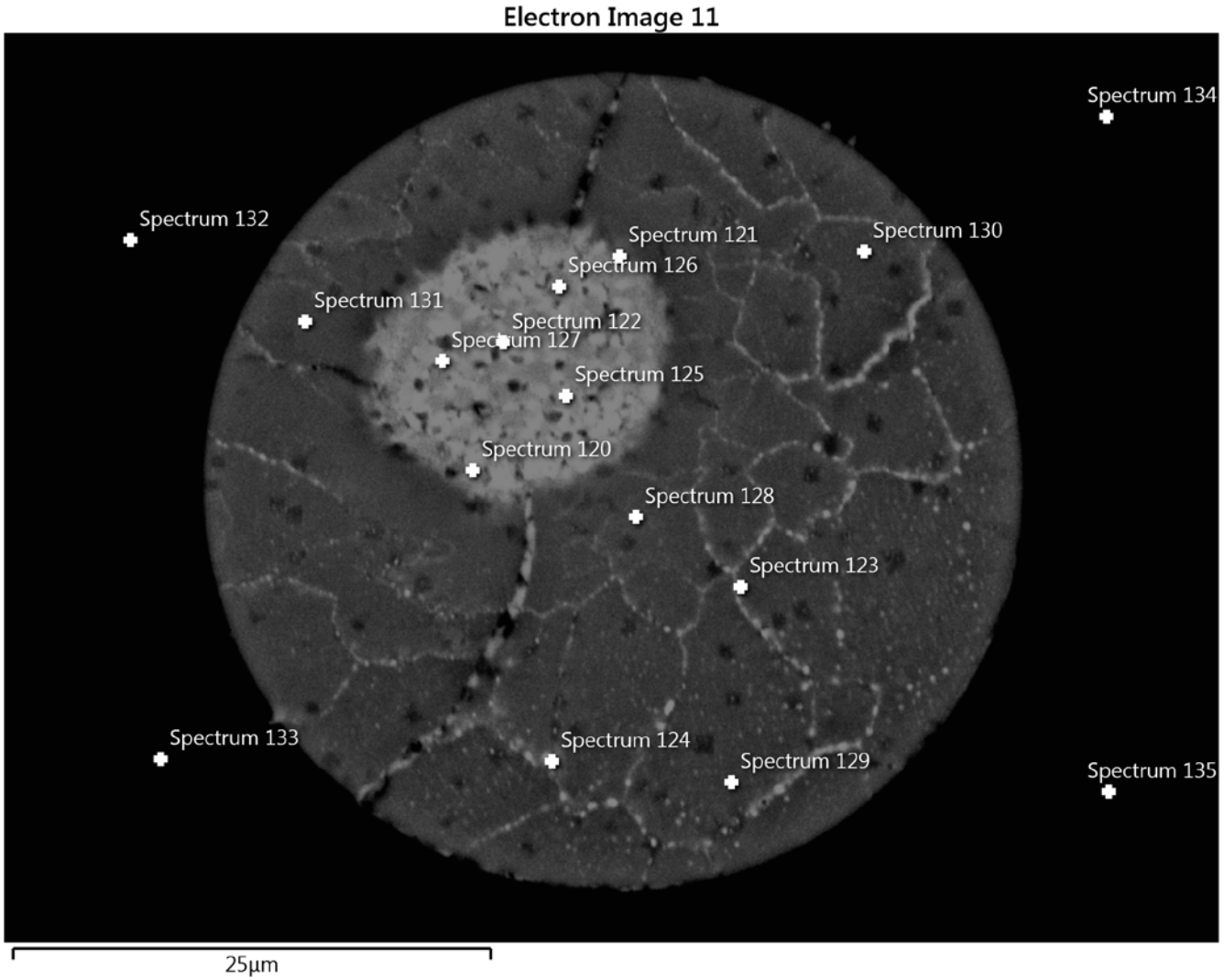

Figure 70: Locations of various spectra obtained at Site 3 of sample MA

Table 52: Elemental composition of material at each spectrum (wt. %)

Spectrum Label	C	O	Mg	Al	Si	S	K	Ca	Ti	Cr	Mn	Fe	Ni	Cu	Zn	Sn	Sb	Pb
Spectrum 120	11.24	8.2		0.51	2.98	2.42						14.36	16.28	29.35	1.26	8.43	1.76	3.2
Spectrum 121	11.37	8.75		0.47	2.96	5.59						13.54	14.08	31.82	1.65	6.34	1.02	2.4
Spectrum 122	11.48	7.96		0.51	3.05	2.06						7.98	9.32	40.9	1.24	10.29	2.82	2.4
Spectrum 123	14.33	8.61		0.43	2.72	15.14		0.14				14.43	1.97	38.08	1.32			2.82
Spectrum 124	13.93	9		0.39	2.71	15.01		0.15				15.35	2.3	35.27	1.23			4.64
Spectrum 125	11.31	7.86		0.49	3.02	1.3						8.3	11.16	39.56	1.37	11.08	2.6	1.94
Spectrum 126	10.27	7.81		0.65	3.34	1.46						8.88	9.91	45.02	1.72	7.79	1.39	1.76
Spectrum 127	10.46	8.14			3.13	1.76						8.62	10.17	38.22	1.27	11.58	2.74	3.91
Spectrum 128	14.6	8.64		0.39	2.59	16.21						14.12	1.41	36.98	1.77			3.29
Spectrum 129	14.9	9.5		0.49	2.75	15.7						14.27	0.76	38.16	1.46			2.01
Spectrum 130	15.47	9.24		0.46	2.75	15.75		0.12				14.16	0.62	37.58	1.47			2.37
Spectrum 131	14.28	9.61		0.46	2.82	16.24		0.13				14.97	0.41	36.37	1.5			3.21
Spectrum 132	11.39	34.78	0.91	2.07	13.61	0.88	0.24	0.59	0.19	0.11	0.16	30.01		1.14	3.91			0

Spectrum 133	11.27	36.05	0.8	1.8	13.51	0.95	0.2	0.6	0.21			29.75		1.29	3.56			
Spectrum 134	11.92	36.19	0.86	1.99	13.25	0.84	0.21	0.55	0.21			29.14		1.1	3.73			
Spectrum 135	11.8	35.33	0.96	1.92	13.59	0.9	0.24	0.59	0.23		0.16	29.33		1.08	3.88			

Table 53: Overview of the elemental composition at site 3 in Sample MA, based on data from all spectra (wt. %)

Statistics	**C**	**O**	**Mg**	**Al**	**Si**	**S**	**K**	**Ca**	**Ti**	**Cr**	**Mn**	**Fe**	**Ni**	**Cu**	**Zn**	**Sn**	**Sb**	**Pb**
Max	15.47	36.19	0.96	2.07	13.61	16.24	0.24	0.6	0.23	0.11	0.16	30.01	16.28	45.02	3.91	11.58	2.82	4.64
Min	10.27	7.81	0.8	0.39	2.59	0.84	0.2	0.12	0.19	0.11	0.16	7.98	0.41	1.08	1.23	6.34	1.02	0
Average	12.5	15.36			5.55	7.01						16.7		28.25	2.02			
Standard Deviation	1.74	12.08			4.74	7.02						8.08		16.52	1.06			

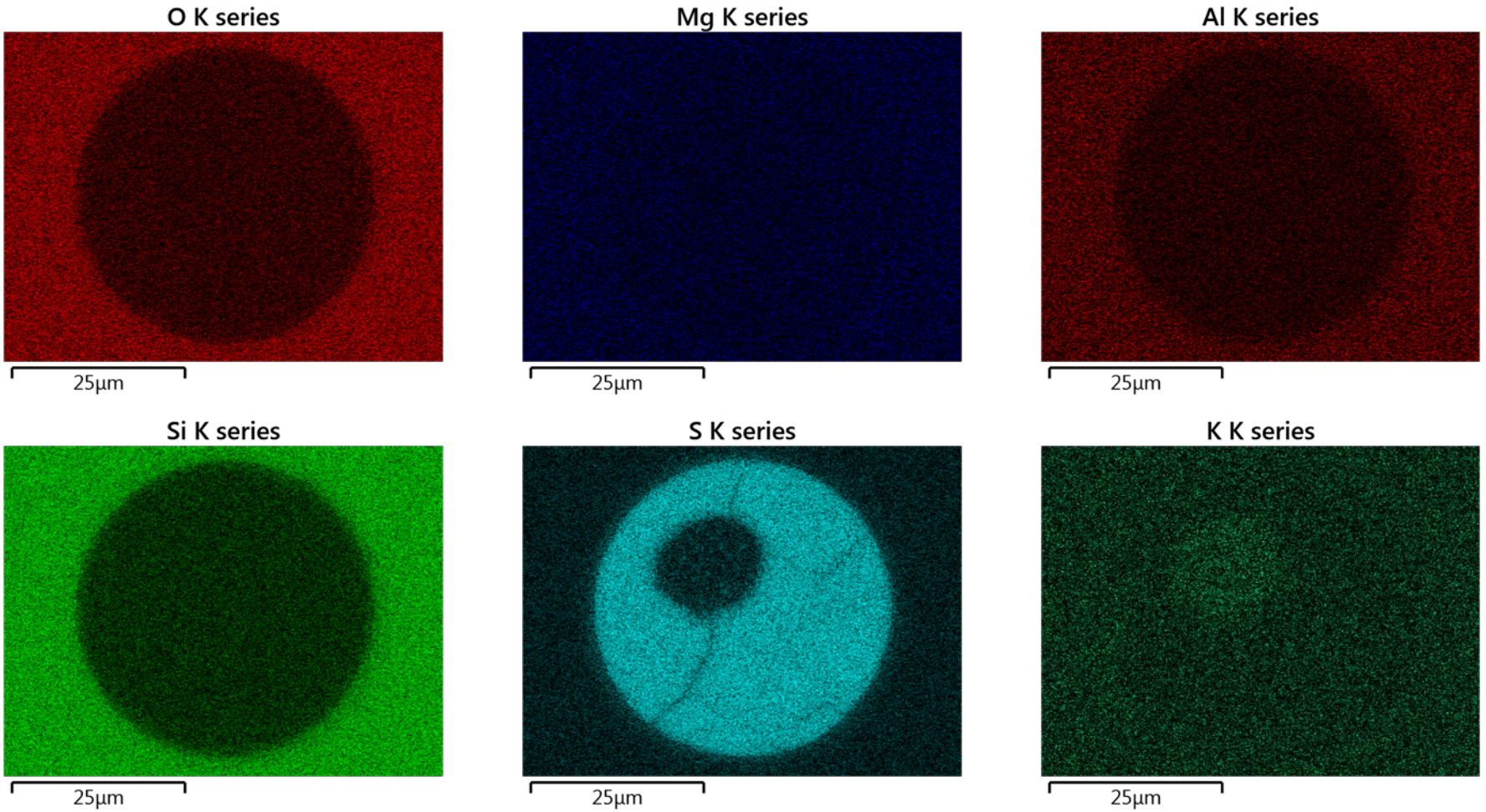
O K series
25µm
Mg K series
25µm
Al K series
25µm
Si K series
25µm
S K series
25µm
K K series
25µm

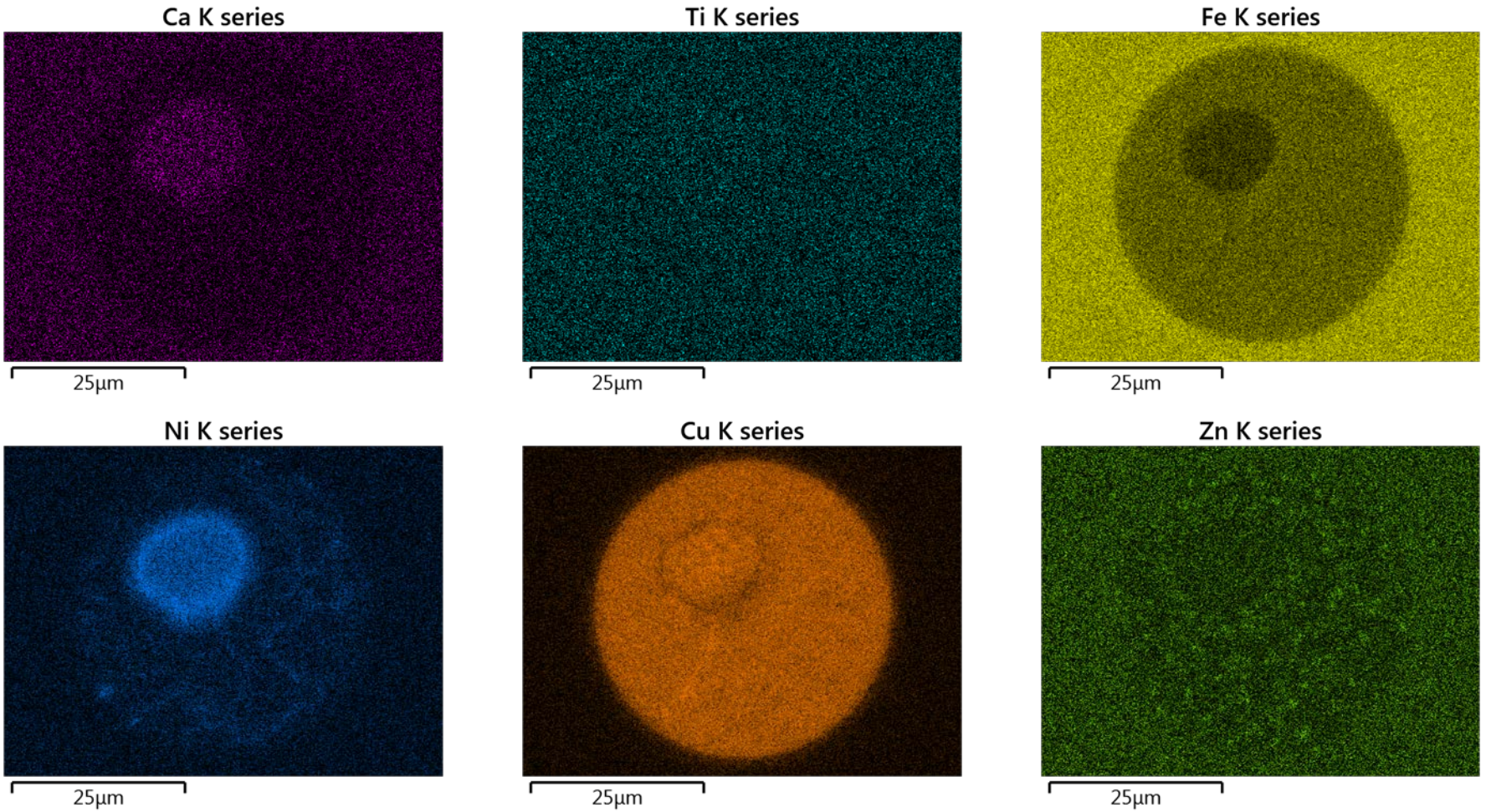
Ca K series
25µm
Ti K series
25µm
Fe K series
25µm
Ni K series
25µm
Cu K series
25µm
Zn K series
25µm

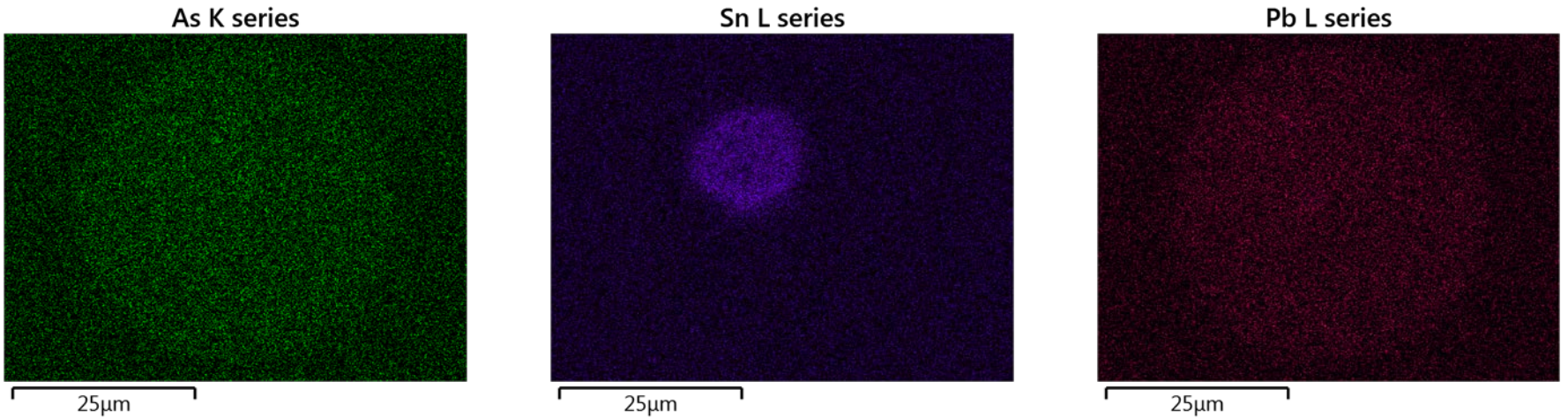

Figure 71: Element maps showing the spatial distribution of various elements at site 3 in sample MA

7h. Sample MA – site 4

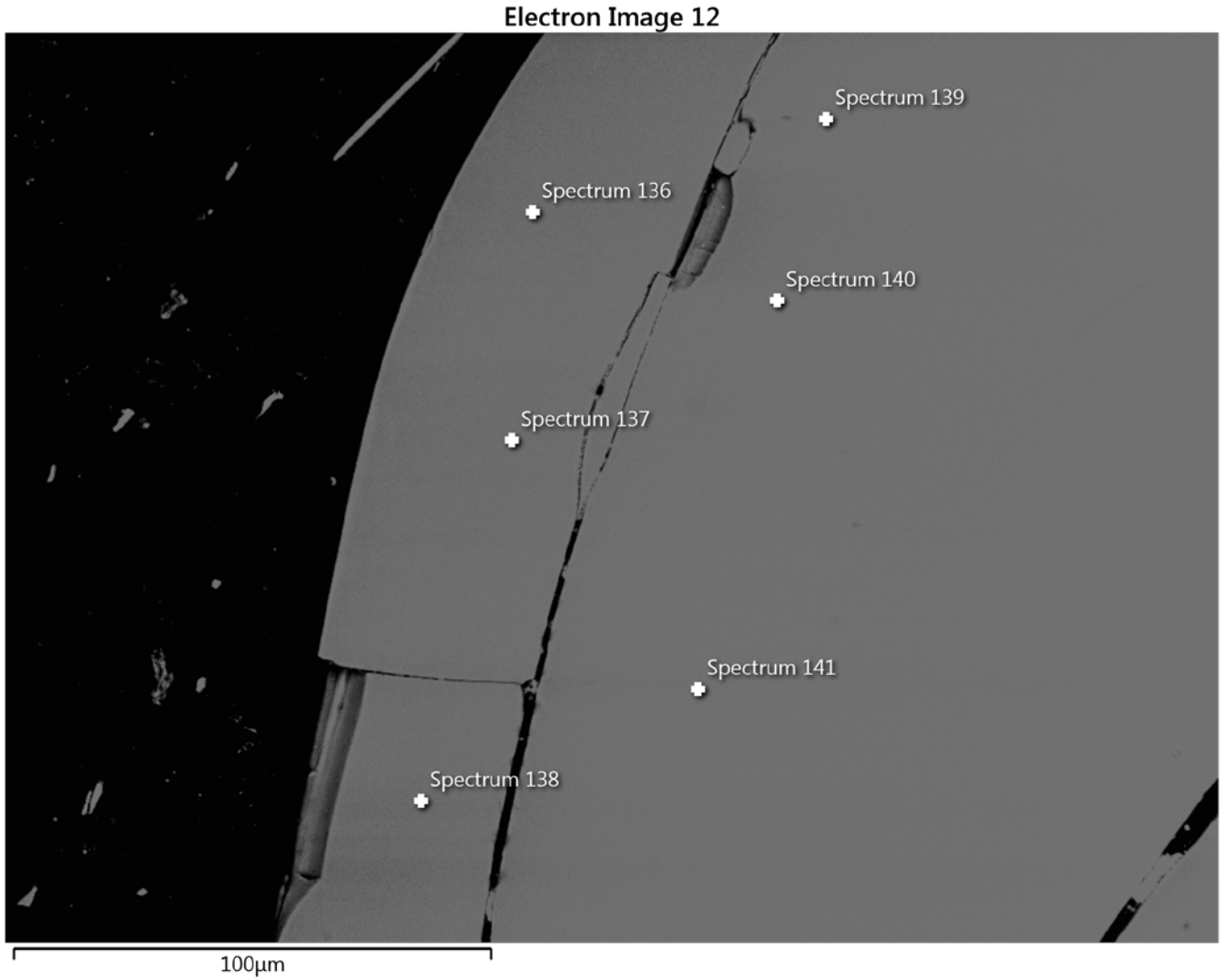

Figure 72: Locations of various spectra obtained at Site 4 of sample MA

Table 54: Elemental composition of material at each spectrum (wt. %)

Spectrum Label	C	O	Mg	Al	Si	S	K	Ca	Ti	Cr	Fe	Co	Zn
Spectrum 136	25.86	35.62	0.68	1.5	10.9	0.58	0.17	0.44	0.18		20.41		3.64
Spectrum 137	24.56	36.37	0.7	1.58	11.3	0.62	0.12	0.47	0.2		20.19	0.31	3.57
Spectrum 138	24.83	36.27	0.72	1.56	11.3	0.6	0.16	0.46			20.37		3.72
Spectrum 139	21.72	37.16	0.8	1.64	12.04	0.6	0.16	0.46	0.14		21.35		3.94
Spectrum 140	20.81	37.07	0.79	1.66	12.16	0.62	0.19	0.44	0.14		22.02		4.1
Spectrum 141	20.21	36.96	0.79	1.74	12.31	0.65	0.22	0.5	0.14	0.14	22.25		4.09

Table 55: Overview of the elemental composition at site 4 in Sample MA, based on data from all spectra (wt. %)

Statistics	C	O	Mg	Al	Si	S	K	Ca	Ti	Cr	Fe	Co	Zn
Max	25.86	37.16	0.8	1.74	12.31	0.65	0.22	0.5	0.2	0.14	22.25	0.31	4.1
Min	20.21	35.62	0.68	1.5	10.9	0.58	0.12	0.44	0.14	0.14	20.19	0.31	3.57
Average	23	36.57	0.75	1.61	11.67	0.61	0.17	0.46			21.1		3.84
Standard Deviation	2.37	0.59	0.05	0.08	0.58	0.02	0.03	0.02			0.9		0.23

Appendix 8. Acid Neutralization Capacity/Acid Generation Capacity of slag

Table 56: Acid Neutralization Capacity/Acid Generation Capacity of four copper slag samples ranging from unweathered to heavily weathered

			Sample ID			
	Units	**LOR**	**MA**	**MB**	**MC**	**MD**
EA033-A: Actual Acidity						
pH KCl (23A)	pH Unit	0.1	6.1	6.2	6.4	6.1
Titratable Actual Acidity (23F)	mole H+ / t	2	<2	<2	<2	<2
sulfidic - Titratable Actual Acidity (s-23F)	% pyrite S	0.02	<0.02	<0.02	<0.02	<0.02
EA033-B: Potential Acidity						
Chromium Reducible Sulfur (22B)	% S	0.005	1.35	1.12	1.18	0.637
Acidity - Chromium Reducible Sulfur (a-22B)	mole H+ / t	10	844	696	739	398
EA033-E: Acid Base Accounting						
ANC Fineness Factor		0.5	1.5	1.5	1.5	1.5
Net Acidity (sulfur units)	% S	0.02	1.35	1.12	1.18	0.64
Net Acidity (acidity units)	mole H+ / t	10	844	696	739	398
Liming Rate	kg CaCO3/t	1	63	52	55	30
Net Acidity excluding ANC (sulfur units)	% S	0.02	1.35	1.12	1.18	0.64
Net Acidity excluding ANC (acidity units)	mole H+ / t	10	844	696	739	398
Liming Rate excluding ANC	kg CaCO3/t	1	63	52	55	30